Astrophysical Tests of General Relativity

Alexander F. Zakharov

A. I. Alikhanov ITEP -- NRC "Kurchatov Institute"

BLTP, JINR, Dubna

The XXV International Workshop on High Energy Physics "From Quarks to Galaxies: Elucidating Dark Sides"

Logunov Institute for High Energy Physics, Protvino, Russia

28 November 2023

Outline of my talk

- Introduction
- Compact stars (White Dwarfs, Neutron Stars are the first astronomical applications of quantum mechanics)
- Early development of GR and cosmology (Friedmann, Lemaitre, Gamow)
- Bright star trajectories near GC
- Shadow from a theoretical concept to GR test
- Conclusions

Our recent publications on the subject

AFZ, Phys. Part. Nucl. Lett. (2023)

AFZ, Universe (2022)

AFZ, Astron. Astrophys. Trans. (2022)

P. Jovanovic, D. Borka, V. Borka Jovanovic, AFZ, JCAP (2023)

AFZ, Phys. Part. Nucl. (2023)

AFZ, IJMPD (2023)

AFZ, arxiv:2305.15446

2023

1953 -- I. S. Shklovsky proposed the synchrotron model for Crab Nebula

1963 -- The first Texas Symposium on Relativistic Astrophysics

The discovery of quasars, Kerr metric

75 years since A. A. Friedmann birthday (the ban on dynamical cosmological models was lifted in USSR). The nuclear “shield” did not protect physical cosmology in 1930s -1960s.

Institute for High Energy Physics (Protvino) was found

1968 -- Discovery of pulsars (rotating NSs), J. A. Wheeler introduced the BH concept

L.I. Pomomarev (1937- 2019): For physicist, the history of science is a necessary element of education, without which he risks remaining a craftsman

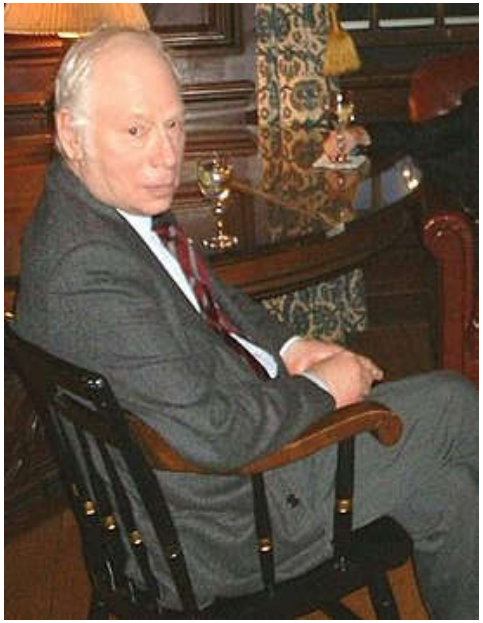

Steven Weinberg: “I am a physicist, not a historian, but over the years I have become increasingly fascinated by the history of science. It is an extraordinary story, one of the most interesting in human history. Today’s research can be aided and illuminated by a knowledge of its past, and for some scientists knowledge of the history of science helps to motivate resent work.”

The founders of GR studies in Russia

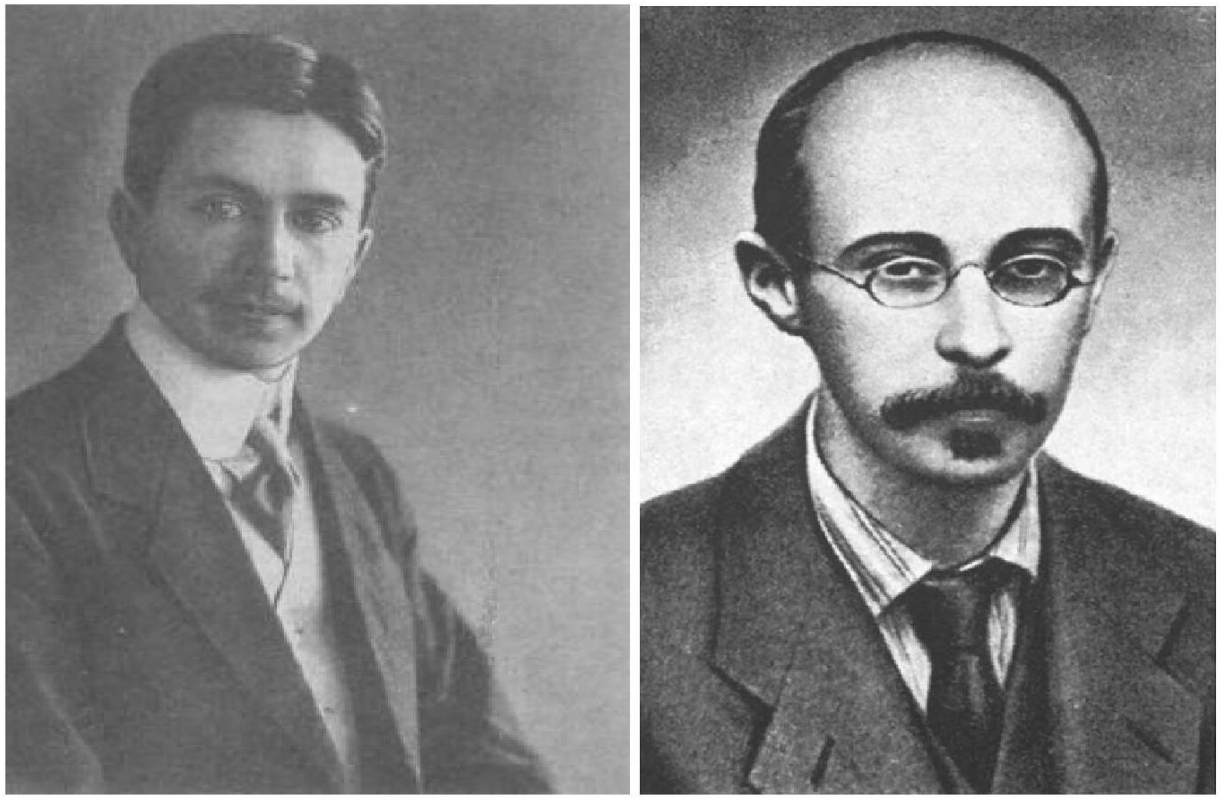

Figure 1. V. K. Frederiks who was a founder of Russian schools in GR and theory of liquid crystals (left) and Alexander Friedmann who was the founde of physical cosmology(right).

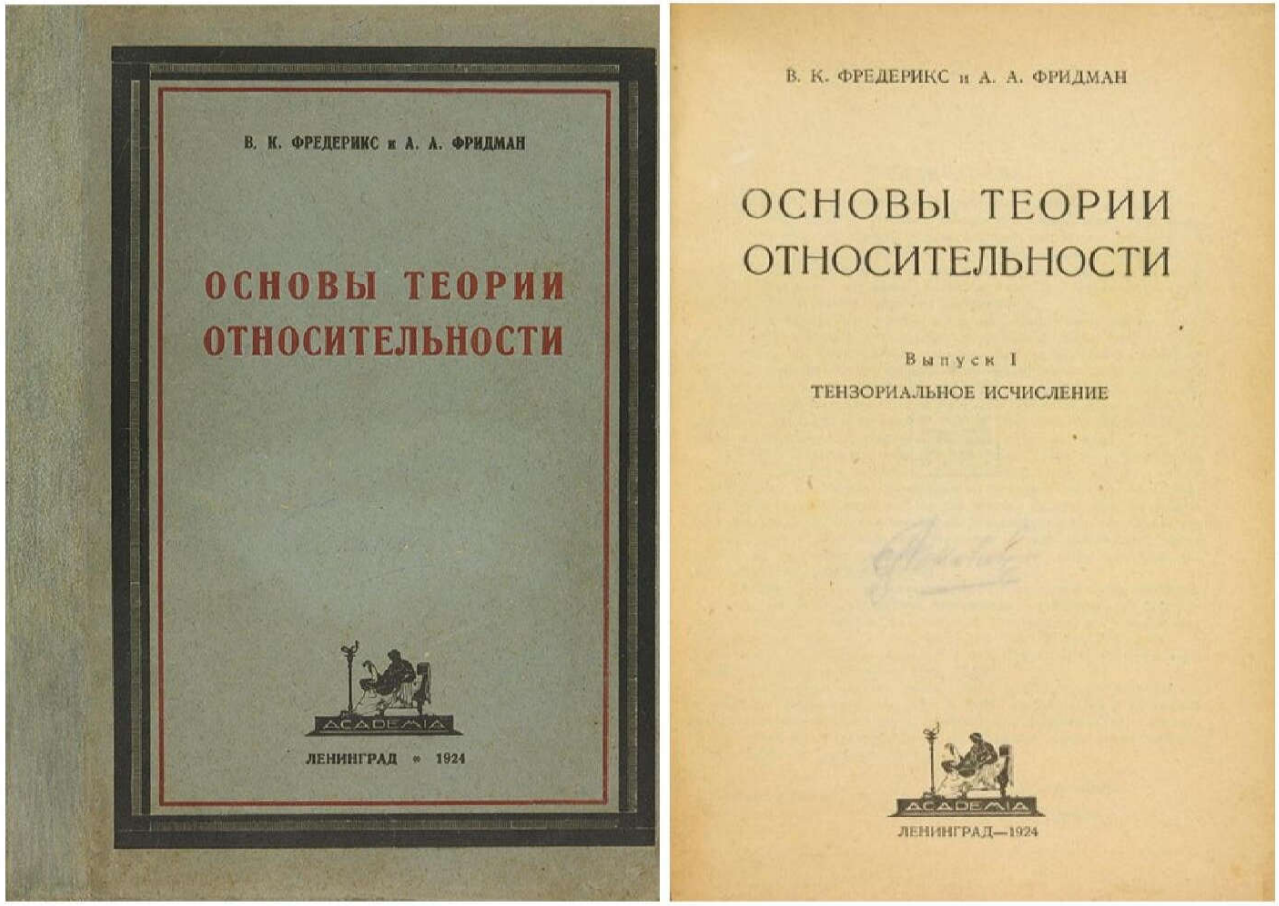

Figure 2. Cover page (left) of joint book "Basics of General Relativity" by V. K. Frederiks and A. A. Friedmann and its first page (right).

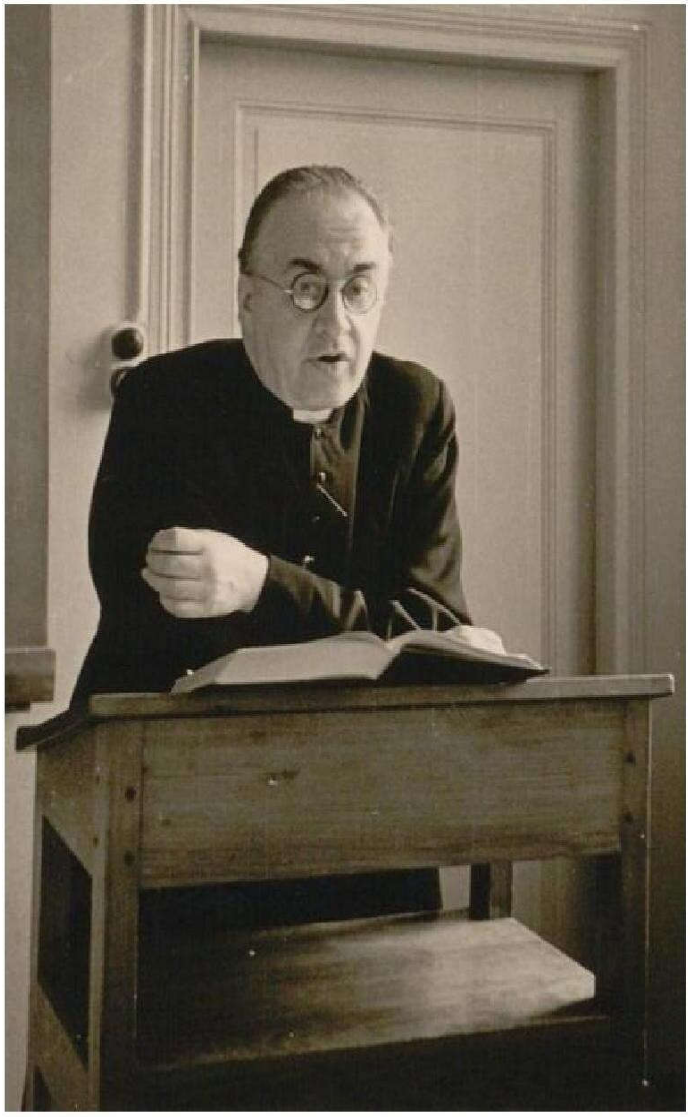

Figure 3. Abbé Georges Lemaitre who firstly discussed observational features of an Universe expansion and introduced a hot Universe model which was later called Big Bang.

In 1933 at Caltech after the Lemaitre's lecture A. Einstein said: "This is the most beautiful and satisfactory explanation of creation to which I have ever listened". This Einstein's opinion was widely distributed through mass media. These circumstances had a negative impact on the development of cosmological studies in USSR for around forty years.

In 1940s G. Gamow proposed the hot Universe model, calculated primary nucleosynthesis and predicted an existence of CMB radiation. Gamow was the youngest corresponding member of Soviet Academy of Sciences (from 1932 to 1938, restored posthumously in 1990).

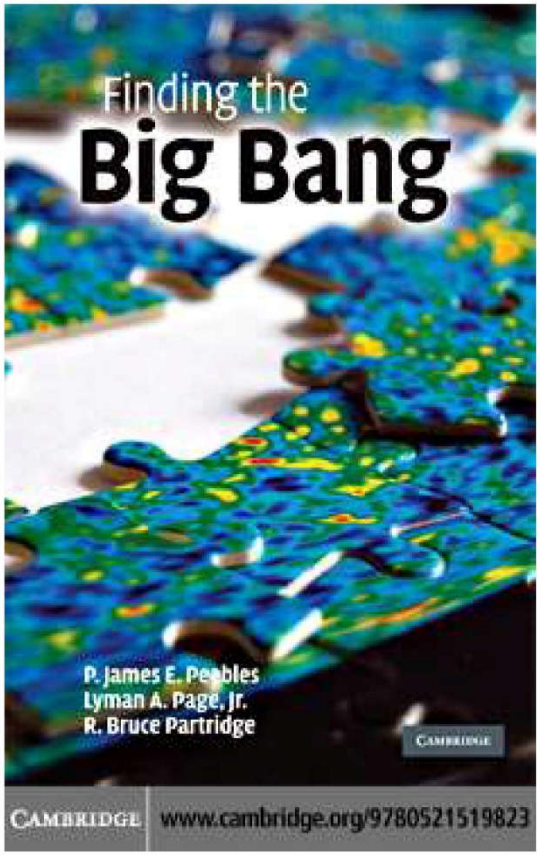
Finding the
Big Bang
P. James E. Peebles
Lyman A. Page, Jr.
R. Bruce Partridge
CAMBRIDGE
CAMBRIDGE
www.cambridge.org/9780521519823

Shmaonov described how, in the middle of the 1950s, he had been doing postgraduate research in the group of the well-known Soviet radio astronomers S. Khaikin and N. Kaidanovsky: he was measuring radio waves coming from space at a wavelength of 3.2 cm. Measurements were done with a horn antenna similar to that used many years later by Penzias and Wilson. Shmaonov carefully studied possible sources of noise. Of course, his instrument could not have been as sensitive as those with which the American astronomers worked in the 1960s. Results obtained by Shmaonov were reported in 1957 in his PhD Thesis and published in a paper (Shmaonov 1957) in the Soviet journal *Pribory i Tekhnika Eksperimenta* (*Instruments and Experimental Methods*)*. The conclusion of the measurements was: "The absolute effective temperature of radiation background ... appears to be 4 ± 3 K." Shmaonov emphasized the independence of the intensity of radiation on direction and time."

*Shmaonov, T., 1957, Method of absolute measurements of the effective temperature of radio emission with a low equivalent temperature [Методика абсолютных измерений эффективной температуры радиоизлучения с низкой эквивалентной температурой], *Pribori i Tekhnika Experimenta* (in Russia), 1, 83

Figure 4. Naum Lvovich Kaidanosky (left) and Semion Emmanuilovich Khaikin (right) who supervised T. A. Shmaonov at the Pulkovo Observatory in 1950s.

Shmaonov in 1957 in Pulkovo

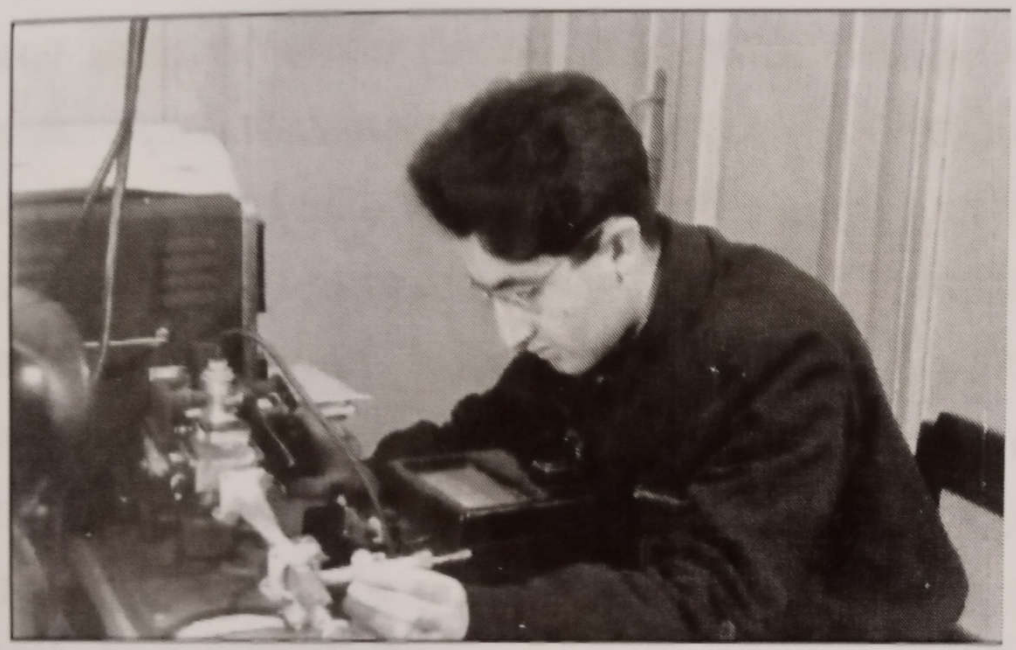

Аспирант Т. А. Шмаонов в лаборатории Главной астрономической обсерватории (1954 г.)

Радиотелескоп ГАО, на котором работал Т. А. Шмаонов

Figure 5. Tigran Aramovich Shmaonov presents his talk about his discovery of CMB in 1957. The talk was delivered in the Institute for History of Natural Sciences and Technology in Moscow on 17 April 2017.

A typical version for an ignorance of Shmaonov's discovery

No one knew an astronomical sense of his discovery in 1950s (including S. E. Khaikin)

However, we have to keep in mind that dynamical models of Universe (Friedmann, Lemaitre, Gamow..) were banned due to Soviet Philosophy opinion on evolution of the Universe until June 1963 when this ban was lifted. In June 1963 Soviet Academy of Sciences changed its point of view on allowed models for the Universe evolution since it celebrated 75th anniversary since the Friedmann's birthday. Therefore, we celebrate 60 years of Russian physical cosmology.

P. L. Kapitsa (1962, 1963) and Ya. B. Zeldovich (1963) played a great role to remove the ban on dynamical models for the Universe

Pre-history of Black holes

- J. Michell, published 1 January 1784, v. 74 (1784) Phil. Trans. R. Soc. – dark star concept
- GRG-0, Bern (1955), Pauli, Fock, Alexandrov
- GRG-1 (1957, Chapel Hill, NC, USA), Feynman, Bondi, Weber, Wheeler, De Witt, Bergmann --The start of GWs race
- GRG-3 (1962, Warsaw, Jablonna, Poland)
- The First Texas Symposium (1963) – R. Kerr, A. Papapetrou, T. Gold

- P. Bergman (GRG1, 1957): “Now to the problems that are more concerned with the special question, where things having physical or model significance are tried out. The most important of these questions which must be settled is, are there gravitational waves? At the present there is no general agreement. The other things to be mentioned are interesting but are of less crucial significance.”

The authors of theoretical foundations for the models of compact stars (E. Fermi and P. A. M. Dirac)

The first applications of fermi-statistics for white dwarfs (R. H. Fowler (1926) and Ya. I. Frenkel (1928))

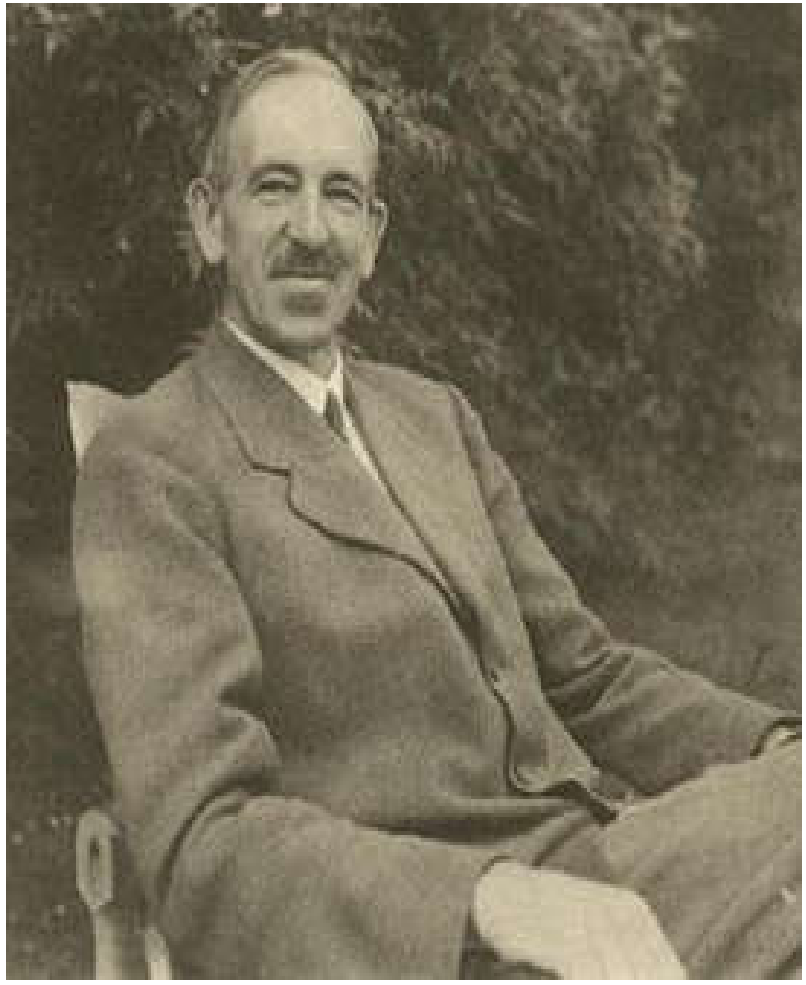

The first evaluations of mass limit for WDs (1929—1934): E. Stoner & S. Chandrasekhar (V. A. Ambarzumyan' proposal)

The first evaluations of mass limit for NSs (J. R. Oppenheimer & G. Volkoff, 1939)

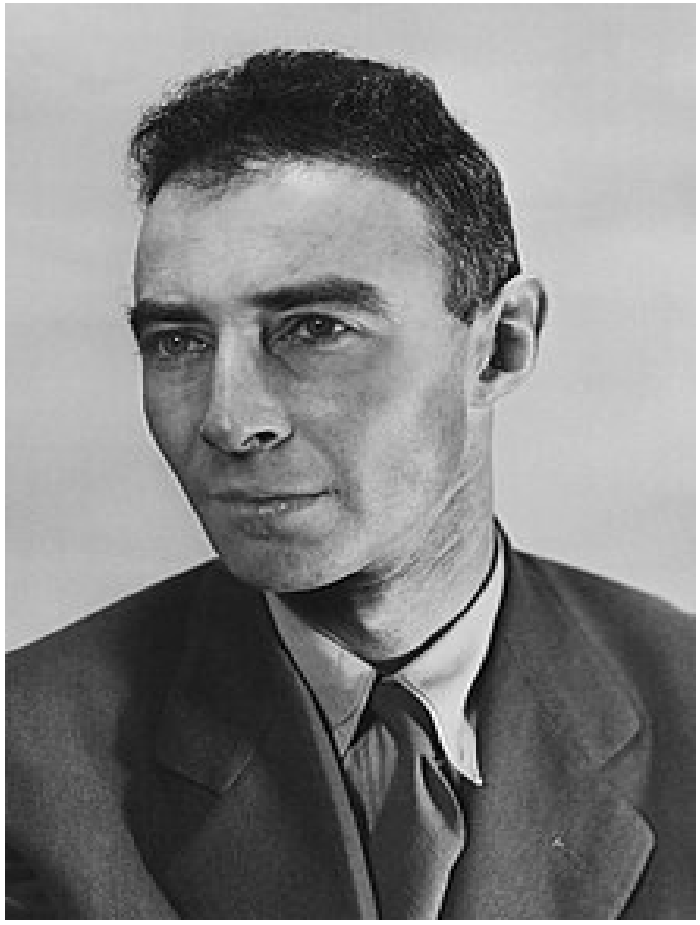

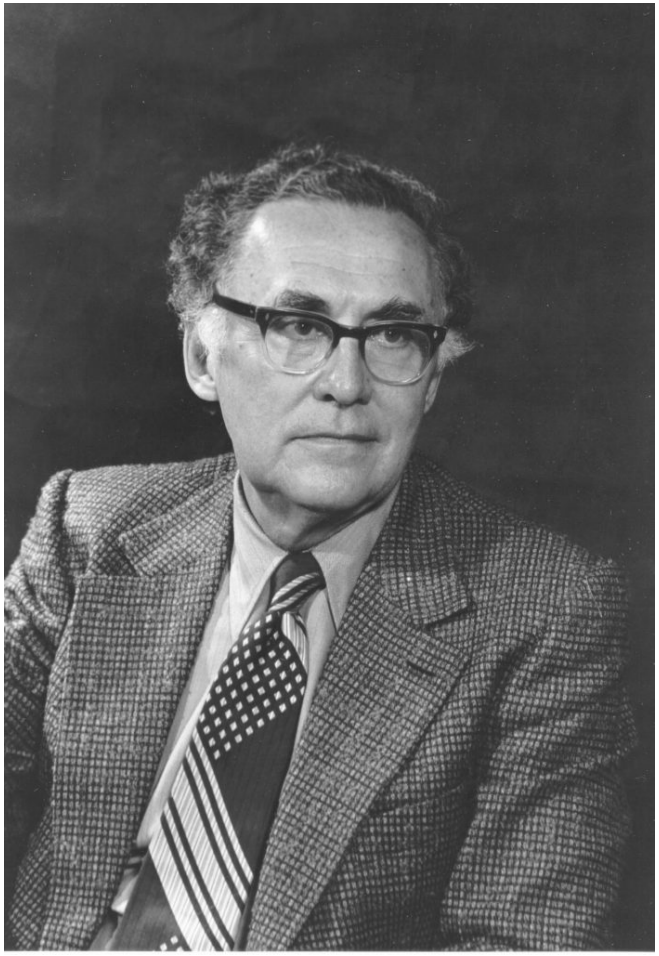

Neutron and NS's

J. Chadwick, Possible existence of neutron, Nature, 129(3252), p. 312 (1932).

W. Baade and F. Zwicky, Remarks on Supernovae and Cosmic Rays, Proc. Nat. Acad. Sc. May (1934) "We have tentatively suggest that the supernova represents the transition of an ordinary star."

K. Thorne about the First Texas Symposium: “ The astronomers and astrophysicists had come to Dallas to discuss quasars; they were not at all interested in Kerr's esoteric mathematical topic. So, as Kerr got up to speak, many slipped out of the lecture hall and into the foyer to argue with each other about their favorite theories of quasars. Others, less polite, remained seated in the hall and argued in whispers. Many of the rest catnapped in a fruitless effort to remedy their sleep deficits from late-night science. Only a handful of relativists listened, with rapt attention.
This was more than Achilles Papapetrou, one of the world's leading relativists, could stand. As Kerr finished Papapetrou demanded the floor, stood up, and with deep feeling explained the importance of Kerr's feat. He, Papapetrou, had been trying for thirty years to find such a solution of Einstein's equation, and had failed, as had many other relativists. The astronomers and astrophysicists nodded politely, and then, as the next speaker began to hold forth on a theory of quasars, they refocused their attention, and the meeting picked up pace.”

- T. Gold (1963) : “[The mystery of the quasars] allows one to suggest that the relativists with their sophisticated work are not only magnificent cultural ornaments but might actually be useful to science! Everyone is pleased: the relativists who feel they are being appreciated and are experts in a field they hardly knew existed, the astrophysicists for having enlarged their domain, their empire, by the annexation of another subject general relativity. It is all very pleasing, so let us all hope that it is right. What a shame it would be if we had to go and dismiss all the relativists again.”

Franco Pacini & Thomas Gold: Pulsars are NSs!

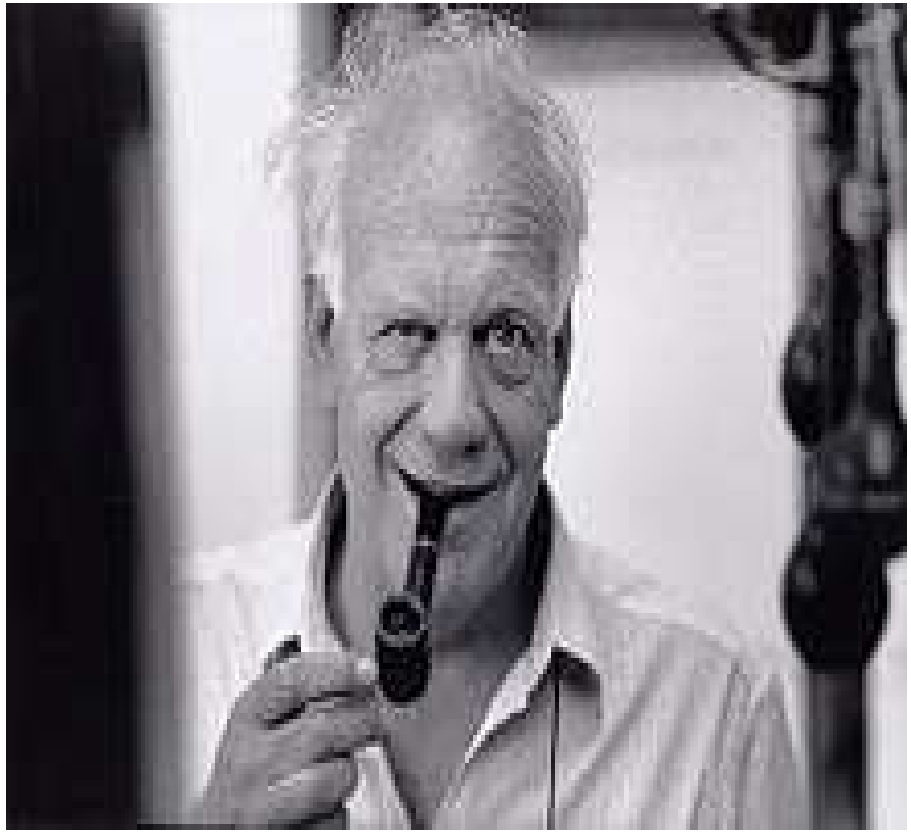

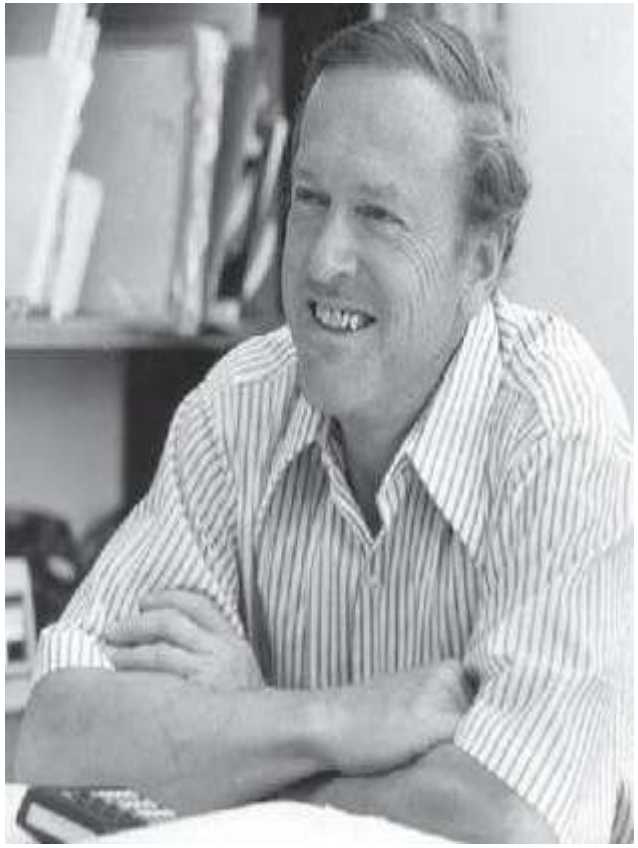

J. A. Wheeler :

In the fall of 1967, Vittorio Canuto, administrative head of NASA's Goddard Institute for Space Studies, invited me to a conference to consider possible interpretations of the exciting new evidence just arriving from England on pulsars. What were these pulsars? Vibrating white dwarfs? Rotating neutron stars? What? In my talk, I argued that we should consider the possibility that at the center of a pulsar is a gravitationally completely collapsed object. I remarked that one couldn't keep saying "gravitationally completely collapsed object" over and over. One needed a shorter descriptive phrase. "How about black hole?" asked someone in the audience. (As it turned out, a pulsar is powered by "merely" a neutron star, not a black hole.) Several years later, Feynman called my language unfit for polite company when I tried to summarize the remarkable simplicity of a black hole by saying, "A black hole has no hair." … The black hole, it has turned out, shows only three characteristics to the outside world: Its mass, its electric charge , and its angular momentum, or spin.

- "The extent to which the Chinese records of guest stars remain of living interest to current astronomical research may be seen in the field of radio-astronomy, where during the past few years great additions to knowledge have been made. The rapid upsurge of this new and powerful method of study of the birth and death of stars....makes urgently necessary the reduction of the information contained in the ancient and medieval Chinese texts to a form utilizable by modern astronomers in all lands. For this purpose, however, collaboration between competent sinologists and practical astronomers and radio astronomers is indispensable."
  Joseph Needham, F.R.S. - distinguished historian
  of Chinese Science (1959) in Vol. III. *Mathematics and the Sciences of the Heavens and Earth*

- “The investigation of the remnants of supernovae and their relation to historical records, both written and unwritten, will be one of the most fascinating tasks awaiting the next generation of astronomers…”
  Fritz Zwicky (1965)

Crab nebula (remnant of SN AD1054) in different bands

The 3rd Earl of Rosse (William Parsons), the President of RS (1848—1854), a member of St. Peterburg's Academy of Sciences since 1853.

Leviathan of Parsonstown (1.83 m telescope) started in 1845

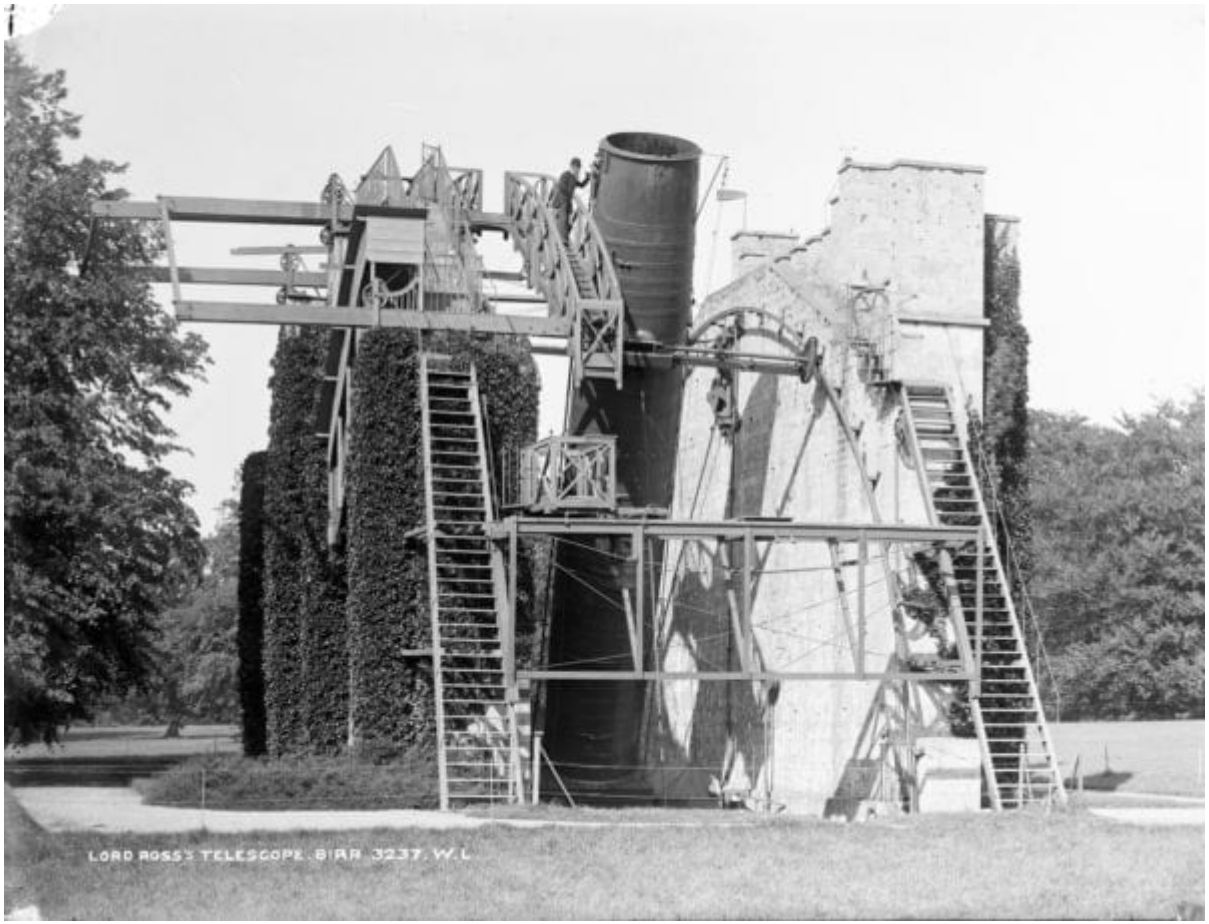

J. A. Wheeler: in “Our Universe: the known and unknown”: “Take up the telescope and turn it on the Grab Nebula. There was no Crab Nebula a thousand years ago. At that time astronomy was at a low level in Europe. Not so in China. There astronomers regularly swept the skies and recorded their observations. In July 1054 they reported a new star. It grew in brightness from day to day. In a few days it out shone every star in the firmament. Then it sank in brilliance, falling off in intensity from week to week. At each date the nova, or supernova as we more appropriately call it, could be compared with neighbor stars for brightness. Out of these comparisons by our Chinese colleagues of long ago one has today constructed a light curve. “

The identification of old Chinese records with Crab Nebula has been done by J. J. L. Duyvendak (1942). In 1054-1056 the Crab Nebula was observed for 21 months (many Chinese records)

NS's were discovered as pulsars

A. Hewish, S. J. Bell, J. D. H. Pilkington, P. F. Scott, R. A. Collins,
Observation of a Rapidly Pulsating Radio Source, Nature, 217, p. 709 (1968).
NJT (2021): "She Changed Astronomy Forever. He Won the Nobel Prize For It."

The Crab nebula was identified with a radio source in 1963 and as a X-ray source in 1964 and as a pulsar in 1968.

These Chinese observations helped to confirm observationally the Baade – Zwicky hypothesis that neutron stars could be formed in supernova explosions.

Conclusions from Wheeler's statements: First, sometimes, a time distance between an action and a result may be centuries (or even Millennium) and at this period one could think that the action was useless but it is not. Second a scientific knowledge is a result of activity of skilful people working in different areas.

The Astrophysical Journal, 757:55 (13pp), 2012 September 20 doi:10.1088/0004-637X/757/1/55

ON THE MASS DISTRIBUTION AND BIRTH MASSES OF NEUTRON STARS

Feryal Özel[1], Dimitrios Psaltis[1], Ramesh Narayan[2], and Antonio Santos Villarreal[1]
[1] Department of Astronomy, University of Arizona, 933 North Cherry Avenue, Tucson, AZ 85721, USA
[2] Harvard-Smithsonian Center for Astrophysics, 60 Garden Street, Cambridge, MA 02138,USA
Received 2011 December 26; accepted 2012 July 12; published 2012 September 5

ABSTRACT

We investigate the distribution of neutron star masses in different populations of binaries, employing Bayesian statistical techniques. In particular, we explore the differences in neutron star masses between sources that have experienced distinct evolutionary paths and accretion episodes. We find that the distribution of neutron star masses in non-recycled eclipsing high-mass binaries as well as of slow pulsars, which are all believed to be near their birth masses, has a mean of 1.28 $M_\odot$ and a dispersion of 0.24 $M_\odot$. These values are consistent with expectations for neutron star formation in core-collapse supernovae. On the other hand, double neutron stars, which are also believed to be near their birth masses, have a much narrower mass distribution, peaking at 1.33 $M_\odot$, but with a dispersion of only 0.05 $M_\odot$. Such a small dispersion cannot easily be understood and perhaps points to a particular and rare formation channel. The mass distribution of neutron stars that have been recycled has a mean of 1.48 $M_\odot$ and a dispersion of 0.2 $M_\odot$, consistent with the expectation that they have experienced extended mass accretion episodes. The fact that only a very small fraction of recycled neutron stars in the inferred distribution have masses that exceed $\sim$2 $M_\odot$ suggests that only a few of these neutron stars cross the mass threshold to form low-mass black holes.

Key words: black hole physics – pulsars: general – stars: neutron – X-rays: binaries

Online-only material: color figures

1. INTRODUCTION

The mass distribution of neutron stars contains information about the supernova explosion mechanisms, the equation of state of neutron star matter, and the accretion history of each neutron star since its formation. Certain populations of neutron stars such as those in double neutron stars and in binaries with high-mass companions are thought to have experienced little-to-no accretion over their lifetimes. In contrast, neutron stars in low-mass X-ray binaries and fast pulsars, which are typically in close orbits around white dwarfs, undergo extended accretion periods that are likely to move the neutron star mass away from its birth value.

The neutron star mass measurements that were available a decade ago allowed a statistical inference of the mass distribution of double neutron stars (Finn 1994) or of pulsars in binaries, without distinguishing between subgroups (Thorsett & Chakrabarty 1999). Finn (1994) found that neutron star masses fall predominantly in the 1.3–1.6 $M_\odot$ range. Thorsett & Chakrabarty (1999) found that the mass distribution for the combined population is consistent with a narrow Gaussian at $1.35 \pm 0.04\,M_\odot$. More recently, Schwab et al. (2010) argued that the distribution of neutron star masses in double neutron stars is actually bimodal, with one peak centered at $\sim$1.25 $M_\odot$ and the other at $\sim$1.35 $M_\odot$, which they attributed to different supernova explosion mechanisms. Kiziltan et al. (2010), Valentim et al. (2011), and Zhang et al. (2011), on the other hand, inferred the mass distribution of different neutron star subgroups based either on the pulsar spin period or the binary companion, both of which were taken to be indicative of the accretion history of the system. All groups found that the neutron stars that are thought to have undergone significant accretion are, on average, 0.2–0.3 $M_\odot$ heavier than those that have not.

One result that is common to all of these studies is the narrowness of the mass distribution of double neutron stars, $\sigma \simeq 0.05\,M_\odot$, which has been taken as indicative of the birth mass distribution of all neutron stars. The mean of the distribution is at 1.35 $M_\odot$, which is significantly larger than the mass of the pre-supernova iron core for neutron stars that form through the core-collapse mechanism. The Chandrasekhar mass for cores with electron fractions in the range $Y_e = 0.42$–0.48 is 1.15–1.34 $M_\odot$. Electrostatic interactions and entropy of the core introduce additional corrections to the pre-collapse mass (see Timmes et al. 1996 for a discussion). Taking into account the binding energy of the neutron star results in gravitational masses for the collapsed cores in the range 1.06–1.22 $M_\odot$. Even the largest of these masses is well below the mean of the observed distribution of double neutron stars. Fallback of stellar matter onto the collapsing core during the supernova explosion allows for the remnant to increase. However, this is also expected to increase the dispersion of masses by a comparable amount (see Zhang et al. 2008), which is inconsistent with the narrowness of the inferred mass distribution of double neutron star masses.

Considering a bimodal underlying distribution in the population of double neutron stars, as in Schwab et al. (2010), makes the width of each distribution even narrower: 0.008 $M_\odot$ and 0.025 $M_\odot$ for the two components. For the lower mass component centered around $\sim$1.25 $M_\odot$, such a narrow distribution may be reasonably obtained through an electron capture supernova, the onset of which occurs at a particular mass threshold of an ONeMg white dwarf (Podsiadlowski et al. 2005). However, the second component, which is centered at 1.35 $M_\odot$ cannot be explained as a result of the electron capture supernovae and poses the same challenge in its narrowness when explained via the core-collapse mechanism.

In order to model the distribution of neutron star masses both at their births and throughout their lives, one important question to address is whether double neutron stars are a representative sample for neutron stars at their birth masses. In this paper, we address this question by identifying a different population of neutron stars at or near their birth masses and compare the inferred mass distribution with that of double neutron stars.

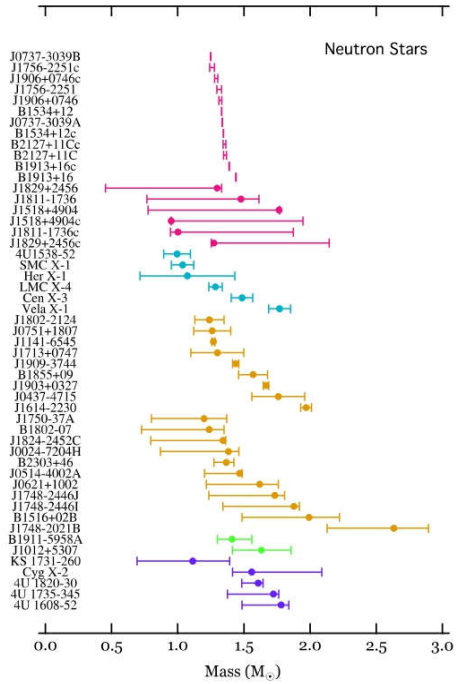

Figure 13. Masses of neutron stars measured in double neutron stars (magenta; categories Ia and IIa), in eclipsing binaries with primarily high-mass companions (cyan; category IV; these are the numerical values from Rawls et al. 2011 given in Column 2 of Table 6), with white dwarf companions (gold; categories Ib and IIb), with optical observations of the white dwarf companions (green; category III), and in accreting bursters (purple; category V).

(A color version of this figure is available in the online journal.)

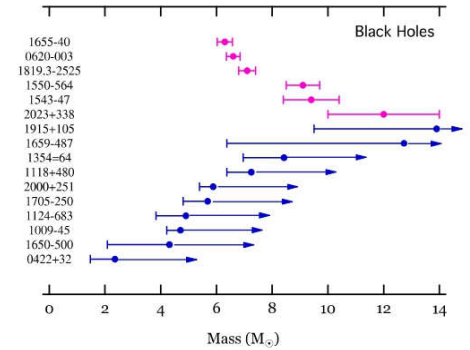

Figure 14. Measured masses of Galactic black holes (after Özel et al. 2010a).

(A color version of this figure is available in the online journal.)

the most likely mean value and the dispersion are $1.46\,M_\odot$ and $0.21\,M_\odot$, respectively. We, therefore, attribute the small difference with the Kiziltan et al. (2010) results to our handling of the posterior likelihood distributions for each measurement.

4. DISCUSSION

In this paper, we investigated the distribution of neutron star masses in different types of binary systems and at different stages of evolution based on currently available measurements. We summarize the neutron star mass measurements and their uncertainties in each subgroup in Figure 13 and compare them to those of black holes in Figure 14 (compiled and analyzed in Özel et al. 2010a). In these figures, the error bars correspond to a 68% confidence level calculated from the detailed likelihood distribution presented for each subgroup of sources in Section 2.

In the top panel of Figure 15, we show the inferred mass distributions of the various neutron star populations discussed in Section 2. For each population, we present two different distributions. The dashed lines correspond to the most likely parameters of the underlying distributions inferred in Section 3. Each solid line represents the weighted distribution over the central mass and dispersion for each population. We compute this weighted distribution as

$$P_w(M_{\rm NS}) = \int dM_0 \int d\sigma\, P(M_{\rm NS}; M_0, \sigma) P(M_0, \sigma|{\rm data}), \tag{27}$$

where $P(M_{\rm NS}; M_0, \sigma)$ and $P(M_0, \sigma|{\rm data})$ are given by Equations (20) and (21), respectively. In the Appendix, we provide approximate analytic fitting formulae for these weighted distributions for each population.

In the bottom panel of Figure 15, we compare the inferred mass distribution for recycled neutron stars to that of black holes reported in Özel et al. (2010a). For the latter, we use the exponential model with a lower mass cutoff given by

$$P(M_{\rm BH}; M_{\rm scale}, M_{\rm c}) = \frac{\exp(M_{\rm c}/M_{\rm scale})}{M_{\rm scale}} \times \begin{cases} \exp(-M_{\rm BH}/M_{\rm scale}), & M_{\rm BH} > M_{\rm c} \\ 0, & M_{\rm BH} \leqslant M_{\rm c} \end{cases}. \tag{28}$$

The most likely values for the parameters of this distribution are $M_{\rm scale} = 1.61\,M_\odot$ and $M_{\rm c} = 6.32\,M_\odot$. In the same panel, we also include the appropriate weighted distribution for the black holes, where we carried out the integration over the posterior likelihood of the parameters $M_{\rm scale}$ and $M_{\rm c}$; we provide an analytic fitting formula for the weighted distribution in the Appendix. This panel highlights the substantial mass gap that exists between the black hole population and even the heaviest neutron star population (see the discussion in Özel et al. 2010a and Farr et al. 2011).

Within the neutron star population, it is evident from these figures that the mass distribution of double neutron star systems is different than those observed in other binary systems, which include both neutron stars near their birth masses as well as neutron stars that experienced significant accretion episodes. Indeed, the most likely values of the mean mass and the dispersion we derived for these populations using the Bayesian inference technique discussed in Section 3 are $1.33 \pm 0.05\,M_\odot$ for double neutron stars, in contrast to $1.28 \pm 0.24\,M_\odot$ for other neutron stars near their birth masses, and $1.48 \pm 0.20\,M_\odot$ for recycled neutron stars. Note that the uncertainties in both the

FAIR, Facility for Antiproton and Ion Research (Darmstadt, Germany) and Nuclotron Based Facility (NICA, Dubna, Russia)

- How does the strong force, which binds the particles comprising atomic nuclei work - and where do their masses come from?
- How does matter behave across the wide range of temperatures and pressures found in the past and present Universe?
- How did matter in the early Universe evolve and why does it look the way it does today?
- Where do the atomic elements come from?
- How does the electromagnetic force, which binds atoms and molecules, work under extreme conditions?
- The search for signs of the phase transition between hadronic matter and QGP;
- Search for new phases of baryonic matter Study of basic properties of the strong interaction vacuum and QCD symmetries

- **The Universe in Laboratory**

Pulsars and GWs

Mikhail Sazhin
(1951—2023)

Opportunities for detecting ultralong gravitational waves

M. V. Sazhin

Shternberg Astronomical Institute, Moscow

(Submitted June 14, 1977)
Astron. Zh. **55**, 65–68 (January–February 1978)

The influence of ultralong gravitational waves on the propagation of electromagnetic pulses is examined. Conditions are set forth whereby it might be possible to detect gravitational waves arriving from binary stars. There are some prospects for detecting gravitational radiation from double superstars with masses $\mathfrak{M}_1 \approx \mathfrak{M}_2 \approx 10^{10}\,\mathfrak{M}_\odot$.

PACS numbers: 97.80.—d, 97.60.Gb, 95.30.Gv

Several methods have been proposed for detecting ultralong gravitational waves.[1] One possible technique would involve recording the change in the frequency of electromagnetic radiation in the gravitational wave field.[2] For pulses of electromagnetic radiation, this effect would be manifested as a change in the period between pulses. The time required for a pulse of electromagnetic radiation moving in a gravitational wave field to cover the path from the transmitter to the receiver will depend on the amplitude and the phase of the gravitational waves. If the pulses are radiated by the transmitter at equal time intervals Δ, the receiver will record them at time intervals $\Delta + \delta(t)$. The quantity $\delta(t)$ describes the shift in the pulses with respect to time.

Let us apply the geometrical optics approximation to find the change $\delta(t)$ in the interpulse period. Light rays move along trajectories for which ds = 0. We orient the coordinate system such that photons will travel along the x axis when gravitational waves are absent. The equation of motion will then have the form c dt = dx. If gravitational radiation comes into play, this equation will become

$$c\,dt = \left[1 + \frac{1}{2}h(t,x)\right]dx,$$

where h(t, x) represents the corrections to the metric. Pulses radiated at different instants t_1, t_2 will traverse equal distances dx in different elapsed times:

$$c\,d\delta t = \frac{1}{2}[h(t_1,x) - h(t_2,x)]\,dx. \qquad (1)$$

The principal time shift between two pulses will build up while they traverse a distance L comparable to the wavelength. If L should be shorter than the wavelength, then $\delta(t) \approx h(t)\Delta \cdot L/\lambda$. If $L \gg \lambda$, then $\delta(t) \approx h(t)\Delta$, and the amplitude of the shift during the half-period of the gravitational waves will be $\theta \approx h\tau$, to order of magnitude.

We shall apply the theory outlined above to the pulse propagation scheme illustrated in Fig. 1. Suppose that the line joining the source of the electromagnetic pulses and the observer lies in the orbit plane of a binary star. Then the wave corrections to the metric will be

$$h(t,x) = -\frac{\alpha}{2}\frac{a^4 - a^2x^2}{(a^2+x^2)^{7/2}}\cos 2\omega\left(t - \frac{\sqrt{x^2+a^2}}{c}\right), \qquad (2)$$

where $\tau = 2\pi/\omega$ is the period of the binary star, a is the distance from the center of the binary system to the trajectory of the light rays, the coordinate x is measured along this trajectory from the point A (Fig. 1), and $\alpha = 6\pi^{2/3}ct_g^{5/3}\tau^{2/3}$. Here $t_g = (2G/c^3)(M_1M_2)^{3/5}/(M_1+M_2)^{1/3}$; M_1 and M_2 are the masses of the two stars.

Substituting the expression (2) into Eq. (1) and integrating, we find that the interpulse period will change by

$$\delta(t) = \frac{\pi\alpha}{c}\frac{\Delta}{\tau}\int_{-b}^{s} dx\,\frac{a^4 - a^2x^2}{(a^2+x^2)^{7/2}}\sin\left[2\omega t + 2\frac{\omega}{c}(x - \sqrt{x^2+a^2})\right],$$

where b is the distance from the source of the electromagnetic pulses to the point A (Fig. 1) and s is the distance from A to the observer. If the binary star is situated close to the path of the light ray, with $a^2 \ll c\tau b$ but $c\tau < a$, then after an elapsed time $\tau/4$ the shift will amount to

$$\theta = c^2 t_g^{5/4}\tau^{1/4}/a^2. \qquad (3)$$

However, if the binary star is far from the light ray, with $c\tau b^3 \ll a^4$ but $a < b$, then

$$\theta = ct_g^{5/4}\tau^{1/4}(a/b)^3/4a, \qquad (4)$$

while if $a \gg b$,

$$\theta = ct_g^{5/4}\tau^{1/4}/4a. \qquad (5)$$

One of the most appealing prospects in the search for ultralong gravitational waves would be to monitor the radiation of pulsars. The high stability of pulsar periods would give the method the requisite sensitivity. Compared to the use of drift-free satellites, pulsars would have two major advantages for detection of such signals: 1) The pulses will traverse a path $L \gg \lambda$, and the equation for

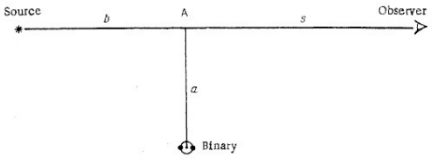

FIG. 1. Relative arrangement of the source of electromagnetic pulses, the observer, and the binary star.

 0038-5301/78/2201-035 $02.70

The Astrophysical Journal Letters, 951:L8 (24pp), 2023 July 1 https://doi.org/10.3847/2041-8213/acdac6

The NANOGrav 15 yr Data Set: Evidence for a Gravitational-wave Background

Gabriella Agazie[1], Akash Anumarlapudi[1], Anne M. Archibald[2], Zaven Arzoumanian[3], Paul T. Baker[4], Bence Bécsy[5], Laura Blecha[6], Adam Brazier[7,8], Paul R. Brook[9], Sarah Burke-Spolaor[10,11], Rand Burnette[5], Robin Case[5], Maria Charisi[12], Shami Chatterjee[7], Katerina Chatziioannou[13], Belinda D. Cheeseboro[10,11], Siyuan Chen[14], Tyler Cohen[15], James M. Cordes[7], Neil J. Cornish[16], Fronefield Crawford[17], H. Thankful Cromartie[7,70], Kathryn Crowter[18], Curt J. Cutler[13,19], Megan E. DeCesar[20], Dallas DeGan[5], Paul B. Demorest[21], Heling Deng[5], Timothy Dolch[22,23], Brendan Drachler[24,25], Justin A. Ellis[26], Elizabeth C. Ferrara[27,28,29], William Fiore[10,11], Emmanuel Fonseca[10,11], Gabriel E. Freedman[1], Nate Garver-Daniels[10,11], Peter A. Gentile[10,11], Kyle A. Gersbach[12], Joseph Glaser[10,11], Deborah C. Good[30,31], Kayhan Gültekin[32], Jeffrey S. Hazboun[5], Sophie Hourihane[13], Kristina Islo[1], Ross J. Jennings[10,11,73], Aaron D. Johnson[1,13], Megan L. Jones[1], Andrew R. Kaiser[10,11], David L. Kaplan[1], Luke Zoltan Kelley[33], Matthew Kerr[34], Joey S. Key[35], Tonia C. Klein[1], Nima Laal[5], Michael T. Lam[24,25], William G. Lamb[12], T. Joseph W. Lazio[19], Natalia Lewandowska[36], Tyson B. Littenberg[37], Tingting Liu[10,11], Andrea Lommen[38], Duncan R. Lorimer[10,11], Jing Luo[39,71], Ryan S. Lynch[40], Chung-Pei Ma[33,41], Dustin R. Madison[42], Margaret A. Mattson[10,11], Alexander McEwen[1], James W. McKee[43,44], Maura A. McLaughlin[10,11], Natasha McMann[12], Bradley W. Meyers[18,45], Patrick M. Meyers[13], Chiara M. F. Mingarelli[30,31,46], Andrea Mitridate[47], Priyamvada Natarajan[48,49], Cherry Ng[50], David J. Nice[51], Stella Koch Ocker[7], Ken D. Olum[52], Timothy T. Pennucci[53], Benetge B. P. Perera[54], Polina Petrov[12], Nihan S. Pol[12], Henri A. Radovan[55], Scott M. Ransom[56], Paul S. Ray[34], Joseph D. Romano[57], Shashwat C. Sardesai[1], Ann Schmiedekamp[58], Carl Schmiedekamp[58], Kai Schmitz[59], Levi Schult[12], Brent J. Shapiro-Albert[10,11,60], Xavier Siemens[1,5], Joseph Simon[61,72], Magdalena S. Siwek[62], Ingrid H. Stairs[18], Daniel R. Stinebring[63], Kevin Stovall[21], Jerry P. Sun[5], Abhimanyu Susobhanan[1], Joseph K. Swiggum[51,72], Jacob Taylor[5], Stephen R. Taylor[12], Jacob E. Turner[10,11], Caner Unal[64,65], Michele Vallisneri[13,19], Rutger van Haasteren[66], Sarah J. Vigeland[1], Haley M. Wahl[10,11], Qiaohong Wang[12], Caitlin A. Witt[67,68], and Olivia Young[24,25]
The NANOGrav Collaboration[69]

[1] Center for Gravitation, Cosmology and Astrophysics, Department of Physics, University of Wisconsin–Milwaukee, P.O. Box 413, Milwaukee, WI 53201, USA
[2] Newcastle University, NE1 7RU, UK
[3] X-Ray Astrophysics Laboratory, NASA Goddard Space Flight Center, Code 662, Greenbelt, MD 20771, USA
[4] Department of Physics and Astronomy, Widener University, One University Place, Chester, PA 19013, USA
[5] Department of Physics, Oregon State University, Corvallis, OR 97331, USA
[6] Physics Department, University of Florida, Gainesville, FL 32611, USA
[7] Cornell Center for Astrophysics and Planetary Science and Department of Astronomy, Cornell University, Ithaca, NY 14853, USA
[8] Cornell Center for Advanced Computing, Cornell University, Ithaca, NY 14853, USA
[9] Institute for Gravitational Wave Astronomy and School of Physics and Astronomy, University of Birmingham, Edgbaston, Birmingham B15 2TT, UK
[10] Department of Physics and Astronomy, West Virginia University, P.O. Box 6315, Morgantown, WV 26506, USA
[11] Center for Gravitational Waves and Cosmology, West Virginia University, Chestnut Ridge Research Building, Morgantown, WV 26505, USA
[12] Department of Physics and Astronomy, Vanderbilt University, 2301 Vanderbilt Place, Nashville, TN 37235, USA
[13] Division of Physics, Mathematics, and Astronomy, California Institute of Technology, Pasadena, CA 91125, USA
[14] Kavli Institute for Astronomy and Astrophysics, Peking University, Beijing, 100871, People's Republic of China
[15] Department of Physics, New Mexico Institute of Mining and Technology, 801 Leroy Place, Socorro, NM 87801, USA
[16] Department of Physics, Montana State University, Bozeman, MT 59717, USA
[17] Department of Physics and Astronomy, Franklin & Marshall College, P.O. Box 3003, Lancaster, PA 17604, USA
[18] Department of Physics and Astronomy, University of British Columbia, 6224 Agricultural Road, Vancouver, BC V6T 1Z1, Canada
[19] Jet Propulsion Laboratory, California Institute of Technology, 4800 Oak Grove Drive, Pasadena, CA 91109, USA
[20] George Mason University, resident at the Naval Research Laboratory, Washington, DC 20375, USA
[21] National Radio Astronomy Observatory, 1003 Lopezville Rd., Socorro, NM 87801, USA
[22] Department of Physics, Hillsdale College, 33 E. College Street, Hillsdale, MI 49242, USA
[23] Eureka Scientific, 2452 Delmer Street, Suite 100, Oakland, CA 94602-3017, USA
[24] School of Physics and Astronomy, Rochester Institute of Technology, Rochester, NY 14623, USA
[25] Laboratory for Multiwavelength Astrophysics, Rochester Institute of Technology, Rochester, NY 14623, USA
[26] Bionic Health, 800 Park Offices Drive, Research Triangle Park, NC 27709, USA
[27] Department of Astronomy, University of Maryland, College Park, MD 20742, USA
[28] Center for Research and Exploration in Space Science and Technology, NASA/GSFC, Greenbelt, MD 20771, USA
[29] NASA Goddard Space Flight Center, Greenbelt, MD 20771, USA
[30] Department of Physics, University of Connecticut, 196 Auditorium Road, U-3046, Storrs, CT 06269-3046, USA
[31] Center for Computational Astrophysics, Flatiron Institute, 162 5th Avenue, New York, NY 10010, USA
[32] Department of Astronomy and Astrophysics, University of Michigan, Ann Arbor, MI 48109, USA
[33] Department of Astronomy, University of California, Berkeley, 501 Campbell Hall #3411, Berkeley, CA 94720, USA
[34] Space Science Division, Naval Research Laboratory, Washington, DC 20375-5352, USA
[35] University of Washington Bothell, 18115 Campus Way NE, Bothell, WA 98011, USA
[36] Department of Physics, State University of New York at Oswego, Oswego, NY, 13126, USA
[37] NASA Marshall Space Flight Center, Huntsville, AL 35812, USA
[38] Department of Physics and Astronomy, Haverford College, Haverford, PA 19041, USA
[39] Department of Astronomy & Astrophysics, University of Toronto, 50 Saint George Street, Toronto, ON M5S 3H4, Canada

[40] Green Bank Observatory, P.O. Box 2, Green Bank, WV 24944, USA
[41] Department of Physics, University of California, Berkeley, CA 94720, USA
[42] Department of Physics, University of the Pacific, 3601 Pacific Avenue, Stockton, CA 95211, USA
[43] E.A. Milne Centre for Astrophysics, University of Hull, Cottingham Road, Kingston-upon-Hull, HU6 7RX, UK
[44] Centre of Excellence for Data Science, Artificial Intelligence and Modelling (DAIM), University of Hull, Cottingham Road, Kingston-upon-Hull, HU6 7RX, UK
[45] International Centre for Radio Astronomy Research, Curtin University, Bentley, WA 6102, Australia
[46] Department of Physics, Yale University, New Haven, CT 06520, USA
[47] Deutsches Elektronen-Synchrotron DESY, Notkestr. 85, D-22607 Hamburg, Germany
[48] Department of Astronomy, Yale University, 52 Hillhouse Ave., New Haven, CT 06511, USA
[49] Black Hole Initiative, Harvard University, 20 Garden Street, Cambridge, MA 02138, USA
[50] Dunlap Institute for Astronomy and Astrophysics, University of Toronto, 50 St. George St., Toronto, ON M5S 3H4, Canada
[51] Department of Physics, Lafayette College, Easton, PA 18042, USA
[52] Institute of Cosmology, Department of Physics and Astronomy, Tufts University, Medford, MA 02155, USA
[53] Institute of Physics and Astronomy, Eötvös Loránd University, Pázmány P.s. 1/A, 1117 Budapest, Hungary
[54] Arecibo Observatory, HC3 Box 53995, Arecibo, PR 00612, USA
[55] Department of Physics, University of Puerto Rico, Mayagüez, PR 00681, USA
[56] National Radio Astronomy Observatory, 520 Edgemont Road, Charlottesville, VA 22903, USA
[57] Department of Physics, Texas Tech University, Box 41051, Lubbock, TX 79409, USA
[58] Department of Physics, Penn State Abington, Abington, PA 19001, USA
[59] Institute for Theoretical Physics, University of Münster, D-48149 Münster, Germany
[60] Giant Army, 915A 17th Ave., Seattle WA 98122, USA
[61] Department of Astrophysical and Planetary Sciences, University of Colorado, Boulder, CO 80309, USA
[62] Center for Astrophysics, Harvard University, 60 Garden St., Cambridge, MA 02138, USA
[63] Department of Physics and Astronomy, Oberlin College, Oberlin, OH 44074, USA
[64] Department of Physics, Ben-Gurion University of the Negev, Be'er Sheva 84105, Israel
[65] Feza Gursey Institute, Bogazici University, Kandilli, 34684, Istanbul, Turkey
[66] Max-Planck-Institut für Gravitationsphysik (Albert-Einstein-Institut), Callinstrasse 38, D-30167, Hannover, Germany
[67] Center for Interdisciplinary Exploration and Research in Astrophysics (CIERA), Northwestern University, Evanston, IL 60208, USA
[68] Adler Planetarium, 1300 S. DuSable Lake Shore Dr., Chicago, IL 60605, USA
Received 2023 May 8; revised 2023 May 31; accepted 2023 June 1; published 2023 June 29

Abstract

We report multiple lines of evidence for a stochastic signal that is correlated among 67 pulsars from the 15 yr pulsar timing data set collected by the North American Nanohertz Observatory for Gravitational Waves. The correlations follow the Hellings–Downs pattern expected for a stochastic gravitational-wave background. The presence of such a gravitational-wave background with a power-law spectrum is favored over a model with only independent pulsar noises with a Bayes factor in excess of 10^{14}, and this same model is favored over an uncorrelated common power-law spectrum model with Bayes factors of 200–1000, depending on spectral modeling choices. We have built a statistical background distribution for the latter Bayes factors using a method that removes interpulsar correlations from our data set, finding $p = 10^{-3}$ ($\approx 3\sigma$) for the observed Bayes factors in the null no-correlation scenario. A frequentist test statistic built directly as a weighted sum of interpulsar correlations yields $p = 5 \times 10^{-5}$ to 1.9×10^{-4} ($\approx 3.5\sigma$–4σ). Assuming a fiducial $f^{-2/3}$ characteristic strain spectrum, as appropriate for an ensemble of binary supermassive black hole inspirals, the strain amplitude is $2.4^{+0.7}_{-0.6} \times 10^{-15}$ (median + 90% credible interval) at a reference frequency of 1 yr^{-1}. The inferred gravitational-wave background amplitude and spectrum are consistent with astrophysical expectations for a signal from a population of supermassive black hole binaries, although more exotic cosmological and astrophysical sources cannot be excluded. The observation of Hellings–Downs correlations points to the gravitational-wave origin of this signal.

Unified Astronomy Thesaurus concepts: Gravitational waves (678); Gravitational wave astronomy (675); Millisecond pulsars (1062); Radio pulsars (1353); Supermassive black holes (1663)

1. Introduction

Almost a century had to elapse between Einstein's prediction of gravitational waves (GWs; Einstein 1916) and their measurement from a coalescing binary of stellar-mass black holes (Abbott et al. 2016). However, their existence had been confirmed in the late 1970s through measurements of the orbital decay of the Hulse–Taylor binary pulsar (Hulse & Taylor 1975; Taylor et al. 1979). Today, pulsars are again at the forefront of the quest to detect GWs, this time from binary systems of central galactic black holes.

Black holes with masses of 10^5–$10^{10}\,M_\odot$ exist at the center of most galaxies and are closely correlated with the global properties of the host, suggesting a symbiotic evolution (Magorrian et al. 1998; McConnell & Ma 2013). Galaxy mergers are the main drivers of hierarchical structure formation over cosmic time (Blumenthal et al. 1984) and lead to the formation of close massive black hole binaries long after the mergers (Begelman et al. 1980; Milosavljević & Merritt 2003). The most massive of these (supermassive black hole binaries

[69] comments@nanograv.org.
[70] NASA Hubble Fellowship: Einstein Postdoctoral Fellow.
[71] Deceased.
[72] NSF Astronomy and Astrophysics Postdoctoral Fellow.
[73] NANOGrav Physics Frontiers Center Postdoctoral Fellow.

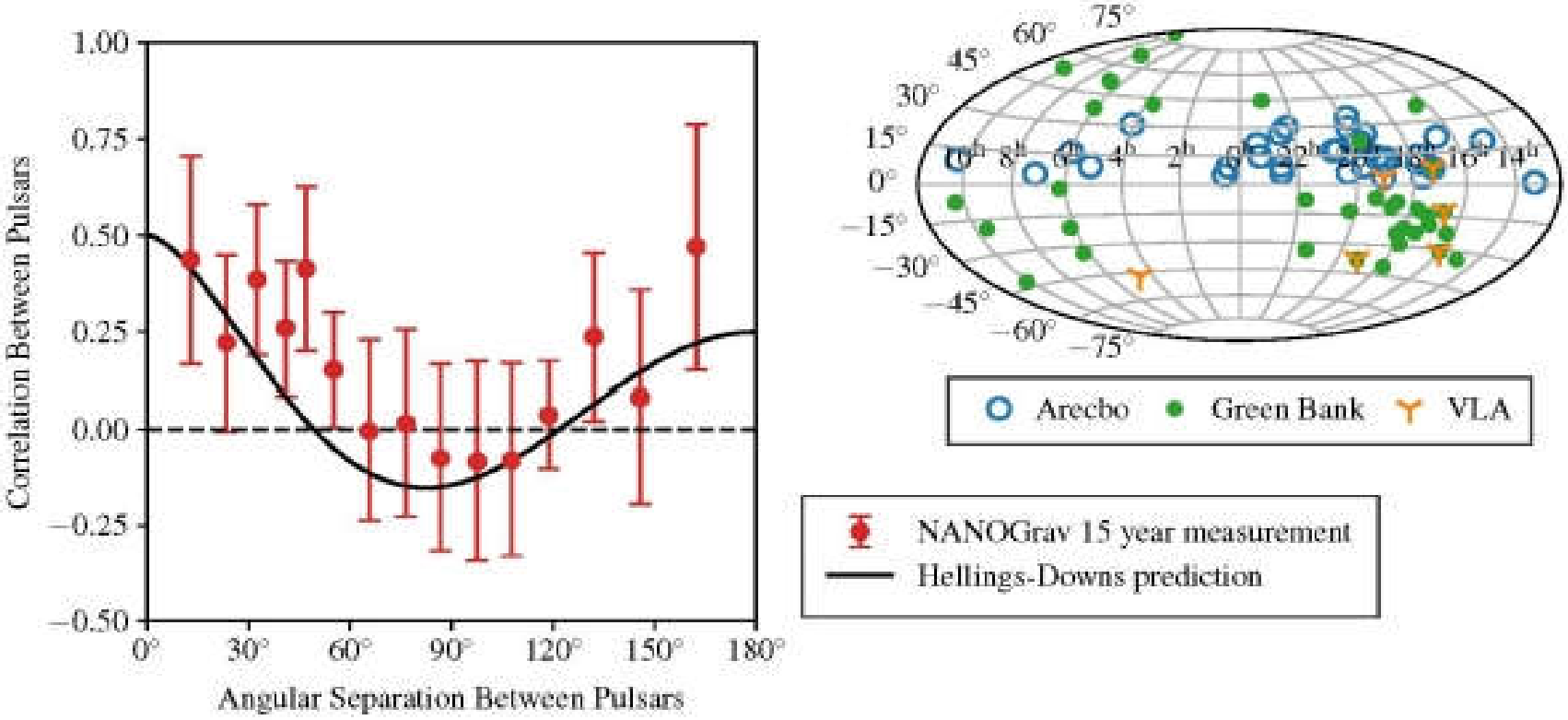
1.00
0.75
0.50
0.25
0.00
−0.25
−0.50
Correlation Between Pulsars
0°
30°
60°
90°
120°
150°
180°
Angular Separation Between Pulsars
75°
60°
45°
30°
15°
0°
−15°
−30°
−45°
−60°
−75°
Arecbo
Green Bank
VLA
NANOGrav 15 year measurement
Hellings-Downs prediction

Arzoumanian, Z., Baker, P. T., Blumer, H., et al. 2021, ApJL, 923, L22
Arzoumanian, Z., Baker, P. T., Brazier, A., et al. 2018, ApJ, 859, 47
Arzoumanian, Z., Brazier, A., Burke-Spolaor, S., et al. 2015, ApJ, 813, 65
Arzoumanian, Z., Brazier, A., Burke-Spolaor, S., et al. 2016, ApJ, 821, 13
Astropy Collaboration, Price-Whelan, A. M., Lim, A. M., et al. 2022, ApJ, 935, 167
Backer, D. C., Kulkarni, S. R., Heiles, C., Davis, M. M., & Goss, W. M. 1982, Natur, 300, 615
Bartolo, N., Bertacca, D., Caldwell, R., et al. 2022, JCAP, 2022, 009
Bécsy, B., Cornish, N. J., & Kelley, L. Z. 2022, ApJ, 941, 119
Begelman, M. C., Blandford, R. D., & Rees, M. J. 1980, Natur, 287, 307
Blumenthal, G. R., Faber, S. M., Primack, J. R., & Rees, M. J. 1984, Natur, 311, 517
Burke-Spolaor, S., Taylor, S. R., Charisi, M., et al. 2019, A&ARv, 27, 5
Caprini, C., & Figueroa, D. G. 2018, CQGra, 35, 163001
Carlin, B. P., & Chib, S. 1995, J. R. Stat. Soc. Series B Stat. Methodol., 57, 473
Chalumeau, A., Babak, S., Petiteau, A., et al. 2022, MNRAS, 509, 5538
Chamberlin, S. J., Creighton, J. D. E., Siemens, X., et al. 2015, PhRvD, 91, 044048
Chen, S., Caballero, R. N., Guo, Y. J., et al. 2021, MNRAS, 508, 4970
Cordes, J. M. 2013, CQGra, 30, 224002
Cornish, N. J., & Littenberg, T. B. 2015, CQGra, 32, 135012
Cornish, N. J., & Sampson, L. 2016, PhRvD, 93, 104047
Cornish, N. J., & Sesana, A. 2013, CQGra, 30, 224005
Demorest, P. B. 2007, PhD thesis, Univ. California, Berkeley
Demorest, P. B., Ferdman, R. D., Gonzalez, M. E., et al. 2013, ApJ, 762, 94
Desvignes, G., Caballero, R. N., Lentati, L., et al. 2016, MNRAS, 458, 3341
Detweiler, S. 1979, ApJ, 234, 1100
Dickey, J. M. 1971, Ann. Math. Stat., 42, 204
Domènech, G. 2021, Univ, 7, 398
DuPlain, R., Ransom, S., Demorest, P., et al. 2008, Proc. SPIE, 7019, 70191D
Einstein, A. 1916, Sitzungsber. Preuss. Akad. Wiss. Berlin (Math. Phys.), 1916, 1
Ellis, J., & van Haasteren, R. 2017, jellis18/PTMCMCSampler: Official Release v1.0.0 Zenodo, doi:10.5281/zenodo.1037579
Ellis, J. A., Vallisneri, M., Taylor, S. R., & Baker, P. T. 2019, ENTERPRISE: Enhanced Numerical Toolbox Enabling a Robust PulsaR Inference SuitE, Astrophysics Source Code Library, ascl:1912.015
Enoki, M., & Nagashima, M. 2007, PThPh, 117, 241
Estabrook, F. B., & Wahlquist, H. D. 1975, GReGr, 6, 439
Ford, J. M., Demorest, P., & Ransom, S. 2010, Proc. SPIE, 7740, 77400A
Foster, R. S., & Backer, D. C. 1990, ApJ, 361, 300
Gair, J., Romano, J. D., Taylor, S., & Mingarelli, C. M. F. 2014, PhRvD, 90, 082001
Gelman, A., Carlin, J., Stern, H., et al. 2013, Bayesian Data Analysis (3rd ed.; London: Chapman and Hall)
Gelman, A., & Meng, X.-L. 1998, StaSc, 13, 163
Gelman, A., Meng, X.-L., & Stern, H. 1996, Stat. Sin., 6, 733
Gelman, A., & Rubin, D. B. 1992, StaSc, 7, 457
Godsill, S. J. 2001, J. Comput. Graph. Stat., 10, 230
Goncharov, B., Reardon, D. J., Shannon, R. M., et al. 2021a, MNRAS, 502, 478
Goncharov, B., Shannon, R. M., Reardon, D. J., et al. 2021b, ApJL, 917, L19
Goncharov, B., Thrane, E., Shannon, R. M., et al. 2022, ApJL, 932, L22
Guzzetti, M. C., Bartolo, N., Liguori, M., & Matarrese, S. 2016, NCimR, 39, 399
Harris, C. R., Millman, K. J., van der Walt, S. J., et al. 2020, Natur, 585, 357
Hazboun, J., Meyers, P. M., Romano, J. D., Siemens, X., & Archibald, A. M. 2023, arXiv:2305.01116
Hazboun, J., Romano, J., & Smith, T. 2019, JOSS, 4, 1775
Hazboun, J. S., Romano, J. D., & Smith, T. L. 2019, PhRvD, 100, 104028
Hazboun, J. S., Simon, J., Madison, D. R., et al. 2022, ApJ, 929, 39
Hazboun, J. S., Simon, J., Taylor, S. R., et al. 2020, ApJ, 890, 108
Heck, D. W., Overstall, A. M., Gronau, Q. F., & Wagenmakers, E.-J. 2019, Stat. Comput., 29, 631
Hee, S., Handley, W. J., Hobson, M. P., & Lasenby, A. N. 2015, MNRAS, 455, 2461
Hellings, R. W., & Downs, G. S. 1983, ApJL, 265, L39
Hinton, S. R. 2016, JOSS, 1, 00045
Hobbs, G., Coles, W., Manchester, R. N., et al. 2012, MNRAS, 427, 2780
Hobbs, G., & Edwards, R. 2012, Tempo2: Pulsar Timing Package, Astrophysics Source Code Library, ascl:1210.015
Hobbs, G., Guo, L., Caballero, R. N., et al. 2020, MNRAS, 491, 5951
Hourihane, S., Meyers, P., Johnson, A., Chatziioannou, K., & Vallisneri, M. 2023, PhRvD, 107, 084045
Hulse, R. A., & Taylor, J. H. 1975, ApJL, 195, L51
Hunter, J. D. 2007, CSE, 9, 90
Jaffe, A. H., & Backer, D. C. 2003, ApJ, 583, 616
Jenet, F. A., Hobbs, G. B., van Straten, W., et al. 2006, ApJ, 653, 1571
Jones, M. L., McLaughlin, M. A., Lam, M. T., et al. 2017, ApJ, 841, 125
Joshi, B. C., Arumugasamy, P., Bagchi, M., et al. 2018, JApA, 39, 51
Kaiser, A. R., Pol, N. S., McLaughlin, M. A., et al. 2022, ApJ, 938, 115
Kaspi, V. M., Taylor, J. H., & Ryba, M. F. 1994, ApJ, 428, 713
Khmelnitsky, A., & Rubakov, V. 2014, JCAP, 2014, 019
Kluyver, T., Ragan-Kelley, B., Pérez, F., et al. 2016, in Positioning and Power in Academic Publishing: Players, Agents and Agendas, ed. F. Loizides & B. Schmidt (Amsterdam: IOS Press), 87
Lam, M. T., Cordes, J. M., Chatterjee, S., et al. 2017, ApJ, 834, 35
Lam, M. T., Ellis, J. A., Grillo, G., et al. 2018, ApJ, 861, 132
Lamb, W. G., Taylor, S. R., & van Haasteren, R. 2023, arXiv:2303.15442
Lee, K. J. 2016, in ASP Conf. Ser. 502, Frontiers in Radio Astronomy and FAST Early Sciences Symposium 2015, ed. L. Qain & D. Li (San Francisco, CA: ASP), 19
Lentati, L., Alexander, P., Hobson, M. P., et al. 2013, PhRvD, 87, 104021
Luo, J., Ransom, S., Demorest, P., et al. 2021, ApJ, 911, 45
Magorrian, J., Tremaine, S., Richstone, D., et al. 1998, AJ, 115, 2285
Manchester, R. N., Hobbs, G., Bailes, M., et al. 2013, PASA, 30, e017
McConnell, N. J., & Ma, C.-P. 2013, ApJ, 764, 184
McLaughlin, M. A. 2013, CQGra, 30, 224008
McWilliams, S. T., Ostriker, J. P., & Pretorius, F. 2014, ApJ, 789, 156
Merritt, D., & Milosavljević, M. 2005, LRR, 8, 8
Meyers, P. M., Chatziioannou, K., Vallisneri, M., & Chua, A. J. K. 2023, arXiv:2306.05559
Milosavljević, M., & Merritt, D. 2003, ApJ, 596, 860
Mingarelli, C. M. F., Lazio, T. J. W., Sesana, A., et al. 2017, NatAs, 1, 886
Mingarelli, C. M. F., & Mingarelli, A. B. 2018, JPhCo, 2, 105002
Mingarelli, C. M. F., & Sidery, T. 2014, PhRvD, 90, 062011
Mingarelli, C. M. F., Sidery, T., Mandel, I., & Vecchio, A. 2013, PhRvD, 88, 062005
Nay, J., Boddy, K. K., Smith, T. L., & Mingarelli, C. M. F. M. 2023, arXiv:2306.06168
Ogata, Y. 1989, NuMat, 55, 137
Park, R. S., Folkner, W. M., Williams, J. G., & Boggs, D. H. 2021, AJ, 161, 105
Perera, B. B. P., DeCesar, M. E., Demorest, P. B., et al. 2019, MNRAS, 490, 4666
Phinney, E. S. 2001, arXiv:astro-ph/0108028
Pirani, F. A. E. 1956, AcPP, 15, 389
Pirani, F. A. E. 2009, GReGr, 41, 1215
Pol, N., Taylor, S. R., & Romano, J. D. 2022, ApJ, 940, 173
Pol, N. S., Taylor, S. R., Kelley, L. Z., et al. 2021, ApJL, 911, L34
Rajagopal, M., & Romani, R. W. 1995, ApJ, 446, 543
Ransom, S., Brazier, A., Chatterjee, S., et al. 2019, BAAS, 51, 195
Roebber, E. 2019, ApJ, 876, 55
Roebber, E., & Holder, G. 2017, ApJ, 835, 21
Romani, R. W. 1989, in Timing Neutron Stars, ed. H. Ögelman & E. P. J. Heuvel, Vol. 262 (Berlin: Springer), 113
Romano, J. D., Hazboun, J. S., Siemens, X., & Archibald, A. M. 2021, PhRvD, 103, 063027
Rosado, P. A., Sesana, A., & Gair, J. 2015, MNRAS, 451, 2417
Sampson, L., Cornish, N. J., & McWilliams, S. T. 2015, PhRvD, 91, 084055
Sardesai, S. C., & Vigeland, S. J. 2023, arXiv:2303.09615
Sazhin, M. V. 1978, SvA, 22, 36
Sesana, A. 2013, MNRAS, 433, L1
Sesana, A., Haardt, F., Madau, P., & Volonteri, M. 2004, ApJ, 611, 623
Sesana, A., Vecchio, A., & Colacino, C. N. 2008, MNRAS, 390, 192
Siemens, X., Ellis, J., Jenet, F., & Romano, J. D. 2013, CQGra, 30, 224015
Speri, L., Porayko, N. K., Falxa, M., et al. 2023, MNRAS, 518, 1802
Stinebring, D. R., Ryba, M. F., Taylor, J. H., & Romani, R. W. 1990, PhRvL, 65, 285
Taylor, J. H., Fowler, L. A., & McCulloch, P. M. 1979, Natur, 277, 437
Taylor, S. R. 2021, Nanohertz Gravitational Wave Astronomy (Boca Raton, FL: CRC Press)
Taylor, S. R., Baker, P. T., Hazboun, J. S., Simon, J. J., & Vigeland, S. J. 2018, enterprise_extensions, https://github.com/nanograv/enterprise_extensions
Taylor, S. R., & Gair, J. R. 2013, PhRvD, 88, 084001
Taylor, S. R., Lentati, L., Babak, S., et al. 2017, PhRvD, 95, 042002
Taylor, S. R., Simon, J., Schult, L., Pol, N., & Lamb, W. G. 2022, PhRvD, 105, 084049
Taylor, S. R., van Haasteren, R., & Sesana, A. 2020, PhRvD, 102, 084039
Tiburzi, C., Hobbs, G., Kerr, M., et al. 2016, MNRAS, 455, 4339

“Gravity has not revealed all its secrets. Achievements of the general theory of relativity a century after its formulation”
by M. Sazhin and O. Sazhina, Independent Newspaper,
November 25, 2015

“Now astronomers know many such objects both in our Galaxy and in other galaxies. Also open supermassive black holes with masses ranging from several million solar masses to a billion solar masses. They “settled” in the centers of galaxies. So, in the center of our Milky Way Galaxy there is a black hole with a mass of 4 million solar masses. Now astronomers, using a giant telescope-interferometer, are trying to measure the “shadow” of black holes in the center of our Galaxy, predicted by Russian physicist A. Zakharov. Such observations will allow us to measure characteristics of the “horizon” of a black hole.”

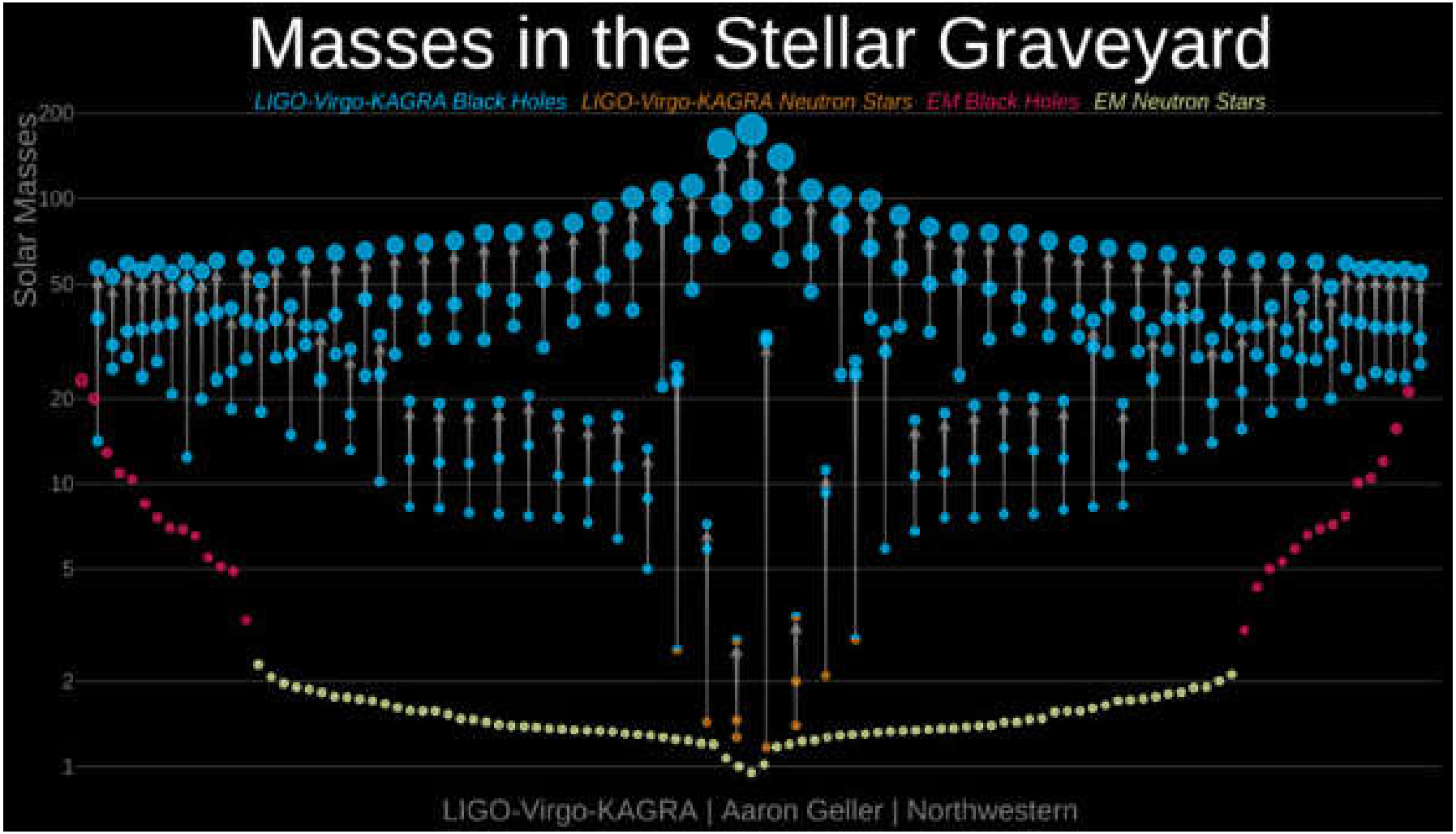
Masses in the Stellar Graveyard
LIGO-Virgo-KAGRA Black Holes
LIGO-Virgo-KAGRA Neutron Stars
EM Black Holes
EM Neutron Stars
Solar Masses
200
100
50
20
10
5
2
1
LIGO-Virgo-KAGRA | Aaron Geller | Northwestern

Black hole types

- Black holes with stellar masses 10 -- 10^2 M_{Sun}
- Massive black holes 10^2 -- 10^5 M_{Sun}
- Supermassive black holes 10^5 – 10^{10} M_{sun}

How to probe a black hole

Albert Einstein's theory of gravity, general relativity, predicts that the collapse of enough mass can leave a self-sustaining gravitational field so strong that, inside a distance called the event horizon, nothing can escape, not even light. But are black holes exactly the inscrutable things general relativity predicts? Observers may now have the tools to find out.

1. Trace the stars

Tracking the orbits of stars around the black hole in our Galaxy's center can reveal whether the black hole warps space and time exactly as general relativity predicts.

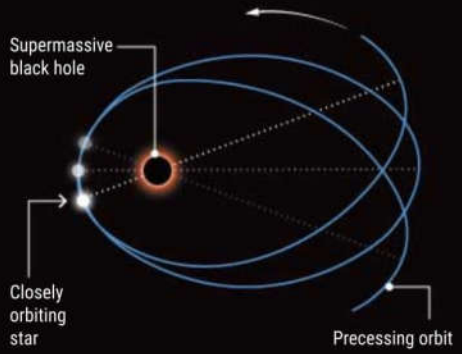

2. Take a picture

An image of a supermassive black hole holds clues to whether, as general relativity predicts, it has an event horizon rather than a surface, and mass and spin are its sole properties.

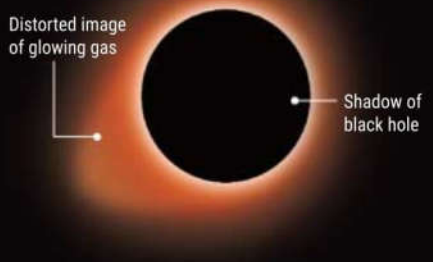

3. Catch the waves

When two small black holes spiral together, they radiate gravitational waves, which could reveal whether the supposed black holes are instead material objects. The final black hole reverberates at frequencies and overtones that provide another test of whether its only properties are mass and spin.

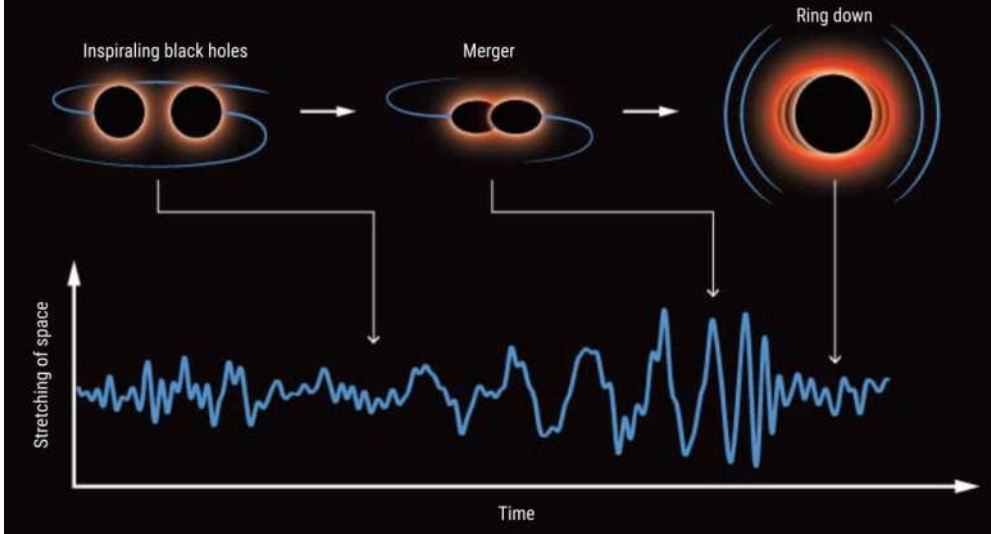

Great success of relativistic astrophysics

Three Nobel prizes in last five years (2017, 2019, 2020)

LIGO-Virgo: BBHs, BNS (kilonova) GW 170817;

GRAVITY, Keck and new tests of GR (gravitational redshift for S2 near its periapsis passage)

The confirmation of relativistic precession for S2 (GRAVITY)

Shadow reconstructions in M87* and Sgr A*

Four woman against more than 200 men (in 2020)

In 2023 the gender proportion for Nobel prize laureates started to be slightly better (Anne Genevieve L’Huillier)

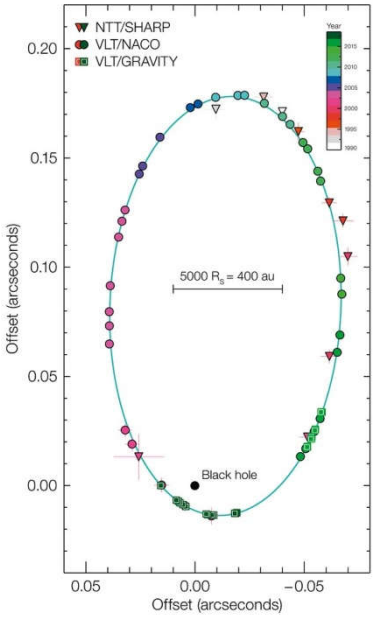
NTT/SHARP
VLT/NACO
VLT/GRAVITY
Year
2015
2010
2005
2000
1995
1990
5000 R_s = 400 au
Black hole
0.20
0.15
0.10
0.05
0.00
Offset (arcseconds)
0.05
0.00
−0.05
Offset (arcseconds)

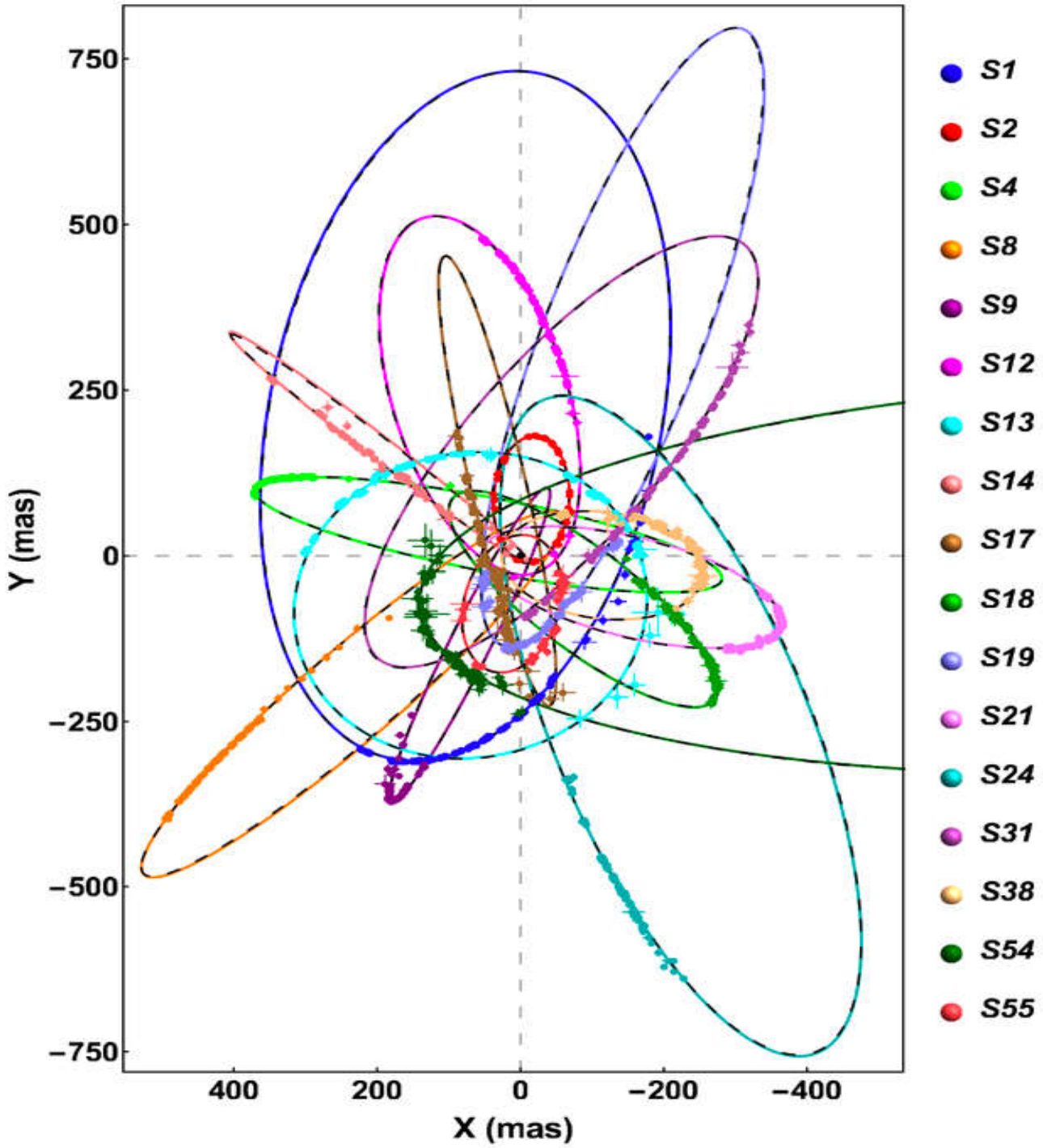
750
500
250
0
−250
−500
−750
Y (mas)
400
200
0
−200
−400
X (mas)
S1
S2
S4
S8
S9
S12
S13
S14
S17
S18
S19
S21
S24
S31
S38
S54
S55

Scalar field effects on the orbit of S2 star

The GRAVITY Collaboration: A. Amorim,[1,4] M. Bauböck,[5] M. Benisty,[6] J.-P. Berger,[5] Y. Clénet,[7] V. Coudé du Forest,[7] T. de Zeeuw,[8,5] J. Dexter,[5] G. Duvert,[6] A. Eckart,[9] F. Eisenhauer,[5] Miguel C. Ferreira,[1⋆] F. Gao,[5] Paulo J.V. Garcia,[1,2,3†] E. Gendron,[7] R. Genzel,[5,10] S. Gillessen,[5] P. Gordo,[1,4] M. Habibi,[5] M. Horrobin,[9] A. Jimenez-Rosales,[5] L. Jocou,[6] P. Kervella,[7] S. Lacour,[7,5] J.-B. Le Bouquin, P. Léna,[7] T. Ott,[5] M. Pössel,[11] T. Paumard,[7] K. Perraut,[6] G. Perrin,[7] O. Pfuhl,[5] G. Rodriguez Coira,[7] G. Rousset,[7] O. Straub,[5] C. Straubmeier,[9] E. Sturm,[5] F. Vincent,[7] S. von Fellenberg,[5] I. Waisberg[5] and F. Widmann[5]

[1] *CENTRA, Centro de Astrofísica e Gravitação, Instituto Superior Técnico, Avenida Rovisco Pais 1, 1049 Lisboa, Portugal*
[2] *Universidade do Porto, Faculdade de Engenharia, Rua Dr. Roberto Frias, 4200-465 Porto, Portugal*
[3] *European Southern Observatory, Casilla 19001, Santiago 19, Chile*
[4] *Universidade de Lisboa - Faculdade de Ciências, Campo Grande, 1749-016 Lisboa, Portugal*
[5] *Max Planck Institute for Extraterrestrial Physics (MPE), Giessenbachstr.1, 85748 Garching, Germany*
[6] *Univ. Grenoble Alpes, CNRS, IPAG, 38000 Grenoble, France*
[7] *LESIA, Observatoire de Paris, Université PSL, CNRS, Sorbonne Université, Université de Paris, 5 place Jules Janssen, 92195 Meudon, France*
[8] *Sterrewacht Leiden, Leiden University, Postbus 9513, 2300 RA Leiden, The Netherlands*
[9] *Physikalisches Institut, Universität zu Köln, Zülpicher Str. 77, 50937 Köln, Germany*
[10] *Departments of Physics and Astronomy, Le Conte Hall, University of California, Berkeley, CA 94720, USA*
[11] *Max Planck Institute for Astronomy (MPIA) and Haus der Astronomie, Königstuhl 17, D-69117 Heidelberg, Germany*

Accepted XXX. Received YYY; in original form ZZZ

ABSTRACT

Precise measurements of the S-stars orbiting SgrA* have set strong constraints on the nature of the compact object at the centre of the Milky Way. The presence of a black hole in that region is well established, but its neighboring environment is still an open debate. In that respect, the existence of dark matter in that central region may be detectable due to its strong signatures on the orbits of stars: the main effect is a Newtonian precession which will affect the overall pericentre shift of S2, the latter being a target measurement of the GRAVITY instrument. The exact nature of this dark matter (e.g., stellar dark remnants or diffuse dark matter) is unknown. This article assumes it to be an scalar field of toroidal distribution, associated with ultra-light dark matter particles, surrounding the Kerr black hole. Such a field is a form of "hair" expected in the context of superradiance, a mechanism that extracts rotational energy from the black hole. Orbital signatures for the S2 star are computed and shown to be detectable by GRAVITY. The scalar field can be constrained because the variation of orbital elements depends both on the relative mass of the scalar field to the black hole and on the field mass coupling parameter.

Key words: black hole physics – celestial mechanics – dark matter – gravitation – Galaxy: centre – quasars: supermassive black holes

⋆ Corresponding author, e-mail: mcferreira@tecnico.ulisboa.pt
† Corresponding author, e-mail: pgarcia@fe.up.pt

Results from nine (!) our papers were used

Table 2. Literature computing extensions/alternatives to GR effects in the orbits of the S-stars.

extension/alternative	results/comments	reference
charged non-rotating black holes	Upper limit to black hole charge from S2 precession upper limit.	De Laurentis et al. (2018a), Iorio (2012), Zakharov (2018)
charged rotating black holes and plasma effects	upper limits from black hole mass, spin and local magnetic field	Zajaček et al. (2018)
fermion ball	Ruled out by Ghez et al. (2005) and Gravity Collaboration et al. (2018a).	Munyaneza & Viollier (2002)
boson "star"	Effects much smaller than GR at S2 orbit, only relevant at a few tens of Schwarzschild radii.	Amaro-Seoane et al. (2010),Boshkayev & Malafarina (2019),Grould et al. (2017a)
Yukawa potential	Upper limits on potential parameters and graviton mass from S2 precession upper limit.	Borka et al. (2013), Hees et al. (2017), Zakharov et al. (2016), Zakharov et al. (2018)
Einstein-Maxwell-Dilaton-Axion gravity	Effects smaller than 10^{-3} of GR for S2, need pulsars or inner stars for further tests.	De Laurentis et al. (2018a)
Brans-Dicke theory	Effects smaller than 10^{-3} of GR for S2, need pulsars or inner stars for further tests.	De Laurentis et al. (2018a), Kalita (2018)
$f(R)$ gravity	Effects smaller than 10^{-3} of GR for S2, need pulsars or inner stars for further tests.	Capozziello et al. (2014), De Laurentis et al. (2018a), De Laurentis et al. (2018b), Kalita (2018)
nonlocal gravity	Precession compatible with observational upper limit, of the order of GR prediction	Dialektopoulos et al. (2019)
scalar tensor gravity	Precession is 13× GR value, ruled out by Hees et al. (2017).	Borka Jovanović et al. (2019)
$f(R,\phi)$ gravity	Best fit precession prediction for S2 is 20× GR value, ruled out by Hees et al. (2017).	Capozziello et al. (2014)
hybrid gravity	Best fit precession prediction too high, ruled out by Hees et al. (2017).	Borka et al. (2016)
R^n gravity	When compared with Hees et al. (2017) upper value, the GR value ($n = 1$) is recovered to < 1%, or smaller if extended mass distributions are present.	Borka et al. (2012), Zakharov et al. (2014)
quadratic Einstein-Gauss-Bonnet gravity	Derive expressions for gravitational redshift in function of theory coupling parameters (scalar/matter & scalar/Gauss-Bonnet invariant).	Hees et al. (2019)
dark matter profiles (See Table 1 for dark matter + black hole studies.)	Dark matter mass required to explain TeV emission compatible with orbital upper limits. Limits on spatial distribution of non-annihilating dark matter.	de Paolis et al. (2011), Hall & Gondolo (2006), Iorio (2013), Lacroix (2018),Zakharov et al. (2007)
scalar fields and ultralight dark matter	Upper limits on scalar field mass (1% of black hole) for particles of mass 4×10^{-19} eV/c^2	Bar et al. (2019)

black holes. To study this possibility, we will analyse the solutions to the Klein-Gordon equation in a Kerr space time. We will follow the analytic results of Detweiler (1980) and then translate the scalar field solution in an effective gravitational potential which can then be treated with the usual perturbation analysis of Keplerian orbits. In this section we will be using Planck units ($\hbar = c = G = 1$) unless otherwise stated.

A black hole-scalar field system, in which the scalar field is minimally coupled to gravity, is described by the following action

$$S = \int d^4x\sqrt{-g}\left(\frac{R}{16\pi} - \frac{1}{2}g^{\alpha\beta}\Psi^*_{,\alpha}\Psi^*_{,\beta} - \frac{\mu^2}{2}\Psi\Psi^*\right) \quad (1)$$

in which R is the Ricci scalar, $g_{\mu\nu}$ and g is the metric and its determinant, $\Psi(t,r,\theta,\phi)$ is a complex scalar field[4] and μ is the mass of the scalar field. The principle of least action results in the Einstein-Klein-Gordon system of equations

$$\begin{cases} G^{\alpha\beta} = & 8\pi T^{\alpha\beta} \\ \nabla_\alpha\nabla^\alpha\Psi = & \mu^2\Psi \end{cases} \quad (2)$$

where $G_{\alpha\beta}$ is the Einstein tensor, ∇_α represents the covariant derivative and

$$T^{\alpha\beta} = \Psi^{*,(\alpha}\Psi^{,\beta)} - \frac{1}{2}g^{\alpha\beta}\left(\Psi^*_{,\sigma}\Psi^{,\sigma} + \mu^2\Psi^*\Psi\right) \quad (3)$$

is the energy-momentum of the scalar field. In this system, the relevant quantity is the dimensionless mass coupling given by

$$\alpha = r_g\mu = \left[\frac{GM}{c^2}\right]\left[\frac{m_s c}{\hbar}\right] = \frac{M_\bullet m_s}{m_p^2}, \quad (4)$$

scalar field can also be considered, as in Brito et al. (2015a) and Ferreira et al. (2017)

[4] We choose to deal with the complex scalar field but the real

Breakthrough Prize in Physics in 2023

Its founding sponsors are Sergey Brin, Priscilla Chan and Mark Zuckerberg, Julia and Yuri Milner, and Anne Wojcicki

Prof John Cardy, an emeritus fellow at the University of Oxford, shares this year's physics prize with Alexander Zamolodchikov for their contributions to statistical physics and quantum field theory – a theoretical framework that describes how different states of matter may be described by fluctuating fields, analogous to magnetic and electric fields.

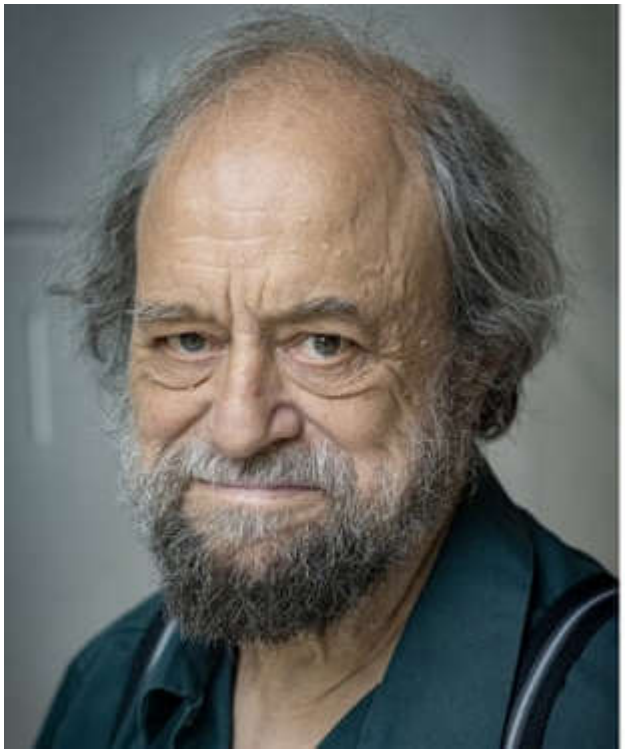

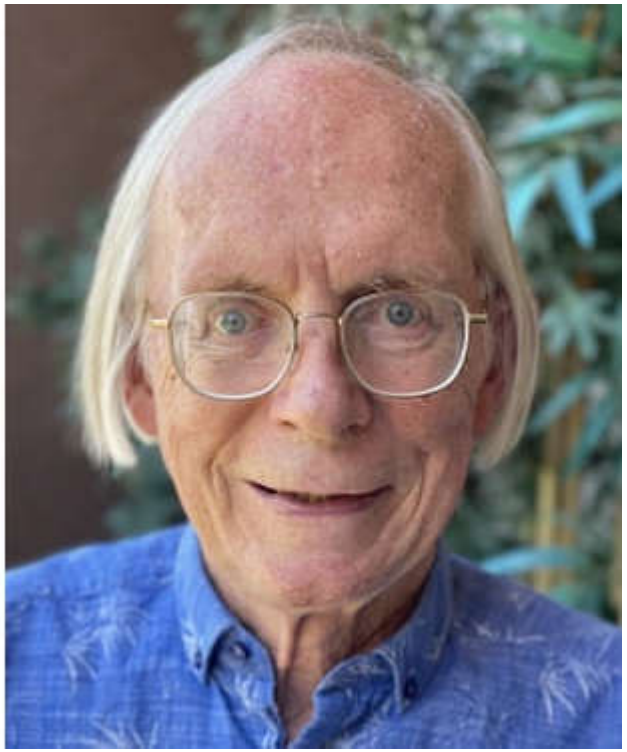

2024 New Horizons in Physics from Breakthrough Prize Foundation for Promising Early-career researchers: Michael Johnson & Alex Lupsasca (EHT coll.)

Coevolution (Or Not) of Supermassive Black Holes and Host Galaxies

John Kormendy[1] and Luis C. Ho[2]

[1]Department of Astronomy, University of Texas at Austin,
2515 Speedway C1400, Austin, TX 78712-1205; email: kormendy@astro.as.utexas.edu

[2]The Observatories of the Carnegie Institution for Science,
813 Santa Barbara Street, Pasadena, CA 91101; email: lho@obs.carnegiescience.edu

Abstract

Supermassive black holes (BHs) have been found in 87 galaxies by dynamical modeling of spatially resolved kinematics. The *Hubble Space Telescope* revolutionized BH research by advancing the subject from its proof-of-concept phase into quantitative studies of BH demographics. Most influential was the discovery of a tight correlation between BH mass $M_\bullet$ and the velocity dispersion σ of the bulge component of the host galaxy. Together with similar correlations with bulge luminosity and mass, this led to the widespread belief that BHs and bulges coevolve by regulating each other's growth. Conclusions based on one set of correlations from $M_\bullet \sim 10^{9.5}\ M_\odot$ in brightest cluster ellipticals to $M_\bullet \sim 10^6\ M_\odot$ in the smallest galaxies dominated BH work for more than a decade.

New results are now replacing this simple story with a richer and more plausible picture in which BHs correlate differently with different galaxy components. A reasonable aim is to use this progress to refine our understanding of BH – galaxy coevolution. BHs with masses of $10^5 - 10^6\ M_\odot$ are found in many bulgeless galaxies. Therefore, classical (elliptical-galaxy-like) bulges are not necessary for BH formation. On the other hand, while they live in galaxy disks, BHs do not correlate with galaxy disks. Also, any $M_\bullet$ correlations with the properties of disk-grown pseudobulges and dark matter halos are weak enough to imply no close coevolution.

The above and other correlations of host galaxy parameters with each other and with $M_\bullet$ suggest that there are four regimes of BH feedback. (1) Local, secular, episodic, and stochastic feeding of small BHs in largely bulgeless galaxies involves too little energy to result in coevolution. (2) Global feeding in major, wet galaxy mergers rapidly grows giant BHs in short-duration, quasar-like events whose energy feedback does affect galaxy evolution. The resulting hosts are classical bulges and coreless-rotating-disky ellipticals. (3) After these AGN phases and at the highest galaxy masses, maintenance-mode BH feedback into X-ray-emitting gas has the primarily negative effect of helping to keep baryons locked up in hot gas and thereby keeping galaxy formation from going to completion. This happens in giant, core-nonrotating-boxy ellipticals. Their properties, including their tight correlations between $M_\bullet$ and core parameters, support the conclusion that core ellipticals form by dissipationless major mergers. They inherit coevolution effects from smaller progenitor galaxies. Also, (4) independent of any feedback physics, in BH growth modes (2) and (3), the averaging that results from successive mergers plays a major role in decreasing the scatter in $M_\bullet$ correlations from the large values observed in bulgeless and pseudobulge galaxies to the small values observed in giant elliptical galaxies.

Table 1 Mass measurements of supermassive black holes in our Galaxy, M 31, and M 32

Galaxy	D	σ_e	$M_\bullet$ ($M_{\rm low}, M_{\rm high}$)	$r_{\rm infl}$	σ_*	$r_{\rm infl}/\sigma_*$	Reference
	(Mpc)	(km s^{-1})	($M_\odot$)	(arcsec)	(arcsec)		
(1)	(2)	(3)	(4)	(5)	(6)	(7)	(8)
Galaxy			4.41(3.98–4.84) e6		0.0146	2868.	Meyer et al. 2012
Galaxy			4.2 (3.9 –4.6) e6		0.0139	3013.	Yelda et al. 2011
Galaxy	0.00828	105	4.30(3.94–4.66) e6	41.9	0.0146	2868.	Genzel, Eisenhauer & Gillessen 2010
Galaxy	0.00828	105	4.30(3.94–4.66) e6	41.9	0.0146	2868.	Gillessen et al. 2009a
Galaxy			4.09(3.74–4.43) e6		0.0148	2829.	Gillessen et al. 2009b
Galaxy			4.25(3.44–4.79) e6		0.0139	3013.	Ghez et al. 2008
Galaxy			3.80(3.60–4.00) e6		0.0056	7478.	Ghez et al. 2005
Galaxy			3.7 (3.3 –4.1) e6		0.0075	5583.	Ghez et al. 2003
Galaxy			3.8 (2.3 –5.4) e6		0.0155	2702.	Schödel et al. 2002
Galaxy			2.1 (1.3 –2.8) e6		0.113	371.	Chakrabarty & Saha 2001
Galaxy			3.1 (2.6 –3.6) e6		0.26	161.	Genzel et al. 2000
Galaxy			2.7 (2.5 –2.9) e6		0.39	107.	Ghez et al. 1998
Galaxy			2.70(2.31–3.09) e6		0.39	107.	Genzel et al. 1997
Galaxy			2.55(2.12–2.95) e6		0.39	107.	Eckart & Genzel 1997
Galaxy			2.8 (2.5 –3.1) e6		2.4	17.4	Genzel et al. 1996
Galaxy			2.0 (0.9 –2.9) e6		4.9	8.5	Haller et al. 1996
Galaxy			2.9 (2.0 –3.9) e6		3.4	12.3	Krabbe et al. 1995
Galaxy			2. e6		5	8.4	Evans & de Zeeuw 1994
Galaxy			3. e6		5	8.4	Kent 1992
Galaxy			5.4 (3.9 –6.8) e6		15	2.8	Sellgren et al. 1990
M 31	0.774	169	1.4 (1.1–2.3) e8	5.75	0.053	109.	Bender et al. 2005
M 31			1.0 e8		0.297	19.4	Peiris & Tremaine 2003
M 31			6.1 (3.6–8.7) e7		0.052	111.	Bacon et al. 2001
M 31			3.3 (1.5–4.5) e7		0.297	19.4	Kormendy & Bender 1999
M 31			6.0 (5.8–6.2) e7		0.297	19.4	Magorrian et al. 1998
M 31			9.5 (7 – 10) e7		0.42	13.7	Emsellem & Combes 1997
M 31			7.5 e7		0.56	10.3	Tremaine 1995
M 31			8.0 e7		0.42	13.7	Bacon et al. 1994
M 31			5 (4.5–5.6) e7		0.59	9.7	Richstone, Bower & Dressler 1990
M 31			3.8 (1.1– 11) e7		0.56	10.3	Kormendy 1988a
M 31			5.6 (3.4–7.8) e7		0.59	9.7	Dressler & Richstone 1988
M 32	0.805	77	2.45(1.4–3.5) e6	0.46	0.052	8.76	van den Bosch & de Zeeuw 2010
M 32			2.9 (2.7–3.1) e6		0.052	8.76	Verolme et al. 2002
M 32			3.5 (2.3–4.6) e6		0.052	8.76	Joseph et al. 2001
M 32			2.4 (2.2–2.6) e6		0.23	1.98	Magorrian et al. 1998
M 32			3.9 (3.1–4.7) e6		0.050	9.11	van der Marel et al. 1998a
M 32			3.9 (3.3–4.5) e6		0.050	9.11	van der Marel et al. 1997a, 1997b
M 32			3.2 (2.6–3.7) e6		0.23	1.98	Bender, Kormendy & Dehnen 1996
M 32			2.1 (1.8–2.3) e6		0.34	1.34	Dehnen 1995
M 32			2.1 e6		0.34	1.34	Qian et al. 1995
M 32			2.1 (1.7–2.4) e6		0.34	1.34	van der Marel et al. 1994a
M 32			2.2 (0.8–3.5) e6		0.59	0.77	Richstone, Bower & Dressler 1990
M 32			9.3 e6		0.59	0.77	Dressler & Richstone 1988
M 32			7.5 (3.5–11.5) e6		0.76	0.60	Tonry 1987
M 32			5.8 e6		1.49	0.31	Tonry 1984

Lines based on HST spectroscopy are in red. Column 2 is the assumed distance. Column 3 is the stellar velocity dispersion inside the "effective radius" that encompasses half of the light of the bulge. Column 4 is the measured BH mass with the one-sigma range that includes 68 % of the probability in parentheses. Only the top four $M_\bullet$ values for the Galaxy include distance uncertainties in the error bars. Column 5 is the radius of the sphere of influence of the BH; the line that lists $r_{\rm infl}$ contains the adopted $M_\bullet$. Column 6 is the effective resolution of the spectroscopy, estimated as in Kormendy (2004). It is a radius that measures the blurring effects of the telescope point-spread function or "PSF," the slit width or aperture size, and the pixel size. The contribution of the telescope is estimated by the dispersion $\sigma_{*\rm tel}$ of a Gaussian fitted to the core of the average radial brightness profile of the PSF. In particular, the HST PSF has $\sigma_{*\rm tel} \simeq 0''.036$ from a single-Gaussian fit to the PSF model in van der Marel, de Zeeuw & Rix (1997a).

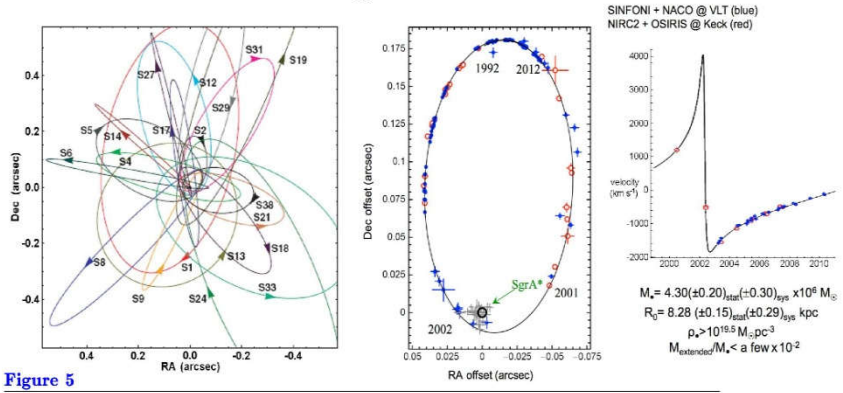

Figure 5

(*left*) Orbits of individual stars near the Galactic center. (*right*) Orbit of star S2 around the BH and associated radio source Sgr A* based on observations of its position from 1992 to 2012. Results from the Ghez group using the Keck telescope and from the Genzel group using the Europen Very Large Telescope (VLT) are combined. This figure is updated from Genzel, Eisenhauer & Gillessen (2010) and is kindly provided by Reinhard Genzel.

These results establish the existence and mass of the central dark object beyond any reasonable doubt. They also eliminate astrophysical plausible alternatives to a BH. These include brown dwarfs and stellar remnants (e. g., Maoz 1995, 1998; Genzel et al. 1997, 2000; Ghez et al. 1998, 2005) and even fermion balls (Ghez et al. 2005; GEG10). Boson balls (Torres et al. 2000; Schunck & Mielke 2003; Liebling & Palenzuela 2012) are harder to exclude; they are highly relativistic, they do not have hard surfaces, and they are consistent with dynamical mass and size constraints. But a boson ball is like the proverbial elephant in a tree: it is OK where it is, but how did it ever get there? GEG10 argue that boson balls are inconsistent with astrophysical constraints based on AGN radiation. Also, the Sołtan (1982) argument implies that at least most of the central dark mass observed in galaxies grew by accretion in AGN phases, and this quickly makes highly relativistic objects collapse into BHs. Finally (Fabian 2013), X-ray AGN observations imply that we see, in some objects, material interior to the innermost stable circular orbit of a non-rotating BH; this implies that these BHs are rotating rapidly and excludes boson balls as alternatives to all central dark objects. Arguments against the most plausible BH alternatives – failed stars and dead stars – are also made for other galaxies in Maoz (1995, 1998) and in Bender et al. (2005). Exotica such as sterile neutrinos or dark matter WIMPs could still have detectable (small) effects, but we conclude that they no longer threaten the conclusion that we are detecting supermassive black holes.

KR95 was titled "Inward Bound – The Search for Supermassive Black Holes in Galactic Nuclei." HST has taken us essentially one order of magnitude inward in radius. A few other telescopes take us closer. But mostly, we are still working at 10^4 to 10^5 Schwarzschild radii. In our Galaxy, we have observed individual stars in to $\sim$ 500 Schwarzschild radii. Only the velocity profiles of relativistically broadened Fe Kα lines (e. g., Tanaka et al. 1995; Fabian 2013) probe radii that are comparable to the Schwarzschild radius. So we are still inward bound. Joining up our measurements made at thousands of r_S with those probed by Fe Kα emission requires that we robustly integrate into our story the rich and complicated details of AGN physics; that is, the narrow– and broad–emission-line regions. That journey still has far to go.

In the last decades of his scientific activity Academician Anatolii Alexeevich Logunov studied astronomical properties of massive gravity theory (this gravity theory was not popular at this time)

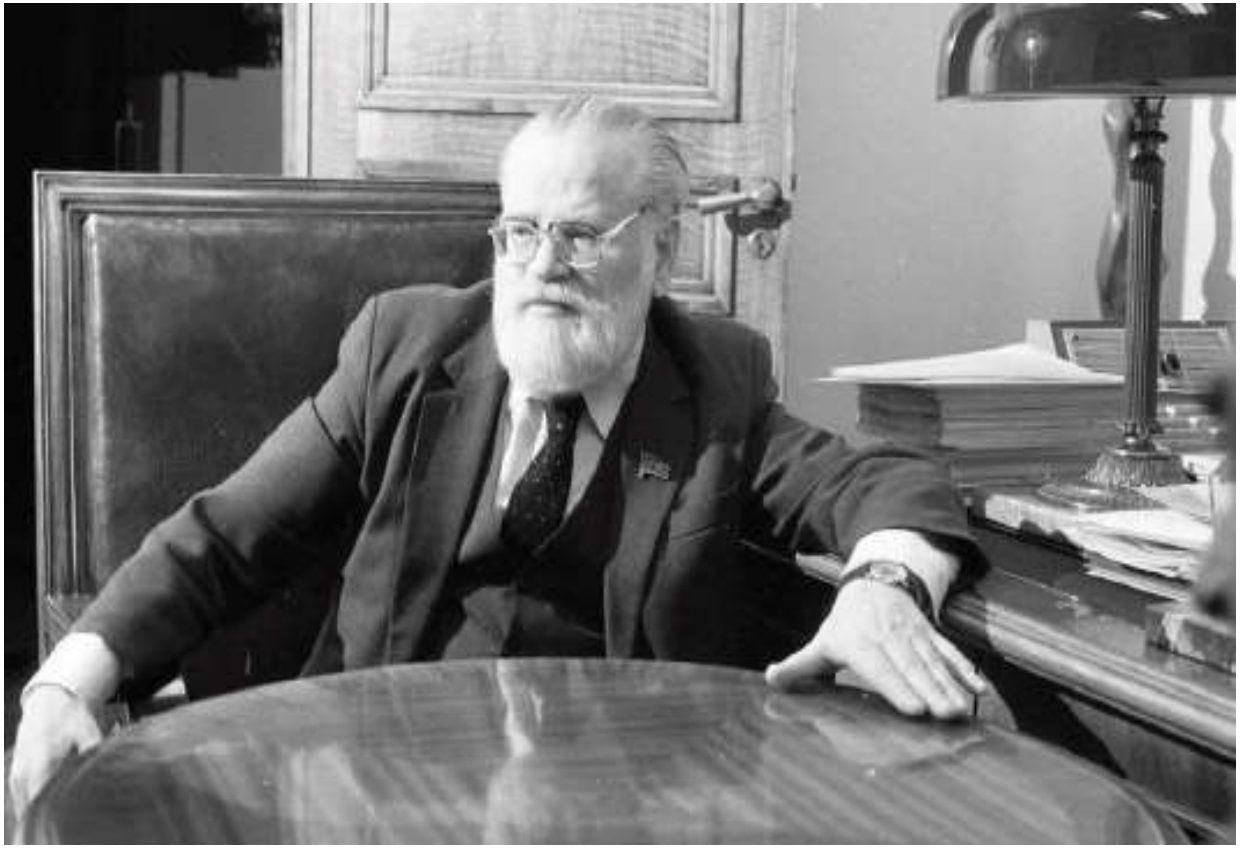

Massive graviton theories

- M. Fierz and W.Pauli-1939
- Zakharov; Veltman, van Dam – 1970
- Vainshtein - 1972
- Boulware, Deser -- 1972
- Logunov, Mestvirishvili, Gershtein et al. (RTG)
- Visser – 1998 (review on such theories)
- Rubakov, Tinyakov – 2008
- de Rham et al.—2011 -- 2016

Observation of Gravitational Waves from a Binary Black Hole Merger

B. P. Abbott *et al.*[*]
(LIGO Scientific Collaboration and Virgo Collaboration)
(Received 21 January 2016; published 11 February 2016)

On September 14, 2015 at 09:50:45 UTC the two detectors of the Laser Interferometer Gravitational-Wave Observatory simultaneously observed a transient gravitational-wave signal. The signal sweeps upwards in frequency from 35 to 250 Hz with a peak gravitational-wave strain of 1.0×10^{-21}. It matches the waveform predicted by general relativity for the inspiral and merger of a pair of black holes and the ringdown of the resulting single black hole. The signal was observed with a matched-filter signal-to-noise ratio of 24 and a false alarm rate estimated to be less than 1 event per 203 000 years, equivalent to a significance greater than 5.1σ. The source lies at a luminosity distance of 410^{+160}_{-180} Mpc corresponding to a redshift $z = 0.09^{+0.03}_{-0.04}$. In the source frame, the initial black hole masses are $36^{+5}_{-4} M_\odot$ and $29^{+4}_{-4} M_\odot$, and the final black hole mass is $62^{+4}_{-4} M_\odot$, with $3.0^{+0.5}_{-0.5} M_\odot c^2$ radiated in gravitational waves. All uncertainties define 90% credible intervals. These observations demonstrate the existence of binary stellar-mass black hole systems. This is the first direct detection of gravitational waves and the first observation of a binary black hole merger.

DOI: 10.1103/PhysRevLett.116.061102

I. INTRODUCTION

In 1916, the year after the final formulation of the field equations of general relativity, Albert Einstein predicted the existence of gravitational waves. He found that the linearized weak-field equations had wave solutions: transverse waves of spatial strain that travel at the speed of light, generated by time variations of the mass quadrupole moment of the source [1,2]. Einstein understood that gravitational-wave amplitudes would be remarkably small; moreover, until the Chapel Hill conference in 1957 there was significant debate about the physical reality of gravitational waves [3].

Also in 1916, Schwarzschild published a solution for the field equations [4] that was later understood to describe a black hole [5,6], and in 1963 Kerr generalized the solution to rotating black holes [7]. Starting in the 1970s theoretical work led to the understanding of black hole quasinormal modes [8–10], and in the 1990s higher-order post-Newtonian calculations [11] preceded extensive analytical studies of relativistic two-body dynamics [12,13]. These advances, together with numerical relativity breakthroughs in the past decade [14–16], have enabled modeling of binary black hole mergers and accurate predictions of their gravitational waveforms. While numerous black hole candidates have now been identified through electromagnetic observations [17–19], black hole mergers have not previously been observed.

The discovery of the binary pulsar system PSR B1913+16 by Hulse and Taylor [20] and subsequent observations of its energy loss by Taylor and Weisberg [21] demonstrated the existence of gravitational waves. This discovery, along with emerging astrophysical understanding [22], led to the recognition that direct observations of the amplitude and phase of gravitational waves would enable studies of additional relativistic systems and provide new tests of general relativity, especially in the dynamic strong-field regime.

Experiments to detect gravitational waves began with Weber and his resonant mass detectors in the 1960s [23], followed by an international network of cryogenic resonant detectors [24]. Interferometric detectors were first suggested in the early 1960s [25] and the 1970s [26]. A study of the noise and performance of such detectors [27], and further concepts to improve them [28], led to proposals for long-baseline broadband laser interferometers with the potential for significantly increased sensitivity [29–32]. By the early 2000s, a set of initial detectors was completed, including TAMA 300 in Japan, GEO 600 in Germany, the Laser Interferometer Gravitational-Wave Observatory (LIGO) in the United States, and Virgo in Italy. Combinations of these detectors made joint observations from 2002 through 2011, setting upper limits on a variety of gravitational-wave sources while evolving into a global network. In 2015, Advanced LIGO became the first of a significantly more sensitive network of advanced detectors to begin observations [33–36].

A century after the fundamental predictions of Einstein and Schwarzschild, we report the first direct detection of gravitational waves and the first direct observation of a binary black hole system merging to form a single black hole. Our observations provide unique access to the

[*]Full author list given at the end of the article.

black hole system in general relativity [94]. A first consistency check involves the mass and spin of the final black hole. In general relativity, the end product of a black hole binary coalescence is a Kerr black hole, which is fully described by its mass and spin. For quasicircular inspirals, these are predicted uniquely by Einstein's equations as a function of the masses and spins of the two progenitor black holes. Using fitting formulas calibrated to numerical relativity simulations [92], we verified that the remnant mass and spin deduced from the early stage of the coalescence and those inferred independently from the late stage are consistent with each other, with no evidence for disagreement from general relativity.

Within the post-Newtonian formalism, the phase of the gravitational waveform during the inspiral can be expressed as a power series in $f^{1/3}$. The coefficients of this expansion can be computed in general relativity. Thus, we can test for consistency with general relativity [95,96] by allowing the coefficients to deviate from the nominal values, and seeing if the resulting waveform is consistent with the data. In this second check [94] we place constraints on these deviations, finding no evidence for violations of general relativity.

Finally, assuming a modified dispersion relation for gravitational waves [97], our observations constrain the Compton wavelength of the graviton to be $\lambda_g > 10^{13}$ km, which could be interpreted as a bound on the graviton mass $m_g < 1.2 \times 10^{-22}$ eV$/c^2$. This improves on Solar System and binary pulsar bounds [98,99] by factors of a few and a thousand, respectively, but does not improve on the model-dependent bounds derived from the dynamics of Galaxy clusters [100] and weak lensing observations [101]. In summary, all three tests are consistent with the predictions of general relativity in the strong-field regime of gravity.

GW150914 demonstrates the existence of stellar-mass black holes more massive than $\simeq 25 M_\odot$, and establishes that binary black holes can form in nature and merge within a Hubble time. Binary black holes have been predicted to form both in isolated binaries [102–104] and in dense environments by dynamical interactions [105–107]. The formation of such massive black holes from stellar evolution requires weak massive-star winds, which are possible in stellar environments with metallicity lower than $\simeq 1/2$ the solar value [108,109]. Further astrophysical implications of this binary black hole discovery are discussed in [110].

These observational results constrain the rate of stellar-mass binary black hole mergers in the local universe. Using several different models of the underlying binary black hole mass distribution, we obtain rate estimates ranging from 2–400 Gpc^{-3} yr^{-1} in the comoving frame [111–113]. This is consistent with a broad range of rate predictions as reviewed in [114], with only the lowest event rates being excluded.

Binary black hole systems at larger distances contribute to a stochastic background of gravitational waves from the superposition of unresolved systems. Predictions for such a background are presented in [115]. If the signal from such a population were detected, it would provide information about the evolution of such binary systems over the history of the universe.

VII. OUTLOOK

Further details about these results and associated data releases are available at [116]. Analysis results for the entire first observational period will be reported in future publications. Efforts are under way to enhance significantly the global gravitational-wave detector network [117]. These include further commissioning of the Advanced LIGO detectors to reach design sensitivity, which will allow detection of binaries like GW150914 with 3 times higher SNR. Additionally, Advanced Virgo, KAGRA, and a possible third LIGO detector in India [118] will extend the network and significantly improve the position reconstruction and parameter estimation of sources.

VIII. CONCLUSION

The LIGO detectors have observed gravitational waves from the merger of two stellar-mass black holes. The detected waveform matches the predictions of general relativity for the inspiral and merger of a pair of black holes and the ringdown of the resulting single black hole. These observations demonstrate the existence of binary stellar-mass black hole systems. This is the first direct detection of gravitational waves and the first observation of a binary black hole merger.

ACKNOWLEDGMENTS

The authors gratefully acknowledge the support of the United States National Science Foundation (NSF) for the construction and operation of the LIGO Laboratory and Advanced LIGO as well as the Science and Technology Facilities Council (STFC) of the United Kingdom, the Max-Planck Society (MPS), and the State of Niedersachsen, Germany, for support of the construction of Advanced LIGO and construction and operation of the GEO 600 detector. Additional support for Advanced LIGO was provided by the Australian Research Council. The authors gratefully acknowledge the Italian Istituto Nazionale di Fisica Nucleare (INFN), the French Centre National de la Recherche Scientifique (CNRS), and the Foundation for Fundamental Research on Matter supported by the Netherlands Organisation for Scientific Research, for the construction and operation of the Virgo detector, and for the creation and support of the EGO consortium. The authors also gratefully acknowledge research support from these agencies as well as by the Council of Scientific and Industrial Research of India, Department of Science and

Tests of General Relativity with GWTC-3

R. Abbott,[1] H. Abe,[2] F. Acernese,[3,4] K. Ackley,[5] N. Adhikari,[6] R. X. Adhikari,[1] V. K. Adkins,[7] V. B. Adya,[8] C. Affeldt,[9,10] D. Agarwal,[11] M. Agathos,[12,13] K. Agatsuma,[14] N. Aggarwal,[15] O. D. Aguiar,[16] L. Aiello,[17] A. Ain,[18] P. Ajith,[19] T. Akutsu,[20,21] P. F. de Alarcón,[22] S. Albanesi,[23,24] R. A. Alfaidi,[25] A. Allocca,[26,4] P. A. Altin,[8] A. Amato,[27] C. Anand,[5] S. Anand,[1] A. Ananyeva,[1] S. B. Anderson,[1] W. G. Anderson,[6] M. Ando,[28,29] T. Andrade,[30] N. Andres,[31] M. Andrés-Carcasona,[32] T. Andrić,[33] S. V. Angelova,[34] S. Ansoldi,[35,36] J. M. Antelis,[37] S. Antier,[38,39] T. Apostolatos,[40] E. Z. Appavuravther,[41,42] S. Appert,[1] S. K. Apple,[43] K. Arai,[1] A. Araya,[44] M. C. Araya,[1] J. S. Areeda,[45] M. Arène,[46] N. Aritomi,[20] N. Arnaud,[47,48] M. Arogeti,[49] S. M. Aronson,[7] K. G. Arun,[50] H. Asada,[51] Y. Asali,[52] G. Ashton,[53] Y. Aso,[54,55] M. Assiduo,[56,57] S. Assis de Souza Melo,[48] S. M. Aston,[58] P. Astone,[59] F. Aubin,[57] K. AultONeal,[37] C. Austin,[7] S. Babak,[46] F. Badaracco,[60] M. K. M. Bader,[61] C. Badger,[62] S. Bae,[63] Y. Bae,[64] A. M. Baer,[65] S. Bagnasco,[24] Y. Bai,[1] J. Baird,[46] R. Bajpai,[66] T. Baka,[67] M. Ball,[68] G. Ballardin,[48] S. W. Ballmer,[69] A. Balsamo,[65] G. Baltus,[70] S. Banagiri,[15] B. Banerjee,[33] D. Bankar,[11] J. C. Barayoga,[1] C. Barbieri,[71,72,73] B. C. Barish,[1] D. Barker,[74] P. Barneo,[30] F. Barone,[75,4] B. Barr,[25] L. Barsotti,[76] M. Barsuglia,[46] D. Barta,[77] J. Bartlett,[74] M. A. Barton,[25] I. Bartos,[78] S. Basak,[19] R. Bassiri,[79] A. Basti,[80,18] M. Bawaj,[41,81] J. C. Bayley,[25] M. Bazzan,[82,83] B. R. Becher,[84] B. Bécsy,[85] V. M. Bedakihale,[86] F. Beirnaert,[87] M. Bejger,[88] I. Belahcene,[47] V. Benedetto,[89] D. Beniwal,[90] M. G. Benjamin,[91] T. F. Bennett,[92] J. D. Bentley,[14] M. BenYaala,[34] S. Bera,[11] M. Berbel,[93] F. Bergamin,[9,10] B. K. Berger,[79] S. Bernuzzi,[13] C. P. L. Berry,[25] D. Bersanetti,[94] A. Bertolini,[61] J. Betzwieser,[58] D. Beveridge,[95] R. Bhandare,[96] A. V. Bhandari,[11] U. Bhardwaj,[39,61] R. Bhatt,[1] D. Bhattacharjee,[97] S. Bhaumik,[78] A. Bianchi,[61,98] I. A. Bilenko,[99] G. Billingsley,[1] S. Bini,[100,101] R. Birney,[102] O. Birnholtz,[103] S. Biscans,[1,76] M. Bischi,[56,57] S. Biscoveanu,[76] A. Bisht,[9,10] B. Biswas,[11] M. Bitossi,[48,18] M.-A. Bizouard,[38] J. K. Blackburn,[1] C. D. Blair,[95] D. G. Blair,[95] R. M. Blair,[74] F. Bobba,[104,105] N. Bode,[9,10] M. Boër,[38] G. Bogaert,[38] M. Boldrini,[106,59] G. N. Bolingbroke,[90] L. D. Bonavena,[82] F. Bondu,[107] E. Bonilla,[79] R. Bonnand,[31] P. Booker,[9,10] B. A. Boom,[61] R. Bork,[1] V. Boschi,[18] N. Bose,[108] S. Bose,[11] V. Bossilkov,[95] V. Boudart,[70] Y. Bouffanais,[82,83] A. Bozzi,[48] C. Bradaschia,[18] P. R. Brady,[6] A. Bramley,[58] A. Branch,[58] M. Branchesi,[33,109] J. E. Brau,[68] M. Breschi,[13] T. Briant,[110] J. H. Briggs,[25] A. Brillet,[38] M. Brinkmann,[9,10] P. Brockill,[6] A. F. Brooks,[1] J. Brooks,[48] D. D. Brown,[90] S. Brunett,[1] G. Bruno,[60] R. Bruntz,[65] J. Bryant,[14] F. Bucci,[57] T. Bulik,[111] H. J. Bulten,[61] A. Buonanno,[112,113] K. Burtnyk,[74] R. Buscicchio,[14] D. Buskulic,[31] C. Buy,[114] R. L. Byer,[79] G. S. Cabourn Davies,[53] G. Cabras,[35,36] R. Cabrita,[60] L. Cadonati,[49] M. Caesar,[115] G. Cagnoli,[27] C. Cahillane,[74] J. Calderón Bustillo,[116] J. D. Callaghan,[25] T. A. Callister,[117,118] E. Calloni,[26,4] J. Cameron,[95] J. B. Camp,[119] M. Canepa,[120,94] S. Canevarolo,[67] M. Cannavacciuolo,[104] K. C. Cannon,[29] H. Cao,[90] Z. Cao,[121] E. Capocasa,[46,20] E. Capote,[69] G. Carapella,[104,105] F. Carbognani,[48] M. Carlassara,[9,10] J. B. Carlin,[122] M. F. Carney,[15] M. Carpinelli,[123,124,48] G. Carrillo,[68] G. Carullo,[80,18] T. L. Carver,[17] J. Casanueva Diaz,[48] C. Casentini,[125,126] G. Castaldi,[127] S. Caudill,[61,67] M. Cavaglià,[97] F. Cavalier,[47] R. Cavalieri,[48] G. Cella,[18] P. Cerdá-Durán,[128] E. Cesarini,[126] W. Chaibi,[38] S. Chalathadka Subrahmanya,[129] E. Champion,[130] C.-H. Chan,[131] C. Chan,[29] C. L. Chan,[132] K. Chan,[132] M. Chan,[133] K. Chandra,[108] I. P. Chang,[131] P. Chanial,[48] S. Chao,[131] C. Chapman-Bird,[25] P. Charlton,[134] E. A. Chase,[15] E. Chassande-Mottin,[46] C. Chatterjee,[95] Debarati Chatterjee,[11] Deep Chatterjee,[6] M. Chaturvedi,[96] S. Chaty,[46] K. Chatziioannou,[1] C. Chen,[135,136] D. Chen,[54] H. Y. Chen,[76] J. Chen,[131] K. Chen,[137] X. Chen,[95] Y.-B. Chen,[138] Y.-R. Chen,[139] Z. Chen,[17] H. Cheng,[78] C. K. Cheong,[132] H. Y. Cheung,[132] H. Y. Chia,[78] F. Chiadini,[140,105] C-Y. Chiang,[141] G. Chiarini,[83] R. Chierici,[142] A. Chincarini,[94] M. L. Chiofalo,[80,18] A. Chiummo,[48] R. K. Choudhary,[95] S. Choudhary,[11] N. Christensen,[38] Q. Chu,[95] Y-K. Chu,[141] S. S. Y. Chua,[8] K. W. Chung,[62] G. Ciani,[82,83] P. Ciecielag,[88] M. Cieślar,[88] M. Cifaldi,[125,126] A. A. Ciobanu,[90] R. Ciolfi,[143,83] F. Cipriano,[38] F. Clara,[74] J. A. Clark,[1,49] P. Clearwater,[144] S. Clesse,[145] F. Cleva,[38] E. Coccia,[33,109] E. Codazzo,[33] P.-F. Cohadon,[110] D. E. Cohen,[47] M. Colleoni,[22] C. G. Collette,[146] A. Colombo,[71,72] M. Colpi,[71,72] C. M. Compton,[74] M. Constancio Jr.,[16] L. Conti,[83] S. J. Cooper,[14] P. Corban,[58] T. R. Corbitt,[7] I. Cordero-Carrión,[147] S. Corezzi,[81,41] K. R. Corley,[52] N. J. Cornish,[85] D. Corre,[47] A. Corsi,[148] S. Cortese,[48] C. A. Costa,[16] R. Cotesta,[113] R. Cottingham,[58] M. W. Coughlin,[149] J.-P. Coulon,[38] S. T. Countryman,[52] B. Cousins,[150] P. Couvares,[1] D. M. Coward,[95] M. J. Cowart,[58] D. C. Coyne,[1] R. Coyne,[151] J. D. E. Creighton,[6] T. D. Creighton,[91] A. W. Criswell,[149] M. Croquette,[110] S. G. Crowder,[152] J. R. Cudell,[70] T. J. Cullen,[7] A. Cumming,[25] R. Cummings,[25] L. Cunningham,[25] E. Cuoco,[48,153,18] M. Curyło,[111] P. Dabadie,[27] T. Dal Canton,[47] S. Dall'Osso,[33] G. Dálya,[87,154] A. Dana,[79] B. D'Angelo,[120,94] S. Danilishin,[155,61] S. D'Antonio,[126] K. Danzmann,[9,10] C. Darsow-Fromm,[129] A. Dasgupta,[86] L. E. H. Datrier,[25] Sayak Datta,[11] Sayantani Datta,[50] V. Dattilo,[48] I. Dave,[96] M. Davier,[47] D. Davis,[1] M. C. Davis,[115] E. J. Daw,[156] R. Dean,[115] D. DeBra,[79] M. Deenadayalan,[11] J. Degallaix,[157] M. De Laurentis,[26,4] S. Deléglise,[110] V. Del Favero,[130] F. De Lillo,[60] N. De Lillo,[25] D. Dell'Aquila,[123] W. Del Pozzo,[80,18] L. M. DeMarchi,[15] F. De Matteis,[125,126] V. D'Emilio,[17] N. Demos,[76] T. Dent,[116] A. Depasse,[60] R. De Pietri,[158,159] R. De Rosa,[26,4] C. De Rossi,[48] R. DeSalvo,[127,160] R. De Simone,[140] S. Dhurandhar,[11] M. C. Díaz,[91] N. A. Didio,[69] T. Dietrich,[113] L. Di Fiore,[4] C. Di Fronzo,[14]

TABLE VII. Results for the modified dispersion analysis (Sec. VI). The table shows 90%-credible upper bounds on the graviton mass m_g and the absolute value of the dimensionless phenomenological parameter $\tilde{A}_\alpha = A_\alpha/\mathrm{eV}^{2-\alpha}$. $Q_{\rm GR} = P(A_\alpha < 0)$ denotes the quantiles corresponding to GR hypothesis. The < and > labels denote the bounds on $|\tilde{A}_\alpha|$ for $A_\alpha > 0$ and $A_\alpha < 0$ respectively. We also included bounds computed from GWTC-2 [10, 11] for comparison.

	m_g	$\lvert\tilde{A}_0\rvert$			$\lvert\tilde{A}_{0.5}\rvert$			$\lvert\tilde{A}_1\rvert$			$\lvert\tilde{A}_{1.5}\rvert$			$\lvert\tilde{A}_{2.5}\rvert$			$\lvert\tilde{A}_3\rvert$			$\lvert\tilde{A}_{3.5}\rvert$			$\lvert\tilde{A}_4\rvert$		
	$[10^{-23}$	<	>	$Q_{\rm GR}$	<	>	$Q_{\rm GR}$	<	>	$Q_{\rm GR}$	<	>	$Q_{\rm GR}$	<	>	$Q_{\rm GR}$	<	>	$Q_{\rm GR}$	<	>	$Q_{\rm GR}$	<	>	$Q_{\rm GR}$
	$\mathrm{eV}/c^2]$	$[10^{-45}]$		[%]	$[10^{-38}]$		[%]	$[10^{-32}]$		[%]	$[10^{-26}]$		[%]	$[10^{-14}]$		[%]	$[10^{-8}]$		[%]	$[10^{-2}]$		[%]	$[10^{4}]$		[%]
GWTC-2	1.76	1.75	1.37	66	0.46	0.28	66	1.00	0.52	79	3.35	1.47	83	1.74	2.43	31	1.08	2.17	17	0.76	1.57	12	0.64	0.88	25
GWTC-3	1.27	1.88	0.89	86	0.51	0.19	91	1.16	0.32	96	3.69	0.93	98	1.16	2.95	13	0.66	2.33	2	0.45	1.16	7	0.30	0.74	15

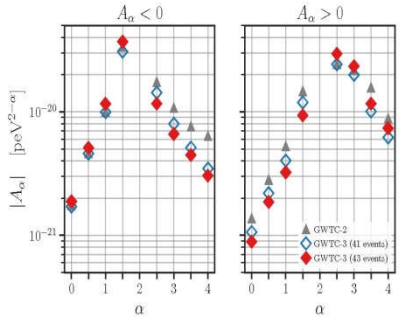

FIG. 12. Results for the modified dispersion analysis (Sec. VI). The scatter plot of 90% credible upper bounds on the modulus of deviation parameters A_α. The one-sided bounds are computed for positive and negative values of the parameters separately. Filled (open) diamond markers represent the GWTC-3 bounds including (excluding) the events GW200219_094415 and GW200225_060421. The gray markers in the background denoted the numbers obtained from the previous analysis [11].

of a signal $\tilde{\boldsymbol{s}}(f)$ and noise $\tilde{\boldsymbol{n}}(f)$, or alternatively, as

$$\tilde{\boldsymbol{d}}(f) = \boldsymbol{F}\tilde{\boldsymbol{h}}(f) + \tilde{\boldsymbol{n}}(f), \tag{10}$$

where $\tilde{\boldsymbol{s}}(f) = \boldsymbol{F}\tilde{\boldsymbol{h}}(f)$, $\boldsymbol{F} \in \mathbb{R}^{D\times M}$ are the beam pattern functions of the detectors and $\tilde{\boldsymbol{h}}(f) \in \mathbb{C}^M$ are the signal's polarization modes. We could interpret the gravitational-wave signal as a geometric projection on the subspace spanned by the basis vectors of $\boldsymbol{F}$. By projecting the data on the subspace orthogonal to these vectors, one can then construct null streams, i.e., linear combinations of the data containing no information on the signal [238, 239]. Given D detectors, it is possible to construct at most $D - M$ null streams. The projection operation can be formalized through the introduction of a null operator $\boldsymbol{P}$ [240]

$$\boldsymbol{P} = \boldsymbol{I} - \boldsymbol{F}(\boldsymbol{F}^\dagger\boldsymbol{F})^{-1}\boldsymbol{F}^\dagger, \tag{11}$$

where $\boldsymbol{I}$ is the identity matrix and † denotes conjugate transpose. The quantities $\boldsymbol{F}$ depend on the sky location of the signal, as well on the polarization angle and event time and, by construction, $\boldsymbol{P}\tilde{\boldsymbol{s}}(f) = 0$.

At least $M + 1$ detectors are needed to apply the null stream method in the most generic case, although for specific sky locations less detectors will suffice to test certain polarization hypotheses [241, 242]. The beam pattern functions of the breathing and longitudinal scalar modes are not linearly independent, and thus the maximum number of independent polarization modes is five [243, 244]. Consequently, past analyses [7, 9, 11, 245] tested only pure polarization hypotheses, as these are fully characterized by two polarisation modes at most, and in this case it is possible to construct a null stream with the strain measured by three detectors.

In this work, we use a method that allows tests of mixed polarization states with 2 and 3 detectors [246]. This enables all our events to be used to compute combined Bayes factors, while the previous analysis [11] was restricted to 3-detector events. The method builds upon an *effective antenna pattern function* $\bar{\boldsymbol{F}} \in \mathbb{C}^{D\times L}$ that is constructed from a subset of $L < M$ polarization modes. For each hypothesis to be tested, the relevant polarization state is projected into the chosen basis: thus, one orthogonalizes the data with respect to a smaller subspace spanned by the basis modes, rather than the assumed polarization modes. Each polarization mode $\tilde{h}_m$ can be rewritten as a linear combination of the basis modes, plus an additional orthogonal component

$$\tilde{h}_m(f) = \sum_{k=1}^{L} C_m^{\parallel}\tilde{h}_{\parallel,k}(f) + C_m^{\perp}\tilde{h}_\perp(f), \tag{12}$$

with $C_m^{\parallel}, C_m^{\perp} \in \mathbb{C}$. We perform the null projection with respect to the subspace spanned by the component of the beam pattern vectors parallel to the basis mode(s). Therefore, the method is sensitive to any component of a given polarization hypothesis that is parallel to the chosen basis modes(s). The subspace removed by the null projection does not need to coincide with the polarization subspace of the hypothesis being tested.

We will conduct analyses employing either one ($L = 1$) or two ($L = 2$) basis modes. The $L = 2$ parameterization allows more freedom in the choice of the basis modes, but at the cost of a weaker distinguishability between different polarization hypotheses. The subspaces spanned by the beam pattern function vectors for different hypotheses, in fact, will generally have a larger overlap in the $L = 2$ than in $L = 1$ case. The polarization content is constrained to be a linear combination of the basis modes and, therefore, the $L = 1$ analysis is expected to produce more stringent results, due to the strongest constraints imposed on the signal. On the other hand, the $L = 2$ analysis will be able to capture orthogonal components missed by the $L = 1$ analysis.

Right ascension, declination and polarization angle are free

Journal of Cosmology and Astroparticle Physics
An IOP and SISSA journal

Constraining the range of Yukawa gravity interaction from S2 star orbits II: bounds on graviton mass

A.F. Zakharov,[a,b,c,d,e] **P. Jovanović,**[f] **D. Borka**[g] **and V. Borka Jovanović**[g]

[a]National Astronomical Observatories of Chinese Academy of Sciences, Datun Road 20A, Beijing, 100012 China
[b]Institute of Theoretical and Experimental Physics, 117259 Moscow, Russia
[c]National Research Nuclear University MEPhI (Moscow Engineering Physics Institute), 115409, Moscow, Russia
[d]Bogoliubov Laboratory for Theoretical Physics, JINR, 141980 Dubna, Russia
[e]North Carolina Central University, Durham, NC 27707, U.S.A.
[f]Astronomical Observatory, Volgina 7, 11060 Belgrade, Serbia
[g]Atomic Physics Laboratory (040), Vinča Institute of Nuclear Sciences, University of Belgrade, P.O. Box 522, 11001 Belgrade, Serbia

E-mail: zakharov@itep.ru, pjovanovic@aob.rs, dusborka@vin.bg.ac.rs, vborka@vin.bg.ac.rs

Received May 4, 2016
Accepted May 7, 2016
Published May 20, 2016

Abstract. Recently LIGO collaboration discovered gravitational waves [1] predicted 100 years ago by A. Einstein. Moreover, in the key paper reporting about the discovery, the joint LIGO & VIRGO team presented an upper limit on graviton mass such as $m_g < 1.2 \times 10^{-22} eV$ [1] (see also more details in another LIGO paper [2] dedicated to a data analysis to obtain such a small constraint on a graviton mass). Since the graviton mass limit is so small the authors concluded that their observational data do not show violations of classical general relativity. We consider another opportunity to evaluate a graviton mass from phenomenological consequences of massive gravity and show that an analysis of bright star trajectories could bound graviton mass with a comparable accuracy with accuracies reached with gravitational wave interferometers and expected with forthcoming pulsar timing observations for gravitational wave detection. It gives an opportunity to treat observations of

doi:10.1088/1475-7516/2016/05/045

JCAP05(2016)045

Constraints on graviton mass from S2 trajectory

- AFZ, D. Borka, P. Jovanovic, V. Borka Jovanovic gr-qc: 1605.00913v; JCAP (2016) :
- $\lambda_g > 2900$ AU $= 4.3 \times 10^{11}$ km with P=0.9 or
- $m_g < 2.9 \times 10^{-21}$ eV $= 5.17 \times 10^{-54}$ g
- Hees et al. PRL (2017) slightly improved our estimates with their new data $m_g < 1.6 \times 10^{-21}$ eV (see discussion below)

graviton MASS

It is likely that the graviton is massless. More than fifty years ago Van Dam and Veltman (VANDAM 1970), Iwasaki (IWASAKI 1970), and Zakharov (ZAKHAROV 1970) almost simultaneously showed that in the linear approximation a theory with a finite graviton mass does not approach GR as the mass approaches zero. Attempts have been made to evade this "vDVZ discontinuity" by invoking modified gravity or nonlinear theory by De Rahm (DE-RHAM 2017) and others. More recently, the analysis of gravitational wave dispersion has led to bounds that are largely independent of the underlying model, even if not the strongest. We quote the best of these as our best limit.

Experimental limits have been set based on a Yukawa potential (YUKA), dispersion relation (DISP), or other modified gravity theories (MGRV).

The following conversions are useful: 1 eV = 1.783×10^{-33} g = $1.957 \times 10^{-6} m_e$; $\lambda_C = (1.973 \times 10^{-7}\ \text{m}) \times (1\ \text{eV}/m_g)$.

VALUE (eV)	*DOCUMENT ID*		*TECN*	*COMMENT*
$< 5 \times 10^{-23}$	[1] ABBOTT	2019	DISP	LIGO Virgo catalog GWTC-1
• • We do not use the following data for averages, fits, limits, etc. • •				
$< 3.2 \times 10^{-23}$	[2] BERNUS	2020	YUKA	Planetary ephemeris INPOP19a
$< 2 \times 10^{-28}$	[3] SHAO	2020	DISP	Binary pulsar Galileon radiation
$< 7 \times 10^{-23}$	[4] BERNUS	2019	YUKA	Planetary ephemeris INPOP17b
$< 3.1 \times 10^{-20}$	[5] MIAO	2019	DISP	Binary pulsar orbital decay rate
$< 1.4 \times 10^{-29}$	[6] DESAI	2018	YUKA	Gal cluster Abell 1689
$< 5 \times 10^{-30}$	[7] GUPTA	2018	YUKA	Using SPT-SZ
$< 3 \times 10^{-30}$	[7] GUPTA	2018	YUKA	Using Planck all-sky SZ
$< 1.3 \times 10^{-29}$	[7] GUPTA	2018	YUKA	Using redMaPPer SDSS-DR8
$< 6 \times 10^{-30}$	[8] RANA	2018	YUKA	Weak lensing in massive clusters
$< 8 \times 10^{-30}$	[9] RANA	2018	YUKA	SZ effect in massive clusters
$< 1.0 \times 10^{-23}$	[10] WILL	2018	YUKA	Perihelion advances of planets
$< 7 \times 10^{-23}$	[1] ABBOTT	2017	DISP	Combined dispersion limit from three BH mergers
$< 1.2 \times 10^{-22}$	[1] ABBOTT	2016	DISP	Combined dispersion limit from two BH mergers
$< 2.9 \times 10^{-21}$	[11] ZAKHAROV	2016	YUKA	S2 star orbit
$< 5 \times 10^{-23}$	[12] BRITO	2013	MGRV	Spinning black holes bounds
$< 6 \times 10^{-32}$	[13] GRUZINOV	2005	MGRV	Solar System observations
$< 6 \times 10^{-32}$	[14] CHOUDHURY	2004	YUKA	Weak gravitational lensing
$< 9.0 \times 10^{-34}$	[15] GERSHTEIN	2004	MGRV	From Ω_{tot} value assuming RTG
$< 8 \times 10^{-20}$	[16, 17] FINN	2002	DISP	Binary pulsar orbital period decrease
$< 7 \times 10^{-23}$	TALMADGE	1988	YUKA	Solar system planetary astrometric data
$< 1.3 \times 10^{-29}$	[18] GOLDHABER	1974	YUKA	Rich clusters
$< 7 \times 10^{-28}$	HARE	1973	YUKA	Galaxy
$< 8 \times 10^{4}$	HARE	1973	YUKA	2γ decay

[1] ABBOTT 2019 , ABBOTT 2017 , and ABBOTT 2016 limits assume a dispersion relation for gravitational waves modified relative to GR.

[2] BERNUS 2020 use the latest solution of the ephemeris INPOP (19a) in order to improve the constraint in BERNUS 2019 on the existence of a Yukawa suppression to the Newtonian potential, generically associated to a gravitons mass.

[3] SHAO 2020 sets limit, 95% CL, based on non-observation of excess gravitational radiation in 14 well-timed binary pulsars in the context of the cubic Galileon model.

[4] BERNUS 2019 use the planetary ephemeris INPOP 17b to constraint the existence of a Yukawa suppression to the Newtonian potential, generically associated to a gravitons mass.

[5] MIAO 2019 90% CL limit is based on orbital period decay rates of 9 binary pulsars using a Bayesian prior uniform in graviton mass. Limit becomes $< 5.2 \times 10^{-21}$ eV for a prior uniform in ln(m_g).

[6] DESAI 2018 limit based on dynamical mass models of galaxy cluster Abell 1689.

VALUE (eV)	*DOCUMENT ID*	*TECN*	*COMMENT*

[7] GUPTA 2018 obtains graviton mass limits using stacked clusters from 3 disparate surveys.

[8] RANA 2018 limit, 68% CL, obtained using weak lensing mass profiles out to the radius at which the cluster density falls to 200 times the critical density of the Universe. Limit is based on the fractional change between Newtonian and Yukawa accelerations for the 50 most massive galaxy clusters in the Local Cluster Substructure Survey. Limits for other CL's and other density cuts are also given.

[9] RANA 2018 limit, 68% CL, obtained using mass measurements via the SZ effect out to the radius at which the cluster density falls to 500 times the critical density of the Universe for 182 optically confirmed galaxy clusters in an Altacama Cosmology Telescope survey. Limits for other CL's and other density cuts are also given.

[10] WILL 2018 limit from perihelion advances of the planets, notably Earth, Mars, and Saturn. Alternate analysis yields $< 6 \times 10^{-24}$.

[11] ZAKHAROV 2016 constrains range of Yukawa gravity interaction from S2 star orbit about black hole at Galactic center. The limit is $< 2.9 \times 10^{-21}$ eV for $\delta = 100$.

[12] BRITO 2013 explore massive graviton (spin-2) fluctuations around rotating black holes.

[13] GRUZINOV 2005 uses the DGP model (DVALI 2000) showing that non-perturbative effects restore continuity with Einstein's equations as the gravition mass approaches zero, then bases his limit on Solar System observations.

[14] CHOUDHURY 2004 concludes from a study of weak-lensing data that masses heavier than about the inverse of 100 Mpc seem to be ruled out if the gravitation field has the Yukawa form.

[15] GERSHTEIN 2004 use non-Einstein field relativistic theory of gravity (RTG), with a massive graviton, to obtain the 95% CL mass limit implied by the value of Ω_{tot} = 1.02 ± 0.02 current at the time of publication.

[16] FINN 2002 analyze the orbital decay rates of PSR B1913+16 and PSR B1534+12 with a possible graviton mass as a parameter. The combined frequentist mass limit is at 90%CL.

[17] As of 2020, limits on dP/dt are now about 0.1% (see T. Damour, "Experimental tests of gravitational theory," in this *Review*).

[18] GOLDHABER 1974 establish this limit considering the binding of galactic clusters, corrected to Planck h_0 = 0.67.

References:

BERNUS	2020	PR D102 021501	Constraint on the Yukawa suppression of the Newtonian potential from the planetary ephemeris INPOP19a
SHAO	2020	PR D102 024069	New Graviton Mass Bound from Binary Pulsars
ABBOTT	2019	PR D100 104036	Tests of General Relativity with the Binary Black Hole Signals from the LIGO-Virgo Catalog GWTC-1
BERNUS	2019	PRL 123 161103	Constraining the mass of the graviton with the planetary ephemeris INPOP
MIAO	2019	PR D99 123015	Bounding the mass of graviton in a dynamic regime with binary pulsars
DESAI	2018	PL B778 325	Limit on graviton mass from galaxy cluster Abell 1689
GUPTA	2018	ANP 399 85	Limit on graviton mass using stacked galaxy cluster catalogs from SPT-SZ, Planck-SZ and SDSS-redMaPPer
RANA	2018	PL B781 220	Bounds on graviton mass using weak lensing and SZ effect in galaxy clusters
WILL	2018	CQG 35 17LT01	Solar system versus gravitational-wave bounds on the graviton mass
ABBOTT	2017	PRL 118 221101	GW170104: Observation of a 50-Solar-Mass Binary Black Hole Coalescence at Redshift 0.2
ABBOTT	2016	PRL 116 061102	Observation of Gravitational Waves from a Binary Black Hole Merger
ZAKHAROV	2016	JCAP 1605 045	Constraining the range of Yukawa gravity interaction from S2 star orbits II: Bounds on graviton mass
BRITO	2013	PR D88 023514	Massive Spin-2 Fields on Black Hole Spacetimes: Instability of the Schwarzschild and Kerr Solutions and Bounds on the Graviton Mass
GRUZINOV	2005	NAST 10 311	On the Graviton Mass
CHOUDHURY	2004	ASP 21 559	Probing Large Distance Higher Dimensional Gravity from Lensing Data
GERSHTEIN	2004	PAN 67 1596	Graviton Mass, Quintessence and Oscillatory Character of the Universe Evolution
FINN	2002	PR D65 044022	Bounding the Mass of the Graviton using Binary Pulsar Observations
TALMADGE	1988	PRL 61 1159	Model Independent Constraints on Possible Modifications of Newtonian Gravity
GOLDHABER	1974	PR D9 1119	Mass of the Graviton
HARE	1973	CJP 51 431	Mass of the Graviton

Mid summer dispute

MGM 16 (July 10, 2021): Saturday round table

https://www.youtube.com/watch?v=pxoq-H4cXqE

Subject: Nature of Galactic Center

Two alternatives: SMBH vs RAR model for DM

Two opponents: R. Genzel vs C. Arguelles

Genzel: «Any theoretical model must
Schwarzschild precession for S2 orbit»

The smallest angle between apocenter and pericenter

- $\Phi_{HO}=\pi/2$
- $\Phi_{N}=\pi$

If astronomers monitor quasi-elliptical trajectories of stars with high eccentricities it is very easy to distinguish $U_{HO}(r)$ and $U_N(r)$ potentials since in the case of the RAR potential stars centers of ellipses should coincide with the Galactic Center while in the case of the Newtonian potential stars foci of the ellipses coincide with the Center.
Orbital periods of stars moving in the harmonic oscillator potential are constant and they do not depend on semi-major axis. Even in the case if the Galactic Center position is not accurately known in respect to quasi-elliptical trajectories, a set of trajectories with high eccentricity clearly showed that the Newtonian potential is preferable and stars are moving around a common focus but not around a common center (Zakharov, arXiv:2108.09709, MNRAS Letters, 2022)

V.I. Arnol'd

HUYGENS AND BARROW, NEWTON AND HOOKE

Pioneers in mathematical analysis and catastrophe theory from evolvents to quasicrystals

Translated from the Russian by Eric J.F. Primrose

1990 Birkhäuser Verlag
Basel · Boston · Berlin

direction than the point of the surface over which it was. Thus, the ball should fall not to the west, but to the east of this point.

If the balls are dropped not on the equator, but at our latitude, then the effect will be somewhat smaller, but nevertheless, says Newton, it should be possible to discover it. Of course, this effect is very small, so Newton advises doing the following. Under the point from which it is dropped and strictly from the plumb-line it is necessary to put a "steel" in the direction from north to south and to drop possibly heavier balls, having suspended them on a thread and burning it through in order to avoid unwanted initial jolts. Then, if we drop a ball sufficiently many times and calculate how many times the ball, on striking the steel, flies off to the east, and how many times to the west, we can, by comparing these two numbers, determine whether one can observe a subtle effect of deflecting to the east or not.

In his remarkable letter to Hooke, Newton touched on one more question. He discussed how a ball would move after reaching the surface if there were a shaft in the Earth (that is, the ball moves through the Earth without meeting any resistance). Newton assumed that the ball would then describe a spiral, and for clarity drew this spiral in the letter (Fig. 3).

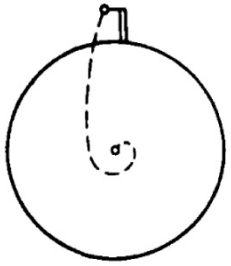

Fig. 3.
A trajectory inside the Earth according to Newton

Hooke read Newton's letter to the session of the Royal Society on 4 December 1679. This caused a lively discussion, in which many scientists took part. Everyone debated animatedly whether it was actually possible to observe the phenomenon described by Newton and on what side the balls must be deflected. For example, The Royal Astronomer Flamsteed came forward, as laid down in the protocol of the Society, with the statement that this effect had been known in the artillery for a long time. Namely, in Flamsteed's opinion, a shot

distances to the centre of the Earth and the shift to the west caused by the difference in the direction of the force of gravity are quantities of the same order, so Newton's qualitative argument is altogether false. If these two effects – deflection to the east and deflection to the west – had a slightly different relation, the qualitative picture would be different.

Secondly, Hooke rightly observed that in the northern hemisphere a ball is deflected not only to the east, but also to the south. Moreover, he asserted (for incomprehensible reasons) that at our latitudes the deflection to the south is even greater than that to the east.

Finally, Hooke made a remark referring to the trajectory of motion of a ball inside the Earth. He says that the spiral drawn by Newton causes him some doubt. In his opinion, inside the Earth approximately the same will happen as under an oscillation of a pendulum on a string, and if a ball moves freely inside the Earth without experiencing resistance, then its trajectory will be closed

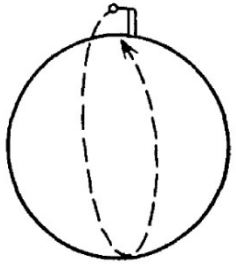

Fig. 4.
Trajectories inside the Earth according to Hooke

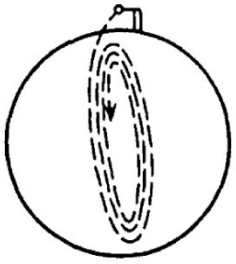

Fig. 5.
Taking account of air resistance according to Hooke

and remind us of an ellipse (Fig. 4), and a spiral can be obtained only by taking account of air resistance. But in this case the spiral obtained is not the same as Newton's, not making one circuit, but slowly winding, with a large number of rotations (Fig. 5).

Robert Hooke met Isaac Newton at the Galactic Center since we have to choose $U_{HO}(r)$ or $U_N(r)$ to fit bright star trajectories. Moreover, EHT estimates of shadow size for Sgr A* are consistent with SMBH model.

Conclusion:

At GC potential must be very close to $U_N(r)$

Shadow reconstructions for M87* and Sgr A* are based on three pillars: Synchrotron radiation, VLBI concept, GR in a strong gravitational field

Synchrotron radiation George A. Schott)

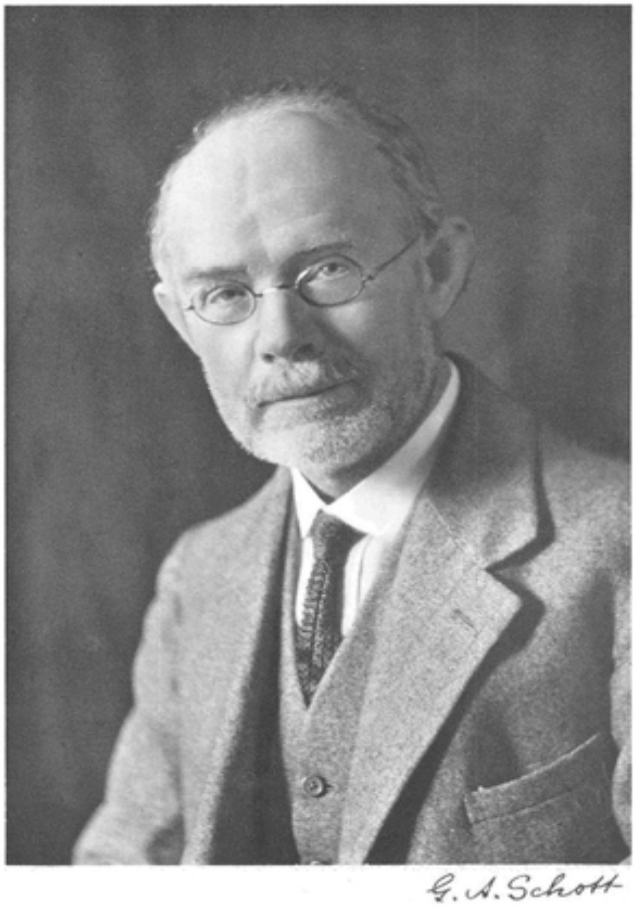

ELECTROMAGNETIC RADIATION

AND THE MECHANICAL REACTIONS ARISING FROM IT

BEING AN ADAMS PRIZE ESSAY IN THE UNIVERSITY OF CAMBRIDGE

by

G. A. SCHOTT, B.A., D.Sc.
Professor of Applied Mathematics in the University College of Wales, Aberystwyth
Formerly Scholar of Trinity College, Cambridge

Cambridge:
at the University Press
1912

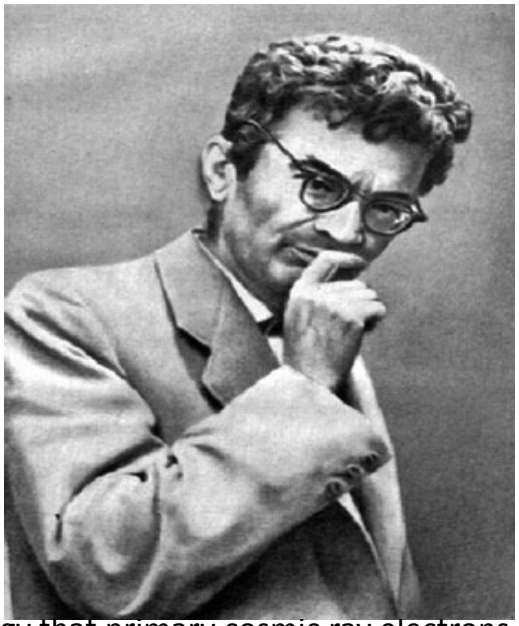

I. Pomeranchuk, The maximum energy that primary cosmic ray electrons can have on the Earth's surface due to radiation in the Earth's magnetic field, J. Phys. USSR, 2, 356 (1940)

D. Ivanenko and I. Pomeranchuk, On the Maximal Energy Attainable in a Betatron, Phys. Rev. 65, 343 (1944)

L.A. Artsimovich and I. Pomeranchuk, The maximum energy that primary cosmic ray electrons can have on the Earth's surface due to radiation in the Earth's magnetic field, J. Phys. USSR, 2, 267 (1945)

Elder, F. R., Gurewitsch, A. M., Langmuir, R. V., & Pollock, H. C. Radiation from Electrons in a Synchrotron. Physical Review, 71(11), 829 (1947)

In 1950 D. Ivanenko, A. A. Sokolov and I. Pomeranchuk were awarded the State prize of the second grade for works on synchrotron radiation, presented in book “Classical Field Theory”

Professor Arsenij Alexandrovich Sokolov and professor Dmitrij Dmitrievich Ivanenko

Academician Lev Andreevich Artsimovich (the founder of the Atomic physics chair at Physical department of MSU, Academician secretary of the General Physics and Astronomy division of the Soviet Acdemy of Sciences, the chairman of the National committee of physicists)

Synchrotron radiation plays a key role in many astrophysical objects (including BH's and pulsars (Crab Nebula)) . In 1946 they predicted emission in radio band from solar corona. In May 1947 they participated in Brazil expedition

The Soviet expedition in Brazil for solar eclipse observations in 20 May 1947 where S. E. Khaikin and B. M. Chikhachev discovered radio emission from solar corona during the solar eclipse aboard the “Griboedov” ship

The idea of VLBI observation was introduced by L. I. Matveenko (1929—2019) in 1960s and it was realized in Soviet – US joint radio observations in 1970s. Matveenko proposed also a project of a ground – space interferometer. This idea was realized later by Japanese (HALCA, VSOP, 1997) and Russian Astronomers (Radioastron, 2011) .

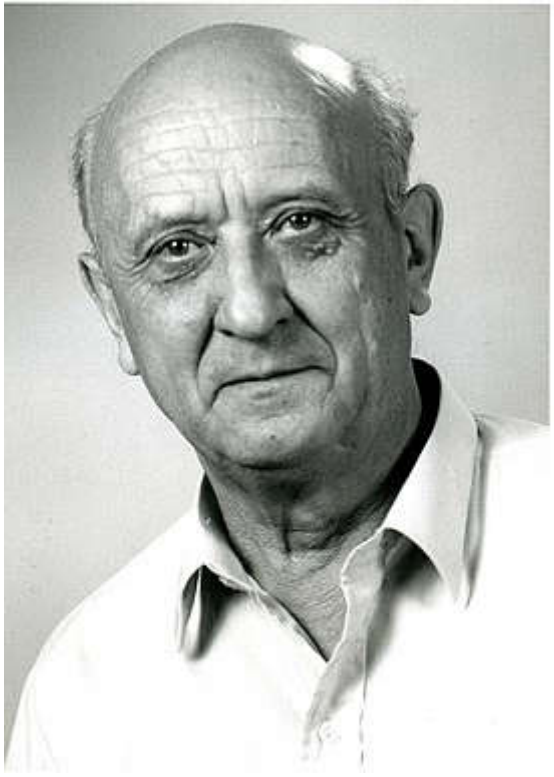

EHT shadow reconstruction for M87* and Sgr A* observed in April 2017

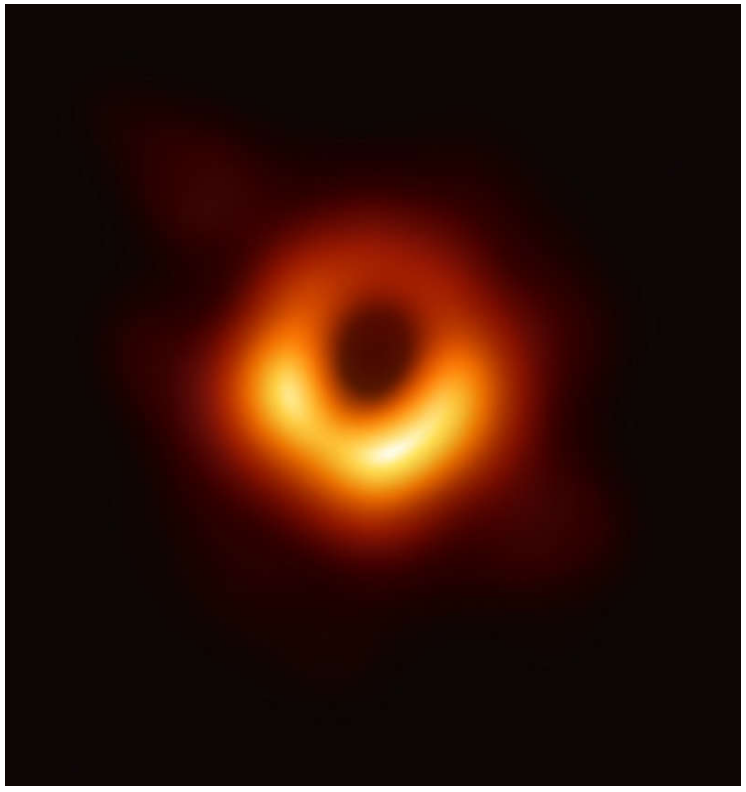

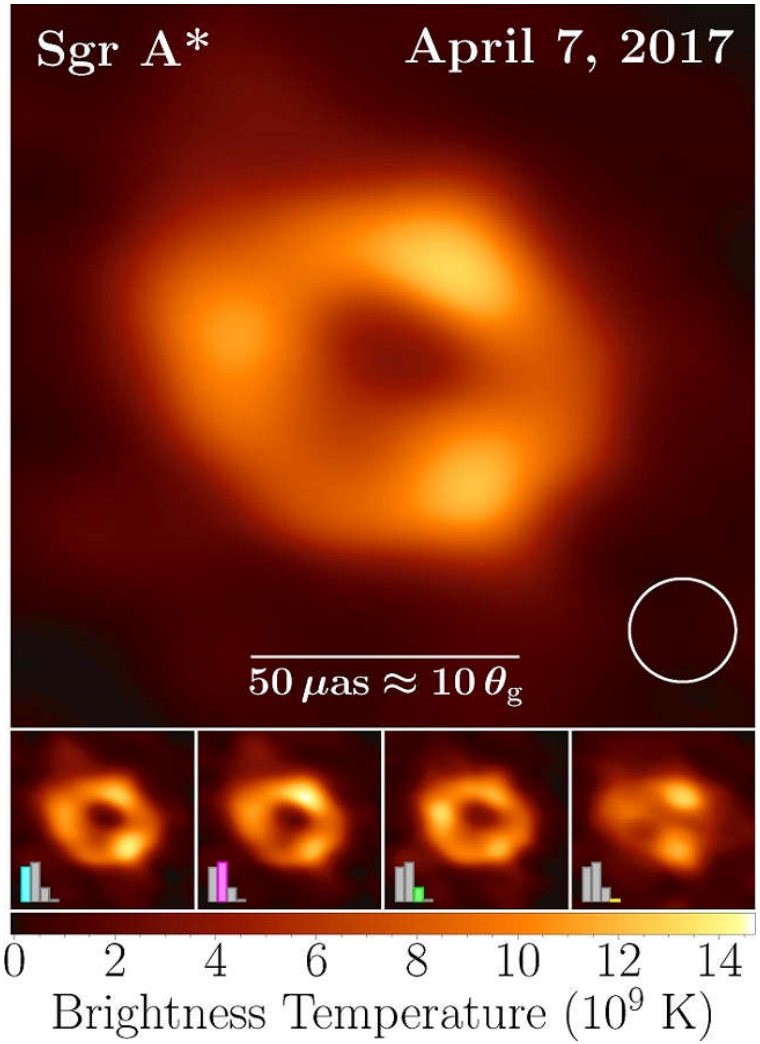

'A majestic story'
Financial Times

MICHIO KAKU

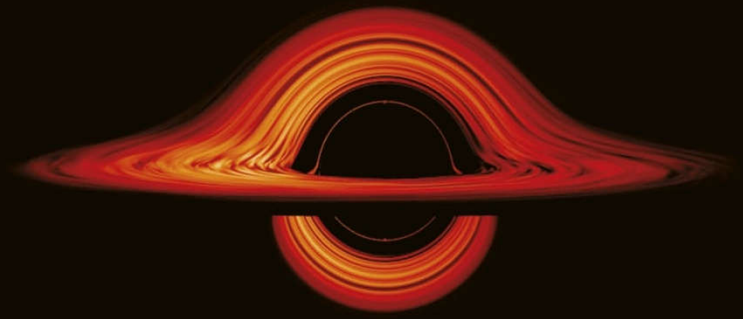

THE GOD EQUATION

The Quest for a Theory of Everything

https://www.gazeta.ru/science/news/2022/06/15/17937578.shtml

- 15 июня 2022, 16:03
- **Сбылось предсказание российского ученого о загадочной тени**
- Борис Ганьжин
-
- Первое изображение сверхмассивной черной дыры в центре Млечного Пути, о получении которого в мае 2022 года **сообщила** коллаборация Телескопа горизонта событий Event Horizon Telescope, послужило подтверждением предсказания ведущего научного сотрудника лаборатории физики плазмы и астрофизики ККТЭФ НИЦ «Курчатовский институт» Александра Захарова и его итальянских коллег, сделанного в 2005 году. Об этом «Газете.Ru» сообщили в НИЦ «Курчатовский институт».

For about 20 years we declared black holes (for theorists) are dark spots (shadows) for observers

Available online at www.sciencedirect.com
SCIENCE DIRECT®
New Astronomy 10 (2005) 479–489
New Astronomy
www.elsevier.com/locate/newast

Measuring the black hole parameters in the galactic center with RADIOASTRON

A.F. Zakharov [a,b,c,*], A.A. Nucita [d], F. DePaolis [d], G. Ingrosso [d]

[a] Institute of Theoretical and Experimental Physics, 25, B. Cheremushkinskaya st., Moscow 117259, Russia
[b] Space Research Centre of Lebedev Physics Institute, Moscow, Russia
[c] Joint Institute for Nuclear Research, Dubna, Russia
[d] Dipartimento di Fisica, Universita di Lecce and INFN, Sezione di Lecce, Italy

Received 19 January 2005; accepted 21 February 2005
Available online 23 March 2005
Communicated by F. Melchiorri

Abstract

Recently, Holz and Wheeler (2002) [ApJ 578, 330] considered a very attracting possibility to detect retro-MACHOs, i.e., retro-images of the Sun by a Schwarzschild black hole. In this paper, we discuss glories (mirages) formed near rapidly rotating Kerr black hole horizons and propose a procedure to measure masses and rotation parameters analyzing these forms of mirages. In some sense that is a manifestation of gravitational lens effect in the strong gravitational field near black hole horizon and a generalization of the retro-gravitational lens phenomenon. We analyze the case of a Kerr black hole rotating at arbitrary speed for some selected positions of a distant observer with respect to the equatorial plane of a Kerr black hole. Some time ago Falcke, Melia, Agol (2000) [ApJ 528, L13S] suggested to search shadows at the Galactic Center. In this paper, we present the boundaries for shadows. We also propose to use future radio interferometer RADIOASTRON facilities to measure shapes of mirages (glories) and to evaluate the black hole spin as a function of the position angle of a distant observer.

PACS: 97.60.L; 04.70; 95.30.S; 04.20; 98.62.S

Keywords: Black hole physics; Gravitational lenses; Microlensing

1. Introduction

Recently Holz and Wheeler (2002) have suggested that a Schwarzschild black hole may form retro-images (called retro-MACHOs) if it is illuminated by the Sun. We analyze a rapidly rotating

* Corresponding author. Tel.:+7 095 1299759; fax: +7 095 8839601.
E-mail address: zakharov@itep.ru (A.F. Zakharov).

1384-1076/$ - see front matter © 2005 Elsevier B.V. All rights reserved.
doi:10.1016/j.newast.2005.02.007

Our proposal

In 2004-2005 we proposed a way to test GR predictions with Radioastron:

Since angular resolution of Radioastron at 1.3 cm is around 8 uas and the size of darkness (shadow) could help us to evaluate a charge, while shape could help us to evaluate a spin (good!)

The shortest wavelength is 1.3 cm (it is too long to detect shadow) (not good for Radioastron!)

So, we propose to test GR predictions about shape and size of BH images with observations. Astronomy is dealing with images. Therefore, establishing the correspondence of theoretical image and reconstructed image using observational data is an aim for further observations.

AFZ et al., NA (2005): “In our old paper
https://ui.adsabs.harvard.edu/.../2005NewA...10.../abstract
we wrote at the end "In spite of the difficulties of measuring the shapes of images near black holes is so attractive challenge to look at the ‘‘faces’’ of black holes because namely the mirages outline the ‘‘faces’’ and
correspond to fully general relativistic description of a region near black hole horizon without any assumption about a specific model for astrophysical processes around black holes (of course we assume that there are sources illuminating black hole surroundings). No doubt that the rapid growth of observational facilities will give a chance to measure the mirage shapes using not only RADIOASTRON facilities but using also other instruments and spectral bands (for example, X-ray interferometer MAXIM (White, 2000; Cash et al., 2000) or sub-mm VLBI array (Miyoshi, 2004)). Astro Space Centre of Lebedev Physics Institute proposed except the RADIOASTRON mission and developed also space based interferometers (Millimetron and Sub-millimetron) for future observations in mm and sub-mm bands. These instruments could be used for the determination of shadow shapes."

Types of unbound geodesics in the Kerr metric

A. F. Zakharov

Institute of Theoretical and Experimental Physics, Academy of Sciences of the USSR, Moscow

(Submitted 4 December 1985)
Zh. Eksp. Teor. Fiz. **91**, 3–6 (July 1986)

Sets of constants of motion of a particle that correspond to different types of r-motion are considered. The topology of these sets is determined and a number of constants characterizing these sets are found.

INTRODUCTION

An important problem in the study of unbound motion of particles in the Kerr metric is the description of the set of constants of motion for which a particle traveling from infinity goes below the horizon of a black hole. We shall give a qualitative description of this set and also of the set of constants of motion for which the particle asymptotically approaches a sphere placed around the black hole, and the sets of constants of motion for which the particle departs to infinity. The solution of this problem is important in connection with the accretion of noninteracting particles on a rotating black hole.

It is well-known that Kepler orbits are characterized by two constants (E and L), since we can identify orbits that can transform into one another by rotations through the Euler angles. Hence, orbits in the Schwarzschild metric are also characterized by two constants. It turns out that a change in the radial coordinate in the Kerr metric is determined by only three constants in the case of moving particles (because the particle mass characterizes the connection between the affine parameter and the proper time of the particle, and the affine parameter can be chosen to be the proper time of the particle), and two constants in the case of the motion of photons (because of the photon energy characterizes the set of different affine parameters in the equation for the change in the r coordinate.)

1. BASIC NOTATION

The equation of motion for the radial variable in the Kerr metric is[1]

$$\rho^4(dr/d\tau)^2=R(r), \tag{1}$$

$$R(r)=r^4+(a^2-\xi^2-\eta)r^2+2M[\eta+(\xi-a)^2]r-a^2\eta \text{ (Photons)},$$

$$R(r)=r^4+(a^2-\xi^2-\eta)r^2+2M[\eta+(\xi-a)^2]r-a^2\eta-r^2\Delta/E \text{ (Particles)},$$

where

$$\rho^2=r^2+a^2\cos^2\theta, \quad \Delta=r^2-2Mr+a^2, \quad a=S/M. \tag{2}$$

The constants S and M refer to the black hole, namely, S is the angular momentum and M the mass of the black hole. The constants E, ξ, and η refer to the particle, namely, E is its energy at infinity, $\xi=L_z/E$ (L_z is the angular momentum of the particle about the axis of rotation of the black hole), and $\eta=Q/E^2$ (Q is given by

$$Q=p_\theta^2+\cos^2\theta[a^2(\mu^2-E^2)+\sin^{-2}\theta L_z^2],$$

and μ is the mass of the particle). It is readily verified that the radial motion of the particle depends on the following constants:

$$\hat{a}=a/M, \quad \hat{E}=E/\mu, \quad \hat{\xi}=\xi/M, \quad \hat{\eta}=\eta/M^2.$$

The radial motion of photons does not depend on the constant $\hat{E}$. Instead of the coordinate r, we now introduce $\hat{r}=r/M$. (The symbol $\wedge$ will be omitted henceforth.) Thus, the character of motion in the r-coordinate for given value of a is determined by the three constants E, ξ, η in the case of a moving particle, and by the two constants ξ and η in the case of photons.

Depending on the multiplicities of the roots of the polynomial $R(r)$ (for $r\geqslant r_g$), we can have three types of motion in the r-coordinate,[2] namely:

(1) the polynomial $R(r)$ has no roots (for $r\geqslant r_g$). The particle then falls into the black hole;

(2) the polynomial $R(r)$ has roots and $r_{\max}>r_g$ ($r_{\max}$ is the maximum root); for $(\partial R/\partial r)(r_{\max})\neq 0$ we then have, $(\partial R/\partial r)(r_{\max})>0$, and the particle departs to infinity after approaching the black hole;

(3) the polynomial $R(r)$ has a root and $R(r_{\max})=(\partial R/\partial r)(r_{\max})=0$; the particle now takes an infinite proper time to approach the sphere of radius $r_{\max}$.

2. DESCRIPTION OF THE SET OF CONSTANTS CORRESPONDING TO DIFFERENT TYPES OF MOTION

We shall now examine the sets of constants of motion E, ξ, and η corresponding to different types of particles motion for a given black-hole rotation parameter $a=\text{const}$. Let us cut the space E,ξ,η with the plane $E=\text{const}\geqslant 1$ and describe in this slice the set of constants corresponding to different types of motion. It then turns out that the boundary of the set of constants corresponding to the second type of motion for $\eta\geqslant 0$ is the set of constants for which the motion belongs to the third type. We shall look upon this set as the graph of the function $\eta=\eta(\xi)$. We note that the set of these constants as functions $\xi(r)$ and $\eta(r)$ was examined by Chandrasekhar[1]. Let us describe some of the properties of the function $\eta(\xi)$. If the motion of the particle is of the third type, we have

$$R(r)=0, \quad (\partial R/\partial r)(r)=0 \tag{3}$$

for $\eta\geqslant 0, r\geqslant r_g$.

Thus, to obtain the function $\eta(\xi)$, we must eliminate r from (3). Assuming that (3) provides an implicit specification of $r(\xi)$ and $\eta(\xi)$, we find that

$$d\eta/d\xi(-\Delta)=2\xi r^2-4(\xi-a)r,$$
$$d\eta/d\xi(-2r+2)+(dr/d\xi)(\partial^2R/\partial r^2)=4\xi r-4(\xi-a) \tag{4}$$

 0038-5646/86/070001-03$04.00

for $r>r_g, \eta>0$. We note that, for $\Delta>0$ and $\partial^2 R/\partial r^2 \neq 0$, the implicit function theorem shows that $r(\xi)$ and $\eta(\xi)$ are single-valued functions. Analysis similar to that given in Ref. 3 then shows that, when $a \neq 1$ or $\xi \neq 2$, we have $\partial^2 R/\partial r^2 > 0$. When $a = 1$ and $\xi = 2$, we find from (3) that $\Delta = 0$. When $a = 1$, it is readily verified that the set corresponding to the third type of motion includes the straight segments $[\xi = 2{,}0 \leqslant \eta \leqslant (3E^4 - 4E^2 + 1)/(E^2(E^2-1))]$ (Ref. 4) (for photons, $\xi = 2{,}0 \leqslant \eta \leqslant 3$, by analogy with Refs. 5 and 6). It can also be shown that the function $\eta(\xi)$ has one maximum and $r(\xi)$ is a monotonically decreasing function.[4] Thus, the set of constants corresponding to the first type of motion is bounded by the curve $\eta(\xi)$ for $\eta \geqslant 0$, as shown in Figs. 1 and 2. It is also readily shown that, when $\eta < 0$ and when η and ξ are such that the motion of the particle is possible, i.e.,

$$-[a(E^2-1)^{1/2}/E - |\xi|]^2 \leqslant \eta < 0, \quad |\xi| \leqslant a(E^2-1)^{1/2}/E,$$

the particle is also captured[2] (this set is illustrated in Fig. 2).

3. UNBOUND MOTION OF PHOTONS

Chandrasekhar[1] has shown that the condition for capture of a particle in the equatorial plane is the inequality

$$6\cos[\arccos(-a)/3 + 2\pi/3] - a \leqslant \xi \leqslant 6\cos[\arccos(-a)/3] - a. \tag{5}$$

Thus, the functions of $r(\xi)$ and $\eta(\xi)$ are defined only for values satisfying the inequalities (5). We also note that the function $\eta(\xi)$ is a maximum for $\xi = -2a, r(-2a) = 3(\eta(-2a) = 27)$. This can be verified by direct evaluation of (3) and (4). Figure 2 shows a plot of the function $\eta(\xi)$ for $a = 1$.

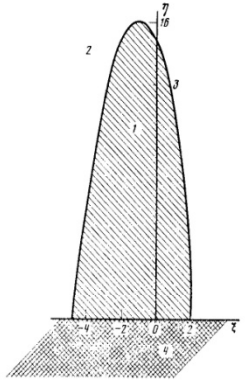

FIG. 1. Different types of particle motion for $E = 1$ and $a = 1$. Region 1—particle trapped, region 2—scattering; curve 3 corresponds to the third type of motion. Region 4 corresponds to values of the constants for which particle motion is impossible.

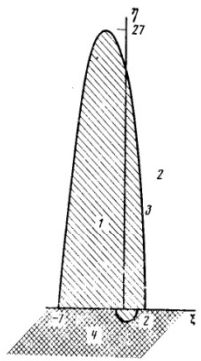

FIG. 2. Same as Fig. 1 for a massless particle and $a = 1$.

4. MOTION OF PARTICLE OF ARBITRARY ENERGY

Consider a moving particle of arbitrary energy at infinity ($E > 1$). It can be verified that, if

$$\eta_{max} = \frac{-(\alpha^2-18\alpha-27) + (\alpha^4+28\alpha^3+270\alpha^2+972\alpha+729)^{1/2}}{2E^2\alpha},$$
$$r_{max} = (8\alpha^3/27 + \eta_{max}E^2\alpha(\alpha/3+1))^{1/2} - 2\alpha/3, \tag{6}$$
$$\xi_{max} = 2a/(r_{max}-2),$$

where $\alpha = (E^2-1)^{-1}$, these values ensure that $R(r)$ and $\partial R/\partial r$ vanish, i.e., they satisfy (3). We also note that, for values chosen in accordance with (6), the right-hand side of the first equation in (4) vanishes, i.e., these values correspond to the maximum of $\eta(\xi)$. The values η_{max} and r_{max} turn out to be equal to the corresponding values of these quantities for $a = 0$ (Schwarzschild metric).[7]

5. ONE CASE OF UNBOUND PARTICLE MOTION

Consider a case of unbound particle motion for $E = 1$. If the motion takes place in the equatorial plane, $\eta = 0$ (Ref. 8) and

$$R(r) = 2r^3 - \xi^2 r^2 + 2(a-\xi)^2 r. \tag{7}$$

The motion then belongs to the third type if $\xi^4 = 16(a-\xi)^2$, and $r = \xi^2/4$. It follows that there are only two values that correspond to the third type of motion in the equatorial plane, namely, $\xi = -2 - 2(1+a)^{1/2}$ and $\xi = 2 + 2(1-a)^{1/2}$. Thus, the domain of definition of $\eta(\xi)$ is the segment $[-2(1+(1+a)^{1/2}), 2(1+(1-a)^{1/2})]$. The domain of variation of the function $r(\xi)$ is the segment $[(1+(1-a)^{1/2})^2, (1+(1+a)^{1/2})^2]$. This follows from the fact that $r(\xi)$ is a monotonically decreasing function of ξ. When $a = 0$, we find that $\eta(\xi) = 16 - \xi^2$. When $E \to 1$, we

Measuring the black hole parameters in the Galactic Center with Radioastron

- Let us consider an illumination of black holes. Then retro-photons form caustics around black holes or mirages around black holes or boundaries around shadows.
- (Zakharov, Nucita, DePaolis, Ingrosso,
- New Astronomy 10 (2005) 479; astro-ph/0411511)

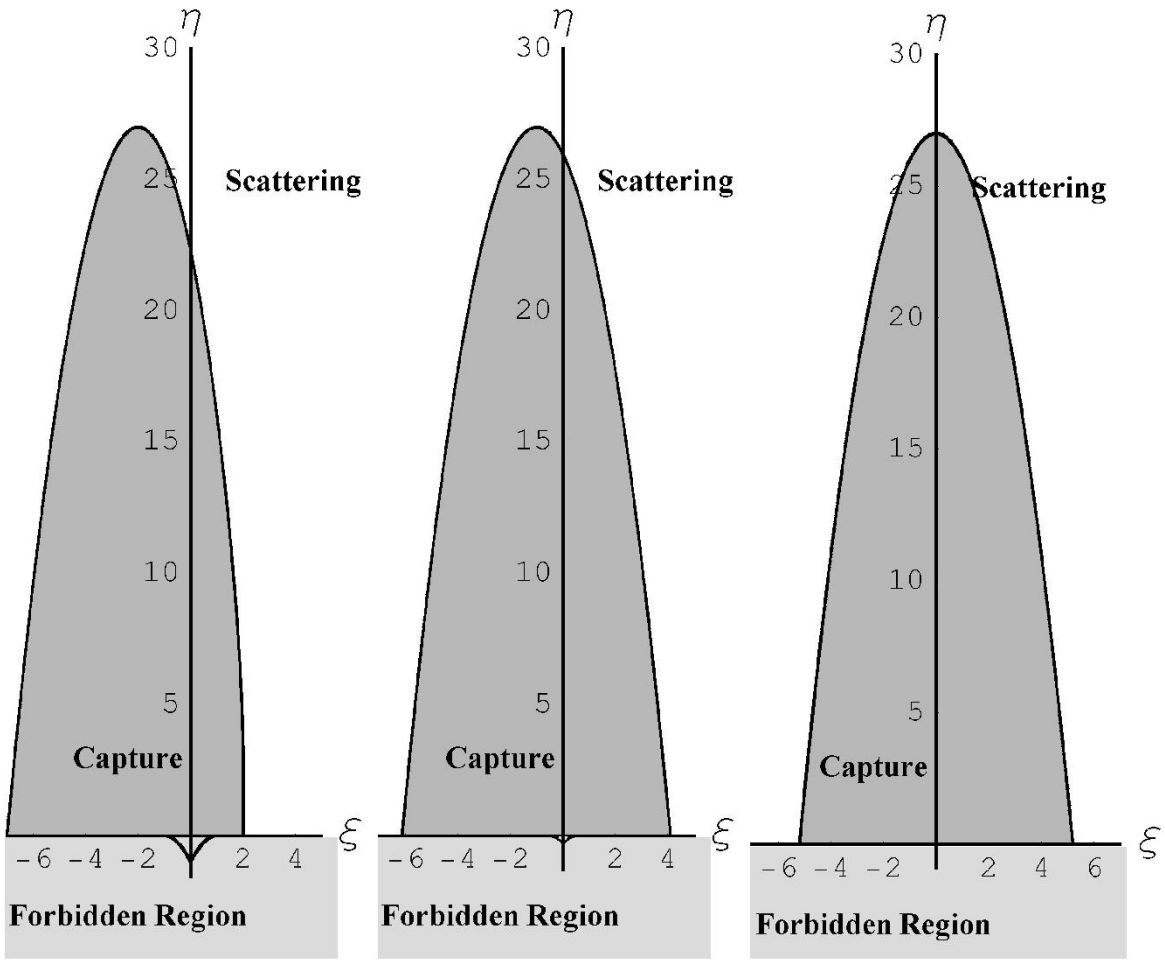

Fig. 1. Different types for photon trajectories and spin parameters ($a = 1., a = 0.5, a = 0.$). Critical curves separate capture and scatter regions. Here we show also the forbidden region corresponding to constants of motion $\eta < 0$ and $(\xi, \eta)\ \bar{\in}\ M$ as it was discussed in the text.

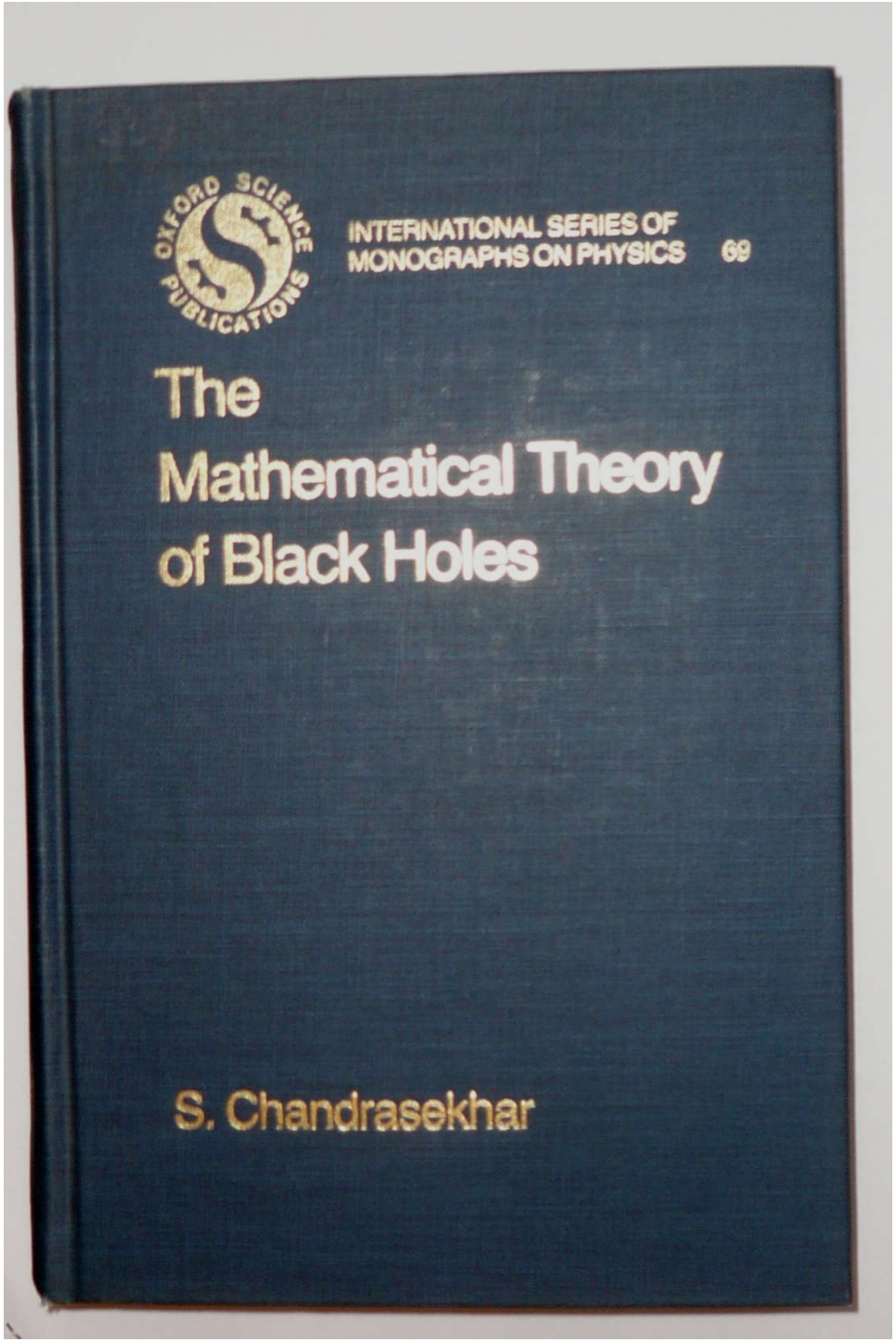
OXFORD SCIENCE PUBLICATIONS
INTERNATIONAL SERIES OF MONOGRAPHS ON PHYSICS 69
The Mathematical Theory of Black Holes
S. Chandrasekhar

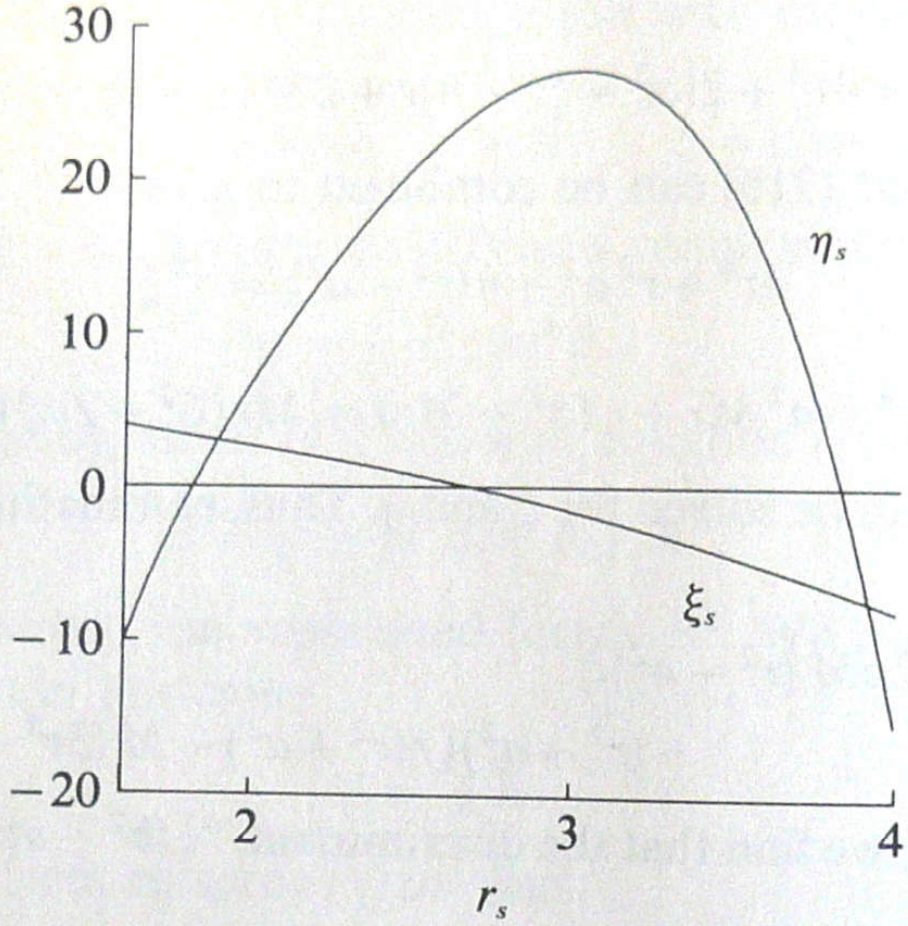

FIG. 34. The locus (ξ_s, η_s) determining the constants of the motion for three-dimensional orbits of constant radius described around a Kerr black-hole with $a = 0.8$. The unit of length along the abscissa is M.

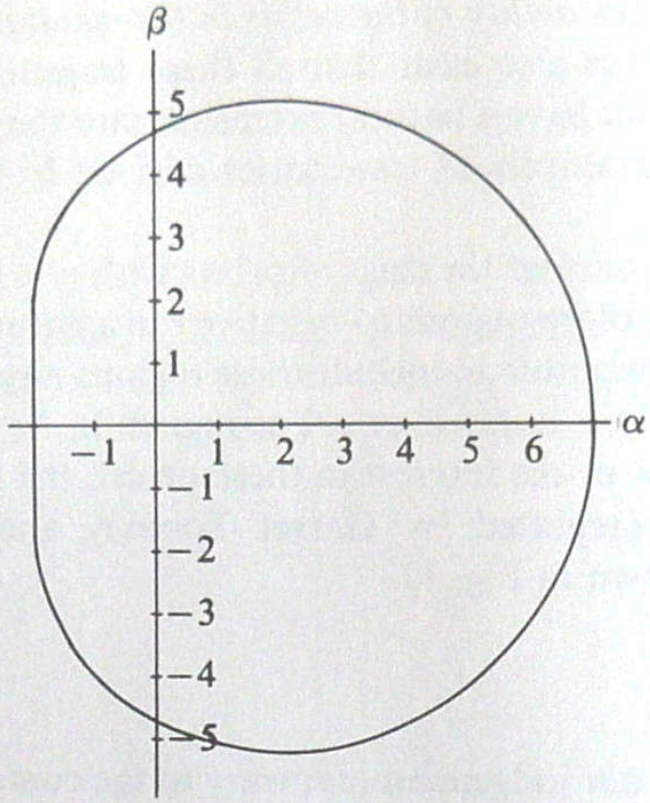

FIG. 38. The apparent shape of an extreme ($a = M$) Kerr black-hole as seen by a distant observer in the equatorial plane, if the black hole is in front of a source of illumination with an angular size larger than that of the black hole. The unit of length along the coordinate axes α and β (defined in equation (241) is M.

black hole from infinity, the apparent shape will be determined by

$$(\alpha, \beta) = [\xi, \sqrt{\eta(\xi)}]. \tag{242}$$

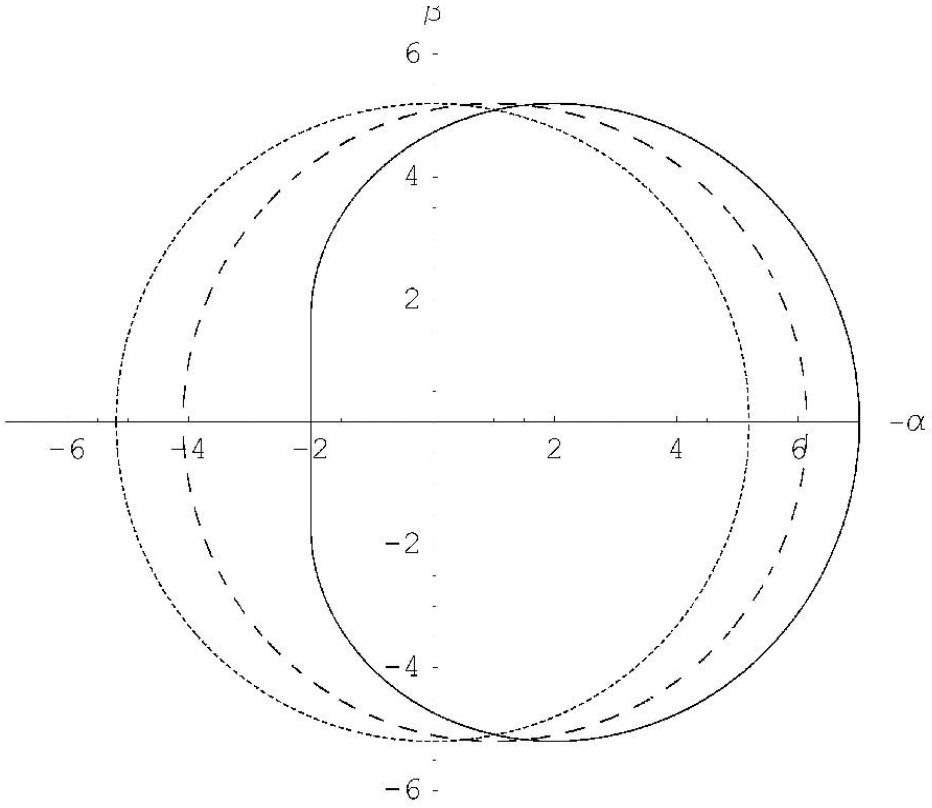

Fig. 2. Mirages around black hole for equatorial position of distant observer and different spin parameters. The solid line, the dashed line and the dotted line correspond to $a = 1, a = 0.5, a = 0$ correspondingly

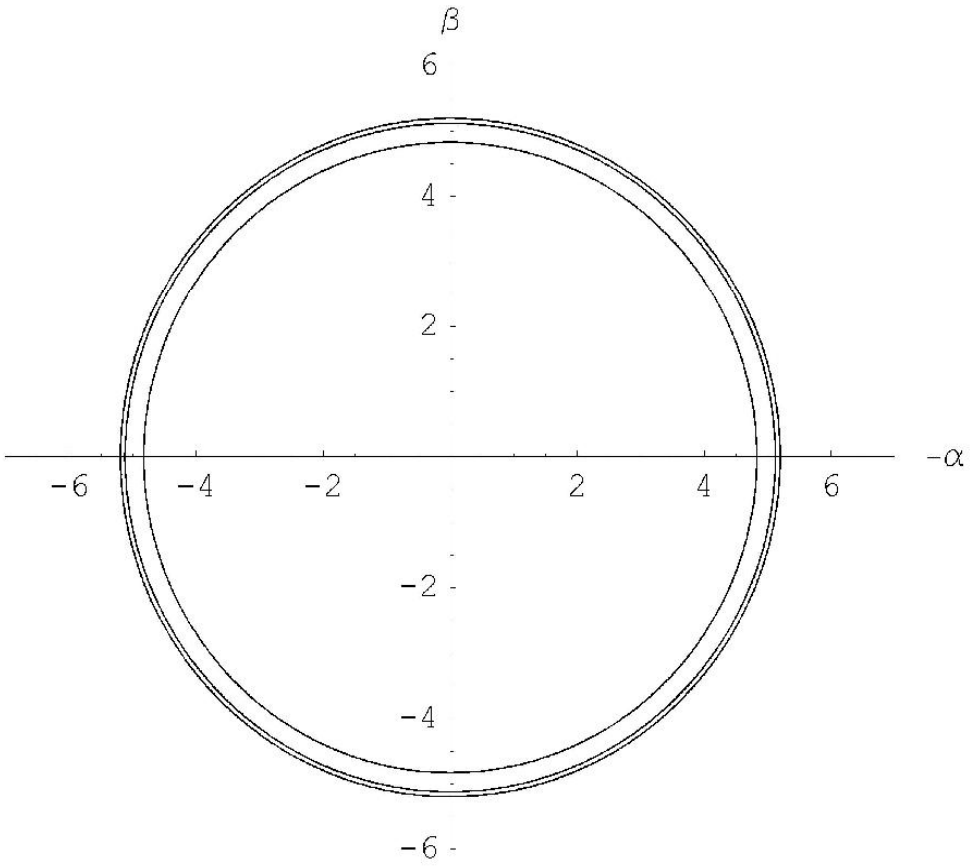

Fig. 3. Mirages around a black hole for the polar axis position of distant observer and different spin parameters ($a = 0, a = 0.5, a = 1$). Smaller radii correspond to greater spin parameters.

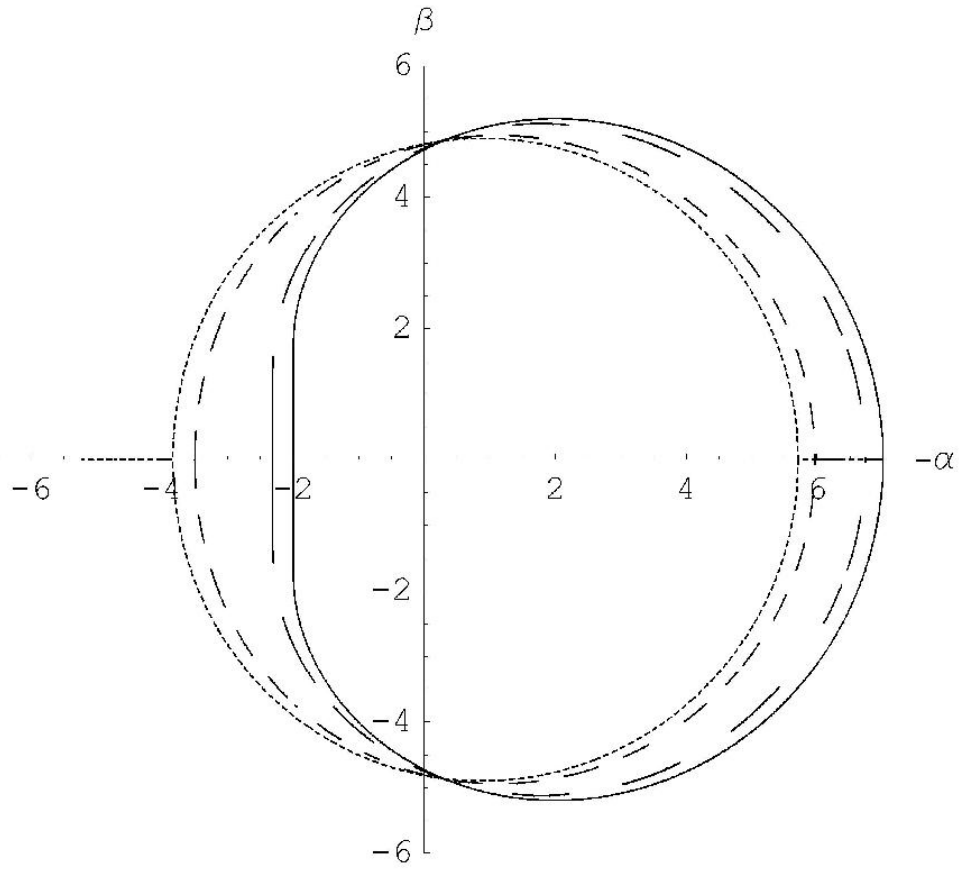

Fig. 5. Mirages around black hole for different angular positions of a distant observer and the spin $a = 1$. Solid, long dashed, short dashed and dotted lines correspond to $\theta_0 = \pi/2, \pi/3, \pi/6$ and $\pi/8$, respectively.

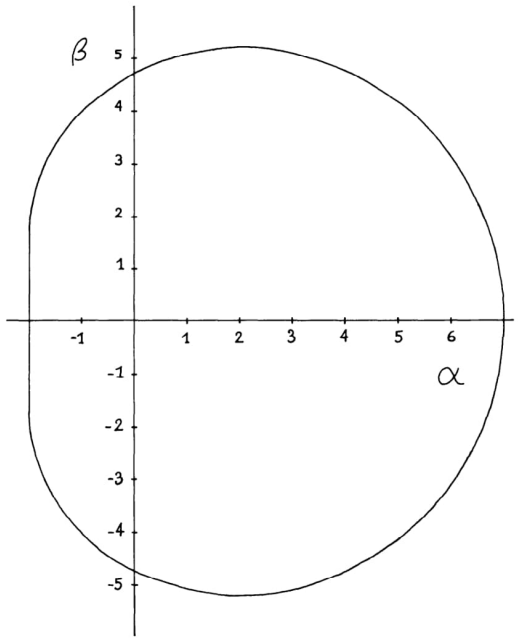

Figure 6. The apparent shape of an extreme ($a = m$) Kerr black hole as seen by a distant observer in the equatorial plane, if the black hole is in front of a source of illumination with an angular size larger than that of the black hole.

is largest there and because of the gravitational focusing effects associated with the bending of the rays toward the equatorial plane. Note that the radiation comes out along the flat portion of the apparent boundary of the extreme black hole as plotted in Figure 6.

D. Geometrical Optics

A detailed calculation of the brightness distribution coming from a source near a Kerr black hole requires more of geometrical optics than the calculation of photon trajectories. I will now review some techniques which are useful in making astrophysical calculations in connection with black holes.

The fundamental principle can be expressed as the conservation of photon density in phase space along each photon trajectory. A phase space element $d^3x\, d^3p$, the product of a proper spatial volume element and a physical momentum-space volume element in a local observer's frame of reference, is a Lorentz invariant, so the particular choice of local observer is arbitrary. The density $N(x^a, p^{(\beta)})$ is defined

James Maxwell Bardeen passed away on June 20, 2022

John Bardeen (1908 -1991), the father of J. M. Bardeen.
E. Wigner was J. Bardeen' supervisor

Direct Measurements of Black Hole Charge with Future Astrometrical Missions

A.F. Zakharov[1,2,3], F. De Paolis[4], G. Ingrosso[4], A.A. Nucita[4]

[1] Institute of Theoretical and Experimental Physics, 25, B.Cheremushkinskaya st., Moscow, 117259, Russia,

[2] Astro Space Centre of Lebedev Physics Institute, 84/32, Profsoyuznaya st., Moscow, 117810, Russia,

[3] Joint Institute for Nuclear Research, Dubna, Russia

[4] Department of Physics, University of Lecce and INFN, Section of Lecce, Via Arnesano, I-73100 Lecce, Italy

Received / accepted

Abstract. Recently, Zakharov et al. (2005a) considered the possibility of evaluating the spin parameter and the inclination angle for Kerr black holes in nearby galactic centers by using future advanced astrometrical instruments. A similar approach which uses the characteristic properties of gravitational retro-lensing images can be followed to measure the charge of Reissner-Nordström black hole. Indeed, in spite of the fact that their formation might be problematic, charged black holes are objects of intensive investigations. From the theoretical point of view it is well-known that a black hole is described by only three parameters, namely, its mass M, angular momentum J and charge Q. Therefore, it would be important to have a method for measuring all these parameters, preferably by model independent way. In this paper, we propose a procedure to measure the black hole charge by using the size of the retro-lensing images that can be revealed by future astrometrical missions. A discussion of the Kerr-Newmann black hole case is also offered.

$$R(r_{max}) = 0, \qquad \frac{\partial R}{\partial r}(r_{max}) = 0, \tag{6}$$

as it was done, for example, by Chandrasekhar (1983) to solve similar problems.

Introducing the notation $\xi^2 = l, Q^2 = q$, we obtain

$$R(r) = r^4 - lr^2 + 2lr - qr. \tag{7}$$

The discriminant Δ of the polynomial $R(r)$ has the form (as it was shown by Zakharov (1991a,b, 1994a)):

$$\Delta = 16l^3[l^2(1-q) + l(-8q^2 + 36q - 27) - 16q^3]. \tag{8}$$

The polynomial $R(r)$ thus has a multiple root if and only if

$$l^3[l^2(1-q) + l(-8q^2 + 36q - 27) - 16q^3] = 0. \tag{9}$$

Excluding the case $l = 0$, which corresponds to a multiple root at $r = 0$, we find that the polynomial $R(r)$ has a multiple root for $r \geq r_+$ if and only if

$$l^2(1-q) + l(-8q^2 + 36q - 27) - 16q^3 = 0. \tag{10}$$

If $q = 0$, we obtain the well-known result for a Schwarzschild black hole (Misner, Thorne and Wheeler 1973; Wald 1984; Lightman et al. 1975), $l = 27$, or $L_{cr} = 3\sqrt{3}$. If $q = 1$, then $l = 16$, or $L_{cr} = 4$, which also corresponds to numerical results given by Young (1976).

The photon capture cross section for an extreme charged black hole turns out to be considerably smaller than the capture cross section of a Schwarzschild black hole. The critical value of the impact parameter, characterizing the capture cross section for a Reissner - Nordström black hole, is determined by the equation (Zakharov 1991a,b, 1994a)

$$l = \frac{(8q^2 - 36q + 27) + \sqrt{(8q^2 - 36q + 27)^2 + 64q^3(1-q)}}{2(1-q)}. \tag{11}$$

Table 1. The fringe sizes (in micro arcseconds) for the standard and advanced apogees $B_{\max}$ (350 000 and 3 200 000 km, respectively).

$B_{\max}$(km)\λ(cm)	92	18	6.2	1.35
3.5×10^5	540	106	37	8
3.2×10^6	59	12	4	0.9

4. The space RADIOASTRON interferometer

The space-based radio telescope RADIOASTRON[1] is planned to be launched within few next years[2]. This space-based 10-m radio telescope will be used for space – ground VLBI observations. The measurements will have extremely high angular resolutions, namely about 1–10 μas (in particular about 8 μas at the shortest wavelength of 1.35 cm and a standard orbit[3], and could be about 0.9 μas for the high orbit configuration at the same wavelength. Four wave bands will be used corresponding to $\lambda = 1.35$ cm, $\lambda = 6.2$ cm, $\lambda = 18$ cm, $\lambda = 92$ cm (see Table 1). A detailed calculation of the high-apogee evolving orbits ($B_{\max}$) can be done, once the exact launch time is known.

After several years of observations, it should be possible to move the spacecraft to a much higher orbit (with apogee radius about 3.2 million km), by additional spacecraft maneuvering using the gravitational force of the Moon. The fringe sizes (in μas) for the apogee of the above-mentioned orbit and for all RADIOASTRON wavelengths are given in Table 1.

By comparing Figs. 1, 2 and Table 1, one can see that there are non-negligible chances to observe such mirages around the black hole at the Galactic Center and in nearby AGNs and microquasars in the radio-band using RADIOASTRON facilities.

We also mention that this high resolution in radio band will be achieved also by Japanese VLBI project VERA (VLBI Exploration of Radio Astrometry), since the angular resolution aimed at will be at the 10 μas level (Sawad-Satoh 2000; Honma 2001). Therefore, the only problem left is to have a powerful enough radio source to illuminate a black hole in order to have retro-lensing images detectable by such radio VLBI telescopes as RADIOASTRON or VERA.

[1] See web-site `http://www.asc.rssi.ru/radioastron/` for more information.

[2] This project was proposed by the Astro Space Center (ASC) of Lebedev Physical Institute of the Russian Academy of Sciences (RAS) in collaboration with other institutions of RAS and RosAviaKosmos. Scientists from 20 countries are developing the scientific payload for the satellite by providing by ground-based support to the mission.

[3] The satellite orbit will have high apogee, and its rotation period around Earth will be 9.5 days, which evolves as a result of the weak gravitational perturbations from the Moon and the Sun. The perigee has been planned to be between 10^4 and 7×10^4 km and the apogee between 310 and 390 thousand kilometers. The basic orbit parameters will be the following: the orbital period is $P = 9.5$ days, the semi-major axis is $a = 189\,000$ km, the eccentricity is $e = 0.853$, the perigee is $H = 29\,000$ km.

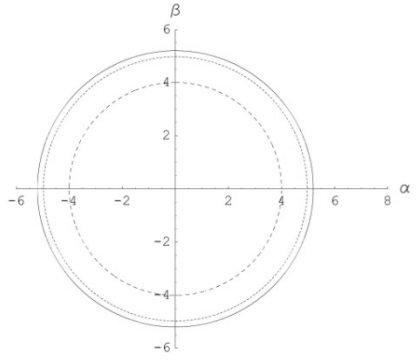

Fig. 1. Shadow (mirage) sizes are shown for selected charges of black holes $Q = 0$ (solid line), $Q = 0.5$ (short dashed line), and $Q = 1$ (long dashed line).

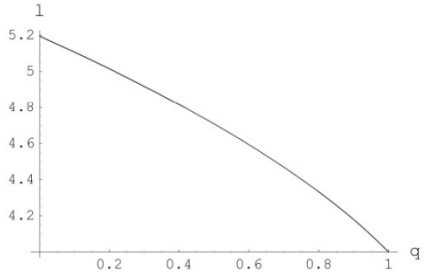

Fig. 2. The mirage radius l is shown as a function of the black hole charge q (l and q are given in units of M).

5. Searches for mirages near Sgr A^* with RADIOASTRON

Radio, near-infrared, and X-ray spectral band observations are developing very rapidly (Lo et al. 1998, 1999; Genzel et al. 2003; Ghez et al. 2004; Baganoff et al. 2001, 2003; Bower et al. 2002, 2003; Narayan 2003; Bower et al. 2004)[4], and it is known that Sgr A^* harbors the closest massive black hole with mass estimated to be $4.07 \times 10^6\ M_\odot$ (Bower et al. 2004; Melia & Falcke 2001; Ghez et al. 2003; Schodel et al. 2003).

Following the idea of Falcke et al. (2000) and of Zakharov et al. (2005a,b,c,d) we propose to use the VLBI technique to observe mirages around massive black holes and, in particular, towards the black hole at Galactic Center. To evaluate the shadow shape Falcke et al. (2000) used the ray-tracing technique. The boundaries of the shadows are black hole mirages.

[4] An interesting idea to use radio pulsars to investigate the region nearby black hole horizon was proposed recently by Pfahl & Loeb (2003).

PHYSICAL REVIEW D **90,** 062007 (2014)

Constraints on a charge in the Reissner-Nordström metric for the black hole at the Galactic Center

Alexander F. Zakharov*

North Carolina Central University, Durham, North Carolina 27707, USA; Institute of Theoretical and Experimental Physics, Moscow 117218, Russia; Joint Institute for Nuclear Research, Dubna 141980, Russia; Institute for Computer Aided Design of RAS, 123056 Moscow, Russia; and National Research Nuclear University (NRNU MEPHI), 115409 Moscow, Russia

(Received 5 March 2013; published 9 September 2014)

Using an algebraic condition of vanishing discriminant for multiple roots of fourth-degree polynomials, we derive an analytical expression of a shadow size as a function of a charge in the Reissner-Nordström (RN) metric [1,2]. We consider shadows for negative tidal charges and charges corresponding to naked singularities $q = \mathcal{Q}^2/M^2 > 1$, where $\mathcal{Q}$ and M are black hole charge and mass, respectively, with the derived expression. An introduction of a negative tidal charge q can describe black hole solutions in theories with extra dimensions, so following the approach we consider an opportunity to extend the RN metric to negative $\mathcal{Q}^2$, while for the standard RN metric $\mathcal{Q}^2$ is always non-negative. We found that for $q > 9/8$, black hole shadows disappear. Significant tidal charges $q = -6.4$ (suggested by Bin-Nun [3–5]) are not consistent with observations of a minimal spot size at the Galactic Center observed in mm-band; moreover, these observations demonstrate that a Reissner-Nordström black hole with a significant charge $q \approx 1$ provides a better fit of recent observational data for the black hole at the Galactic Center in comparison with the Schwarzschild black hole.

DOI: 10.1103/PhysRevD.90.062007 PACS numbers: 04.80.Cc, 04.20.-q, 04.50.Gh, 04.70.Bw

I. INTRODUCTION

Soon after the discovery of general relativity (GR), the first solutions corresponding to spherical symmetric black holes were found [1,2,6]; however, initially people were rather sceptical about possible astronomical applications of the solutions corresponding to black holes [7] (see also, for instance, one of the first textbooks on GR [8]). Even after an introduction to the black hole concept by Wheeler [9] (he used the term in his public lecture in 1967 [10]), we did not know too many examples where we really need GR models with strong gravitational fields that arise near black hole horizons to explain observational data. The cases where we need strong field approximation are very important since they give an opportunity to check GR predictions in a strong field limit; therefore, one could significantly constrain alternative theories of gravity.

One of the most important options to test gravity in the strong field approximation is analysis of relativistic line shape as it was shown in [11], with assumptions that a line emission is originated at a circular ring area of a flat accretion disk. Later on, such signatures of the Fe $K\alpha$ line have been found in the active galaxy MCG-6-30-15 [12]. Analyzing the spectral line shape, the authors concluded the emission region is so close to the black hole horizon that one has to use Kerr metric approximation [13] to fit observational data [12]. Results of simulations of iron $K\alpha$ line formation are given in [14,15] (where we used our approach [16]); see also [17] for a more recent review of the subject.

Now there are two basic observational techniques to investigate a gravitational potential at the Galactic Center, namely, (a) monitoring the orbits of bright stars near the Galactic Center to reconstruct a gravitational potential [18] (see also a discussion about an opportunity to evaluate black hole dark matter parameters in [19] and an opportunity to constrain some class of an alternative theory of gravity [20]) and (b) measuring in mm band, with VLBI technique, the size and shape of shadows around the black hole, giving an alternative possibility to evaluate black hole parameters. The formation of retro-lensing images (also known as mirages, shadows, or "faces" in the literature) due to the strong gravitational field effects nearby black holes has been investigated by several authors [21–24].

Theories with extra dimensions admit astrophysical objects (supermassive black holes in particular) which are rather different from standard ones. Tests have been proposed when it would be possible to discover signatures of extra dimensions in supermassive black holes since the gravitational field may be different from the standard one in the GR approach. So, gravitational lensing features are different for alternative gravity theories with extra dimensions and general relativity.

Recently, Bin-Nun [3–5] discussed the possibility that the black hole at the Galactic Center is described by the tidal Reissner-Nordström metric which may be admitted by the Randall-Sundrum II braneworld scenario [25]. Bin-Nun suggested an opportunity of evaluating the black hole

*zakharov@itep.ru

$$\mathrm{Dis}(s_1,s_2,s_3,s_4)=\begin{vmatrix}1 & 1 & 1 & 1\\ X_1 & X_2 & X_3 & X_4\\ X_1^2 & X_2^2 & X_3^2 & X_4^2\\ X_1^3 & X_2^3 & X_3^3 & X_4^3\end{vmatrix}^2 = \begin{vmatrix}4 & p_1 & p_2 & p_3\\ p_1 & p_2 & p_3 & p_4\\ p_2 & p_3 & p_4 & p_5\\ p_3 & p_4 & p_5 & p_6\end{vmatrix}. \quad (20)$$

Expressing the polynomials $p_k(1\le k\le 6)$ in terms of the polynomials $s_k(1\le k\le 4)$ and using Newton's equations we calculate the polynomials and discriminant of the family X_1,X_2,X_3,X_4 in roots of the polynomial $R(r)$; we obtain

$$p_1=s_1=0,\qquad p_2=-2s_2,\qquad p_3=3s_3,$$
$$p_4=2s_2^2-4s_4,\qquad p_5=-5s_3s_2,$$
$$p_6=-2s_2^3+3s_3^2+6s_4s_2, \quad (21)$$

where $s_1=0, s_2=-l, s_3=-2l, s_4=-ql$, corresponding to the polynomial $R(r)$ in Eq. (8). The discriminant Dis of the polynomial $R(r)$ has the form

$$\mathrm{Dis}(s_1,s_2,s_3,s_4)=\begin{vmatrix}4 & 0 & 2l & -6l\\ 0 & 2l & -6l & 2l(l+2q)\\ 2l & -6l & 2l(l+2q) & -10l^2\\ -6l & 2l(l+2q) & -10l^2 & 2l^2(l+6+3q)\end{vmatrix}$$
$$=16l^3[l^2(1-q)+l(-8q^2+36q-27)-16q^3]. \quad (22)$$

The polynomial $R(r)$ thus has a multiple root if and only if

$$l^3[l^2(1-q)+l(-8q^2+36q-27)-16q^3]=0. \quad (23)$$

Excluding the case $l=0$, which corresponds to a multiple root at $r=0$, we find that the polynomial $R(r)$ has a multiple root for $r\ge r_+$ if and only if

$$l^2(1-q)+l(-8q^2+36q-27)-16q^3=0. \quad (24)$$

If $q=0$, we obtain the well-known result for a Schwarzschild black hole [38,39,49], $l_{\mathrm{cr}}=27$, or $\xi_{\mathrm{cr}}=3\sqrt{3}$ [where l_{cr} is the positive root of Eq. (24)]. If $q=1$, then $l=16$, or $\xi_{\mathrm{cr}}=4$, which also corresponds to numerical results given in paper [50]. The photon capture cross section for an extreme charged black hole turns out to be considerably smaller than the capture cross section of a Schwarzschild black hole. The critical value of the impact parameter, characterizing the capture cross section for a RN black hole, is determined by the equation

$$l_{\mathrm{cr}}=\frac{(8q^2-36q+27)+\sqrt{D_1}}{2(1-q)}, \quad (25)$$

where $D_1=(8q^2-36q+27)^2+64q^3(1-q)=-512(q-\frac{9}{8})^3$. It is clear from the last relation that there are circular unstable photon orbits only for $q\le\frac{9}{8}$ (see also results in [37] about the same critical value). Substituting Eq. (25) into the expression for the coefficients of the polynomial $R(r)$ it is easy to calculate the radius of the unstable circular photon orbit (which is the same as the minimum periastron distance). The orbit of a photon moving from infinity with the critical impact parameter, determined in accordance with Eq. (25) spirals into circular orbit. To find a radius of photon unstable orbit we will solve Eq. (7) substituting l_{cr} in the relation. From trigonometric formula for roots of cubic equation we have

$$r_{\mathrm{crit}}=2\sqrt{\frac{l_{\mathrm{cr}}}{6}}\cos\frac{\alpha}{3}, \quad (26)$$

where

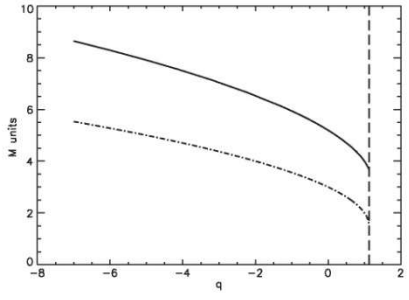

FIG. 1. Shadow (mirage) radius (solid line) and radius of the last circular unstable photon orbit (dot-dashed line) in M units as a function of q. The critical value $q=9/8$ is shown with dashed vertical line.

Jourdain: “For more than forty years I have been speaking prose while knowing nothing of it,” (from “*Bourgeois Gentleman* or *The Middle-Class Aristocrat “,* J. B. Moliere)

We: “For many years we had speaking about BH’s in Randall --- Sundrum model or in (beyond) Horndesky theory (scalar-tensor one) while knowing nothing of the theories…” (tidal charge or “charge” due to scalar-tensor theories)

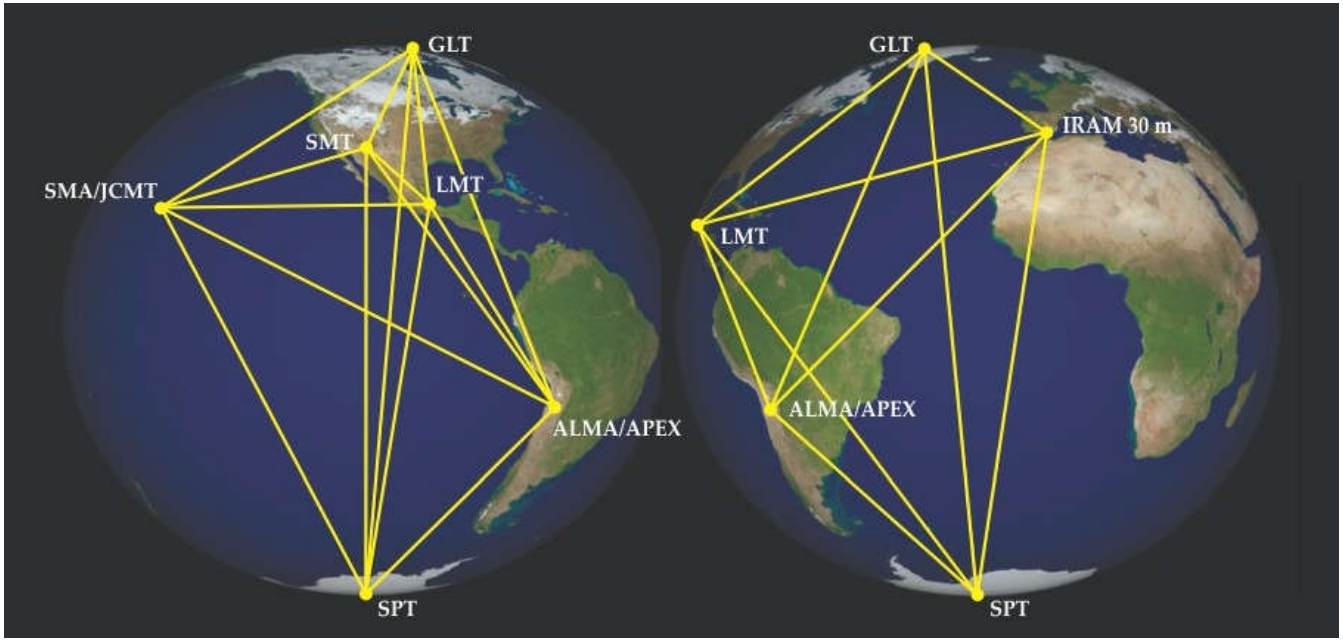

Figure 2. ***The Event Horizon Telescope*** *is a global array of millimeter telescopes (see http://eventhorizontelescope.org/array) that aims to take the first pictures of black holes. (Courtesy of Dan Marrone/University of Arizona.)*

Published in: Dimitrios Psaltis; Feryal Özel; *Physics Today* **2018,** 71, 70-71.
DOI: 10.1063/PT.3.3906

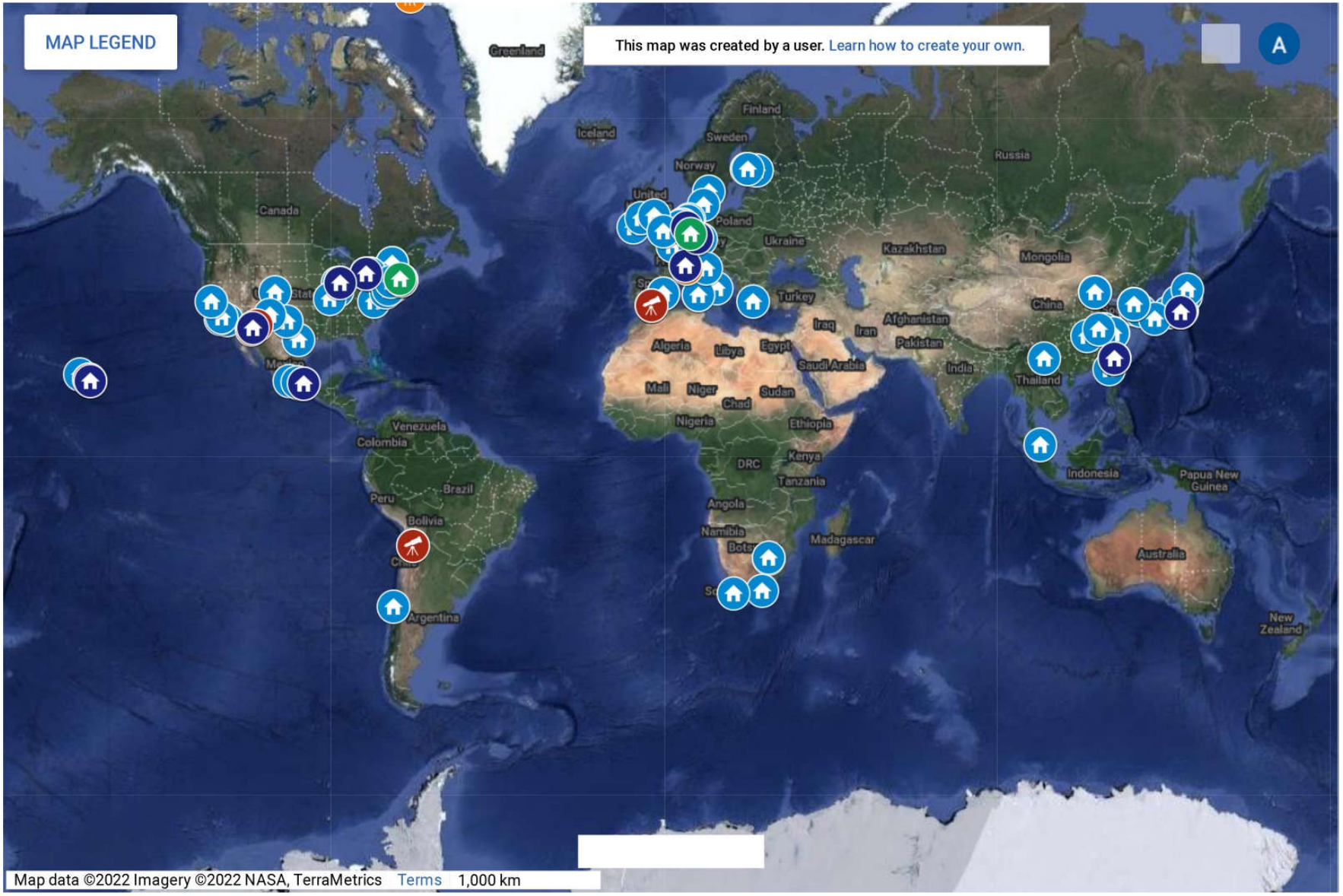
MAP LEGEND
This map was created by a user. Learn how to create your own.
A
Greenland
Iceland
Finland
Sweden
Norway
Russia
Canada
Poland
Ukraine
Kazakhstan
Mongolia
Turkey
China
Iraq
Iran
Afghanistan
Pakistan
Algeria
Libya
Egypt
Saudi Arabia
India
Thailand
Mali
Niger
Sudan
Chad
Nigeria
Ethiopia
Kenya
DRC
Tanzania
Indonesia
Papua New Guinea
Venezuela
Colombia
Brazil
Peru
Bolivia
Angola
Namibia
Madagascar
Australia
Argentina
New Zealand
Map data ©2022 Imagery ©2022 NASA, TerraMetrics
Terms
1,000 km

EHT team: “Similarly, for the EHT, the data we take only tells us only a piece of the story, as there are an infinite number of possible images that are perfectly consistent with the data we measure. But not all images are created equal— some look more like what we think of as images than others. To chose the best image, we essentially take all of the infinite images that explain our telescope measurements, and rank them by how reasonable they look. We then choose the image (or set of images) that looks most reasonable. “

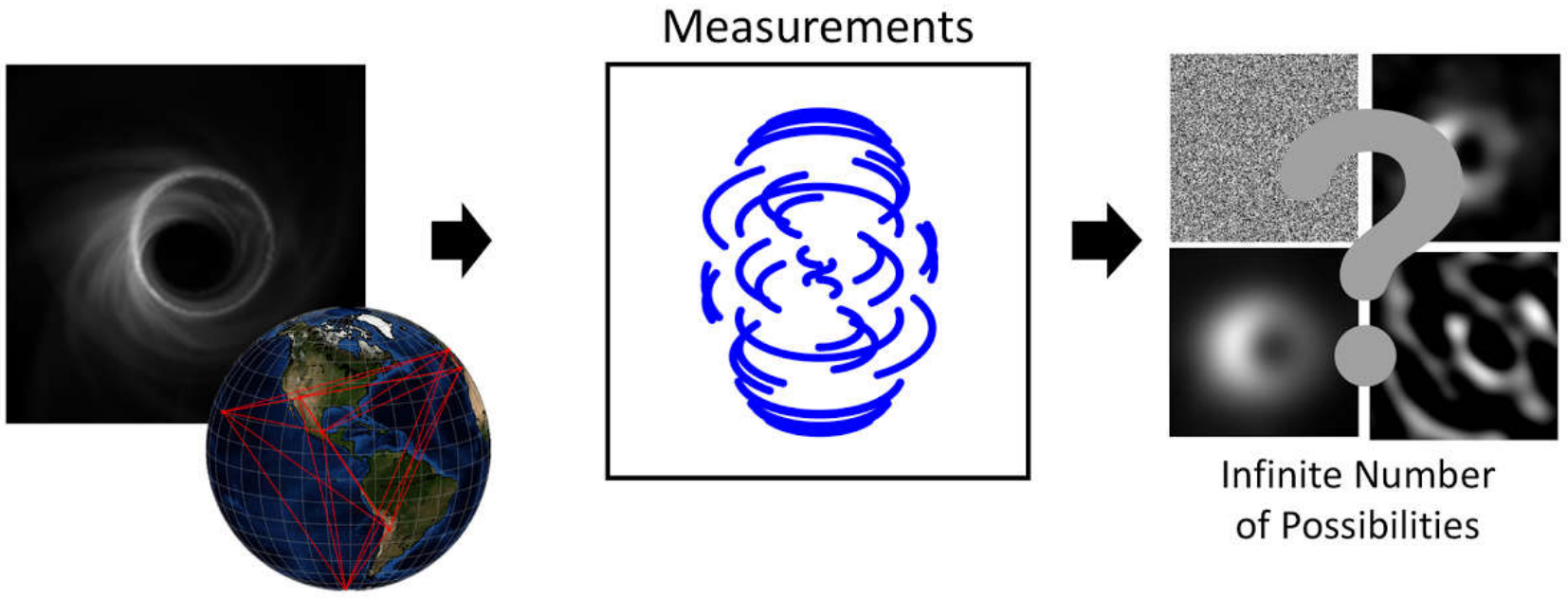

Constraints on black-hole charges with the 2017 EHT observations of M87*

Prashant Kocherlakota,[1] Luciano Rezzolla,[1–3] Heino Falcke,[4] Christian M. Fromm,[5,6,1] Michael Kramer,[7] Yosuke Mizuno,[8,9] Antonios Nathanail,[9,10] Héctor Olivares,[4] Ziri Younsi,[11,9] Kazunori Akiyama,[12,13,5] Antxon Alberdi,[14] Walter Alef,[7] Juan Carlos Algaba,[15] Richard Anantua,[5,6,16] Keiichi Asada,[17] Rebecca Azulay,[18,19,7] Anne-Kathrin Baczko,[7] David Ball,[20] Mislav Baloković,[5,6] John Barrett,[12] Bradford A. Benson,[21,22] Dan Bintley,[23] Lindy Blackburn,[5,6] Raymond Blundell,[6] Wilfred Boland,[24] Katherine L. Bouman,[5,6,25] Geoffrey C. Bower,[26] Hope Boyce,[27,28] Michael Bremer,[29] Christiaan D. Brinkerink,[4] Roger Brissenden,[5,6] Silke Britzen,[7] Avery E. Broderick,[30–32] Dominique Broguiere,[29] Thomas Bronzwaer,[4] Do-Young Byun,[33,34] John E. Carlstrom,[35,22,36,37] Andrew Chael,[38,39] Chi-kwan Chan,[20,40] Shami Chatterjee,[41] Koushik Chatterjee,[42] Ming-Tang Chen,[26] Yongjun Chen (陈永军),[43,44] Paul M. Chesler,[5] Ilje Cho,[33,34] Pierre Christian,[45] John E. Conway,[46] James M. Cordes,[41] Thomas M. Crawford,[22,35] Geoffrey B. Crew,[12] Alejandro Cruz-Osorio,[9] Yuzhu Cui,[47,48] Jordy Davelaar,[49,16,4] Mariafelicia De Laurentis,[50,9,51] Roger Deane,[52–54] Jessica Dempsey,[23] Gregory Desvignes,[55] Sheperd S. Doeleman,[5,6] Ralph P. Eatough,[56,7] Joseph Farah,[6,5,57] Vincent L. Fish,[12] Ed Fomalont,[58] Raquel Fraga-Encinas,[4] Per Friberg,[23] H. Alyson Ford,[59] Antonio Fuentes,[14] Peter Galison,[5,60,61] Charles F. Gammie,[62,63] Roberto García,[29] Olivier Gentaz,[29] Boris Georgiev,[31,32] Ciriaco Goddi,[4,64] Roman Gold,[65,30] José L. Gómez,[14] Arturo I. Gómez-Ruiz,[66,67] Minfeng Gu (顾敏峰),[43,68] Mark Gurwell,[6] Kazuhiro Hada,[47,48] Daryl Haggard,[27,28] Michael H. Hecht,[12] Ronald Hesper,[69] Luis C. Ho (何子山),[70,71] Paul Ho,[17] Mareki Honma,[47,48,72] Chih-Wei L. Huang,[17] Lei Huang (黄磊),[43,68] David H. Hughes,[66] Shiro Ikeda,[13,73–75] Makoto Inoue,[17] Sara Issaoun,[4] David J. James,[5,6] Buell T. Jannuzi,[20] Michael Janssen,[7] Britton Jeter,[31,32] Wu Jiang (江悟),[43] Alejandra Jimenez-Rosales,[4] Michael D. Johnson,[5,6] Svetlana Jorstad,[76,77] Taehyun Jung,[33,34] Mansour Karami,[30,31] Ramesh Karuppusamy,[7] Tomohisa Kawashima,[78] Garrett K. Keating,[6] Mark Kettenis,[79] Dong-Jin Kim,[7] Jae-Young Kim,[33,7] Jongsoo Kim,[33] Junhan Kim,[20,25] Motoki Kino,[13,80] Jun Yi Koay,[17] Yutaro Kofuji,[47,72] Patrick M. Koch,[17] Shoko Koyama,[17] Carsten Kramer,[29] Thomas P. Krichbaum,[7] Cheng-Yu Kuo,[81,17] Tod R. Lauer,[82] Sang-Sung Lee,[33] Aviad Levis,[25] Yan-Rong Li (李彦荣),[83] Zhiyuan Li (李志远),[84,85] Michael Lindqvist,[46] Rocco Lico,[14,7] Greg Lindahl,[6] Jun Liu (刘俊),[7] Kuo Liu,[7] Elisabetta Liuzzo,[86] Wen-Ping Lo,[17,87] Andrei P. Lobanov,[7] Laurent Loinard,[88,89] Colin Lonsdale,[12] Ru-Sen Lu (路如森),[43,44,7] Nicholas R. MacDonald,[7] Jirong Mao (毛基荣),[90–92] Nicola Marchili,[86,7] Sera Markoff,[42,93] Daniel P. Marrone,[20] Alan P. Marscher,[76] Iván Martí-Vidal,[18,19] Satoki Matsushita,[17] Lynn D. Matthews,[12] Lia Medeiros,[94,20] Karl M. Menten,[7] Izumi Mizuno,[23] James M. Moran,[5,6] Kotaro Moriyama,[12,47] Monika Moscibrodzka,[4] Cornelia Müller,[7,4] Gibwa Musoke,[42,4] Alejandro Mus Mejías,[18,19] Hiroshi Nagai,[13,48] Neil M. Nagar,[95] Masanori Nakamura,[96,17] Ramesh Narayan,[5,6] Gopal Narayanan,[97] Iniyan Natarajan,[54,52,98] Joseph Neilsen,[99] Roberto Neri,[29] Chunchong Ni,[31,32] Aristeidis Noutsos,[7] Michael A. Nowak,[100] Hiroki Okino,[47,72] Gisela N. Ortiz-León,[7] Tomoaki Oyama,[47] Feryal Özel,[20] Daniel C. M. Palumbo,[5,6] Jongho Park,[17] Nimesh Patel,[6] Ue-Li Pen,[30,101–103] Dominic W. Pesce,[5,6] Vincent Piétu,[29] Richard Plambeck,[104] Aleksandar PopStefanija,[97] Oliver Porth,[42,9] Felix M. Pötzl,[7] Ben Prather,[62] Jorge A. Preciado-López,[30] Dimitrios Psaltis,[20] Hung-Yi Pu,[105,17,30] Venkatessh Ramakrishnan,[95] Ramprasad Rao,[26] Mark G. Rawlings,[23] Alexander W. Raymond,[5,6] Angelo Ricarte,[5,6] Bart Ripperda,[106,16] Freek Roelofs,[4] Alan Rogers,[12] Eduardo Ros,[7] Mel Rose,[20] Arash Roshanineshat,[20] Helge Rottmann,[7] Alan L. Roy,[7] Chet Ruszczyk,[12] Kazi L. J. Rygl,[86] Salvador Sánchez,[107] David Sánchez-Arguelles,[66,67] Mahito Sasada,[47,108] Tuomas Savolainen,[109,110,7] F. Peter Schloerb,[97] Karl-Friedrich Schuster,[29] Lijing Shao,[7,71] Zhiqiang Shen (沈志强),[43,44] Des Small,[79] Bong Won Sohn,[33,34,111] Jason SooHoo,[12] He Sun (孙赫),[25] Fumie Tazaki,[47] Alexandra J. Tetarenko,[112] Paul Tiede,[31,32] Remo P. J. Tilanus,[4,64,113,20] Michael Titus,[12] Kenji Toma,[114,115] Pablo Torne,[7,107] Tyler Trent,[20] Efthalia Traianou,[7] Sascha Trippe,[116] Ilse van Bemmel,[79] Huib Jan van Langevelde,[79,117] Daniel R. van Rossum,[4] Jan Wagner,[7] Derek Ward-Thompson,[118] John Wardle,[119] Jonathan Weintroub,[5,6] Norbert Wex,[7] Robert Wharton,[7] Maciek Wielgus,[5,6] George N. Wong,[62] Qingwen Wu (吴庆文),[120] Doosoo Yoon,[42] André Young,[4] Ken Young,[6] Feng Yuan (袁峰),[43,68,121] Ye-Fei Yuan (袁业飞),[122] J. Anton Zensus,[7] Guang-Yao Zhao,[14] and Shan-Shan Zhao[43]

(EHT Collaboration)

[1]*Institut für Theoretische Physik, Goethe-Universität, Max-von-Laue-Strasse 1, 60438 Frankfurt, Germany*
[2]*Frankfurt Institute for Advanced Studies, Ruth-Moufang-Strasse 1, 60438 Frankfurt, Germany*
[3]*School of Mathematics, Trinity College, Dublin 2, Ireland*
[4]*Department of Astrophysics, Institute for Mathematics, Astrophysics and Particle Physics (IMAPP), Radboud University, P.O. Box 9010, 6500 GL Nijmegen, Netherlands*
[5]*Black Hole Initiative at Harvard University, 20 Garden Street, Cambridge, Massachusetts 02138, USA*

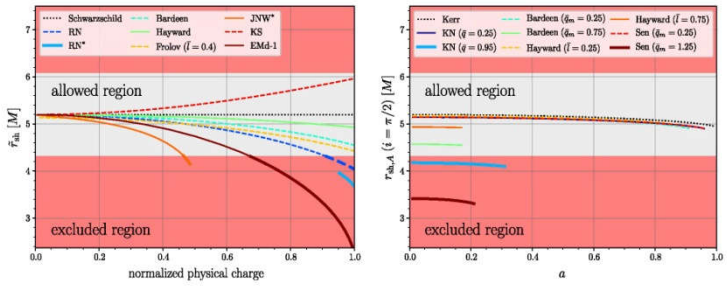

FIG. 2. Left: shadow radii $\tilde{r}_{\rm sh}$ for various spherically symmetric black-hole solutions, as well as for the JNW and RN naked singularities (marked with an asterisk), as a function of the physical charge normalized to its maximum value. The gray/red shaded regions refer to the areas that are 1-σ consistent/inconsistent with the 2017 EHT observations and highlight that the latter set constraints on the physical charges (see also Fig. 3 for the EMd-2 black hole). Right: shadow areal radii $r_{{\rm sh},A}$ as a function of the dimensionless spin a for four families of black-hole solutions when viewed on the equatorial plane ($i=\pi/2$). Also in this case, the observations restrict the ranges of the physical charges of the Kerr-Newman and the Sen black holes (see also Fig. 3).

independent charges—can also produce shadow radii that are incompatible with the EHT observations; we will discuss this further below. The two EMd black-hole solutions (1 and 2) correspond to fundamentally different field contents, as discussed in [70].

We report in the right panel of Fig. 2 the shadow areal radius $r_{{\rm sh},A}$ for a number of stationary black holes, such as Kerr [72], Kerr-Newman (KN) [73], Sen [74], and the rotating versions of the Bardeen and Hayward black holes [75]. The data refers to an observer inclination angle of $i=\pi/2$, and we find that the variation in the shadow size with spin at higher inclinations (of up to $i=\pi/100$) is at most about 7.1% (for $i=\pi/2$, this is 5%); of course, at zero-spin the shadow size does not change with inclination. The shadow areal radii are shown as a function of the dimensionless spin of the black hole $a:=J/M^2$, where J is its angular momentum, and for representative values of the additional parameters that characterize the solutions. Note that—similar to the angular momentum for a Kerr black hole—the role of an electric charge or the presence of a de Sitter core (as in the case of the Hayward black holes) is to reduce the apparent size of the shadow. Furthermore, on increasing the spin parameter, we recover the typical trend that the shadow becomes increasingly noncircular, as encoded, e.g., in the distortion parameter $\delta_{\rm sh}$ defined in [57,83] (see Appendix). Also in this case, while the regular rotating Bardeen and Hayward solutions are compatible with the present constraints set by the 2017 EHT observations, the Kerr-Newman and Sen families of black holes can produce shadow areal radii that lie outside of the 1-σ region allowed by the observations.

To further explore the constraints on the excluded regions for the Einstein-Maxwell-dilaton 2 and the Sen black holes, we report in Fig. 3 the relevant ranges for these two solutions. The Einstein-Maxwell-dilaton 2 black holes are nonrotating but have two physical charges expressed by the coefficients $0<\bar{q}_e<\sqrt{2}$ and $0<\bar{q}_m<\sqrt{2}$, while the Sen black holes spin (a) and have an additional electromagnetic charge $\bar{q}_m$. Also in this case, the gray/red shaded regions refer to the areas that are consistent/inconsistent with the 2017 EHT observations. The figure shows rather easily that for these two black-hole families there are large

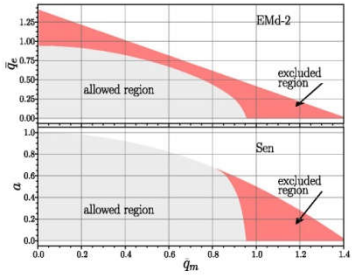

FIG. 3. Constraints set by the 2017 EHT observations on the nonrotating Einstein-Maxwell-dilaton 2 and on the rotating Sen black holes. Also in this case, the gray/red shaded regions refer to the areas that are 1-σ consistent/inconsistent with the 2017 EHT observations).

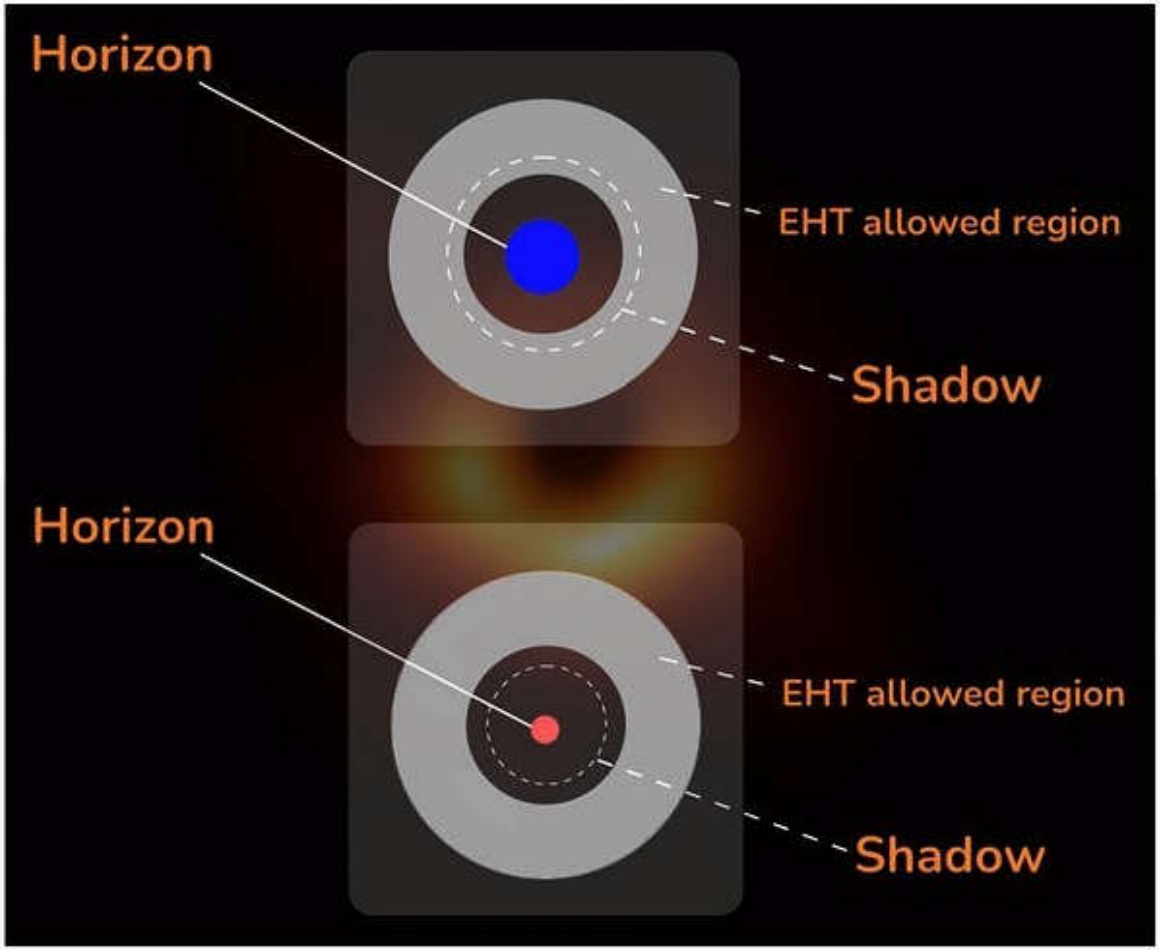
Horizon
EHT allowed region
Shadow
Horizon
EHT allowed region
Shadow

Zakharov, Universe, 2022; arxiv:2108.01533; charge constraint on M87* (for Sgr A* D=51.8±2.3 uas, 12.05.2022). For M87 D=D_Sch (1±0.17)

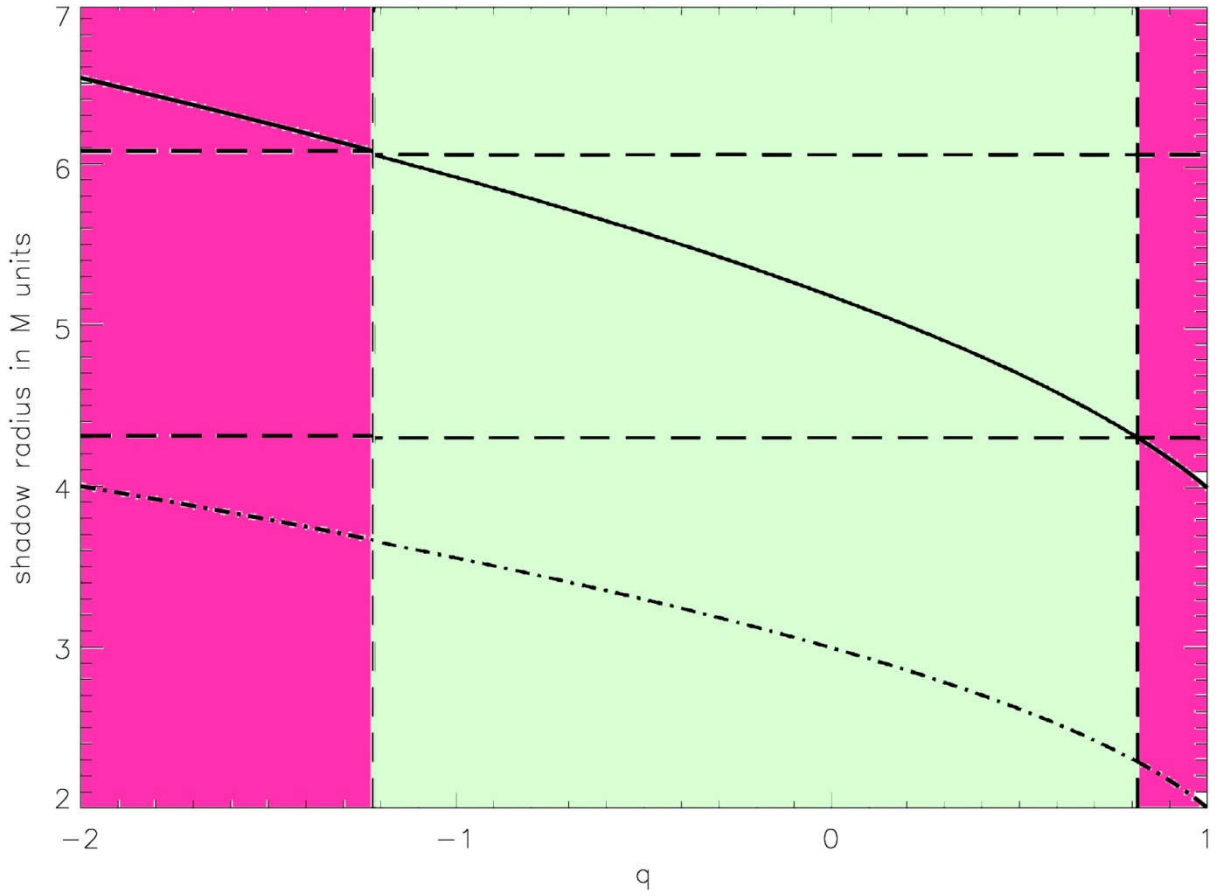

Sgr A* shadow discovery by EHT (reported on May 12, 2022)

Press Conferences around the world (Video Recordings):

Garching, Germany - European Southern Observatory

Madrid, Spain - Consejo Superior de Investigaciones Científicas

México D.F., Mexico - Consejo Nacional de Ciencia y Tecnología

Rome, Italy - Istituto Nazionale di Astrofisica

Santiago de Chile - ALMA Observatory

Washington D.C., USA - National Science Foundation

Tokyo, Japan - National Astronomical Observatory of Japan

For Sgr A* D=51.8±2.3 uas, (EHT collaboration, 12.05.2022)

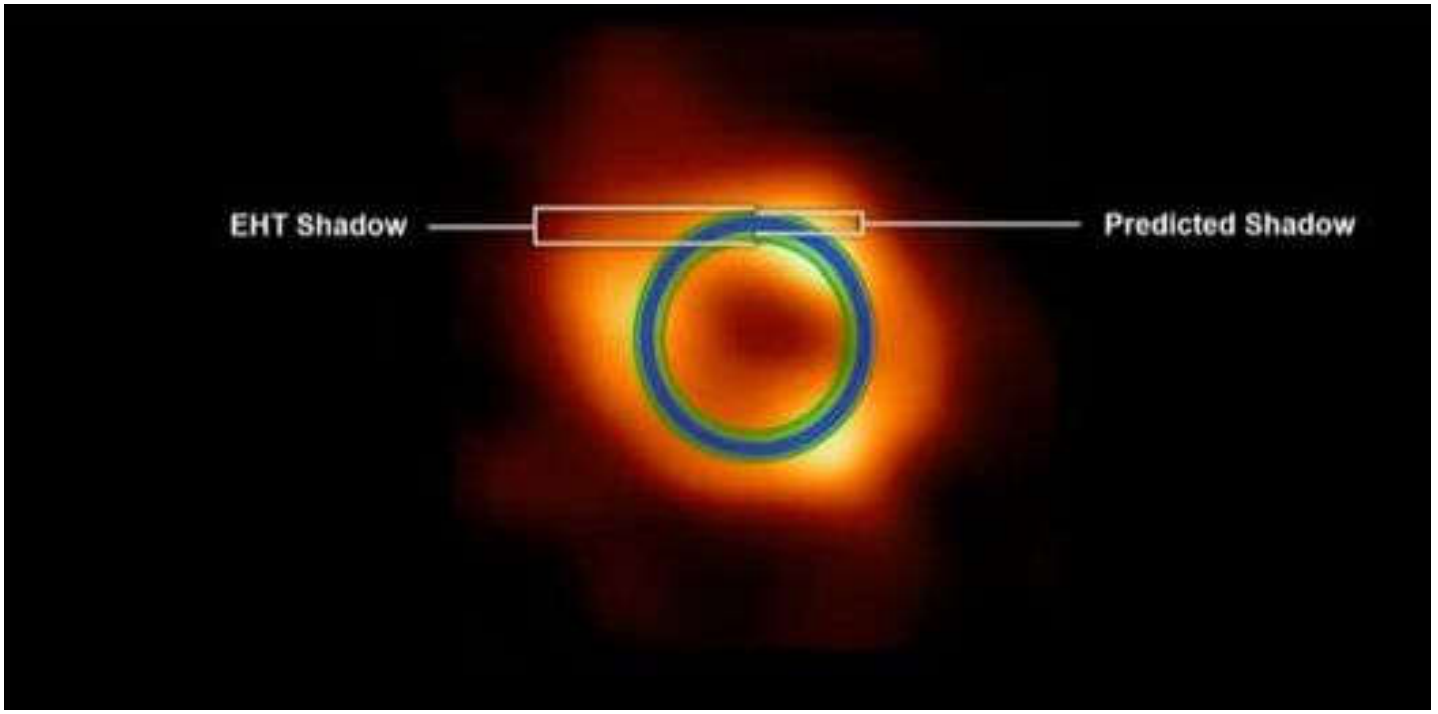

A. F. Zakharov, Physics of Particle and Nuclei Lett. (2023)

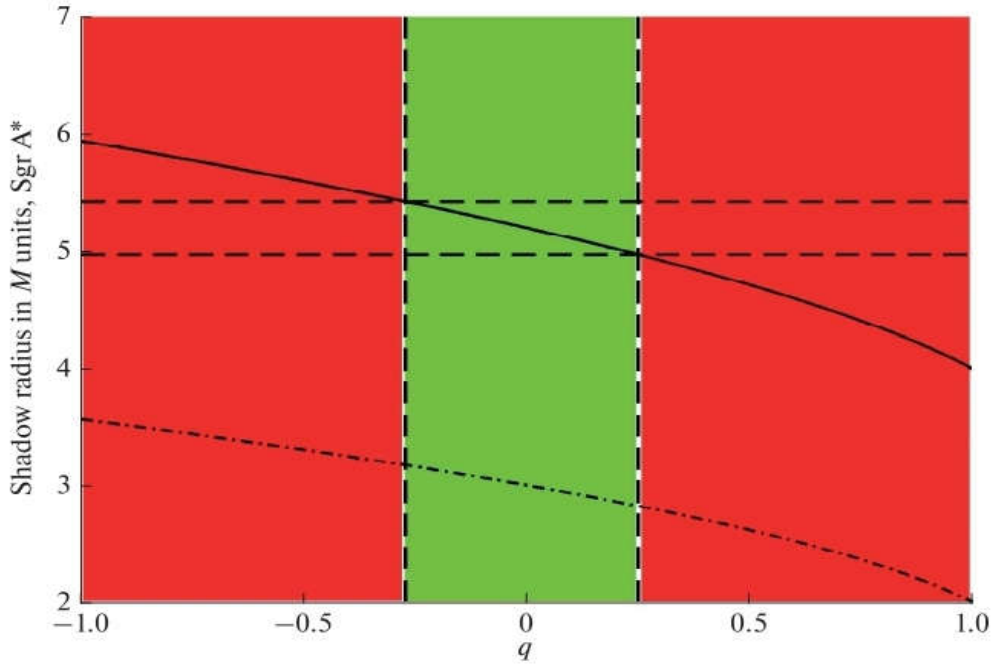

Fig. 1. Shadow radius (solid curve) and radius of the last circular unstable photon orbit (dashed-and-dotted curve) in units M as a function q. Following work [30], we believe that $\theta_{\text{sh SgrA*}} \approx (51.8 \pm 2.3)$ μas at a confidence level of 68%. The horizontal dashed lines correspond to the restrictions on the size of the radius in units M. Accordingly, red vertical stripes for q are inconsistent with these estimates of the size of the shadow in the HC.

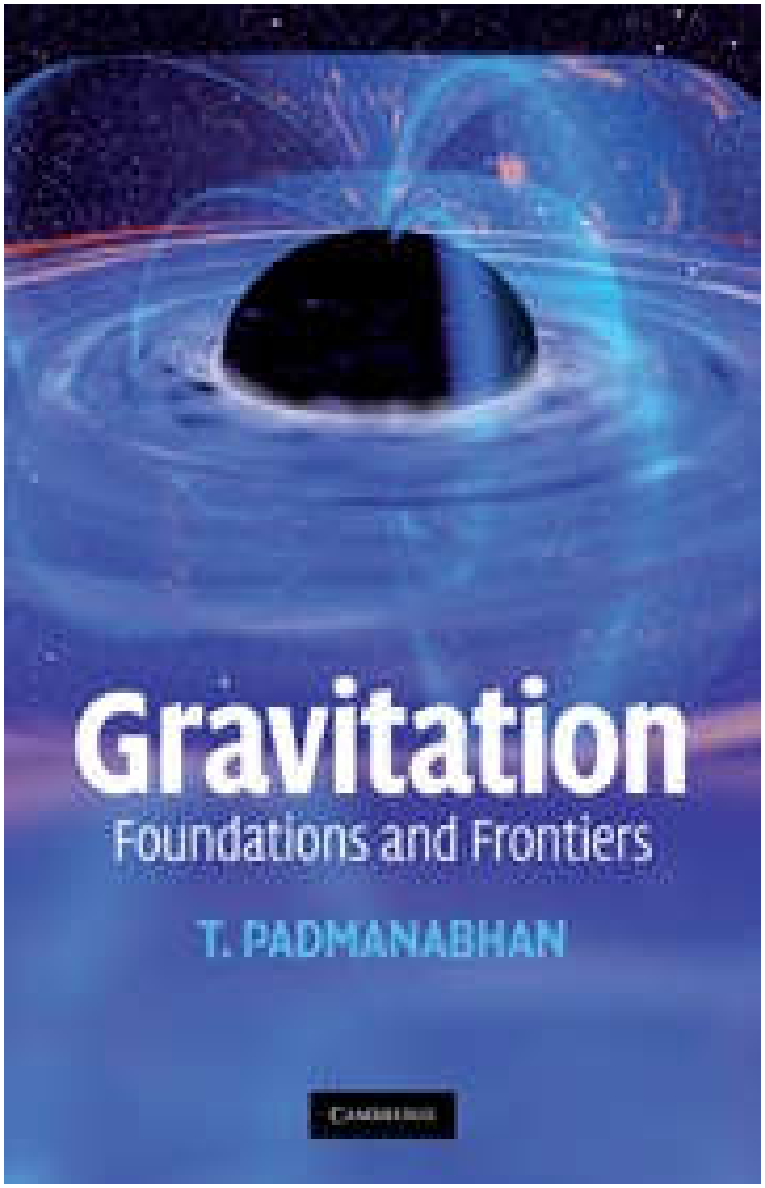
Gravitation
Foundations and Frontiers
T. PADMANABHAN

EXPLORING BLACK HOLES

Introduction to General Relativity

EDWIN F. TAYLOR
JOHN ARCHIBALD WHEELER
EDMUND BERTSCHINGER

SECOND EDITION

The Event Horizon Telescope Picture

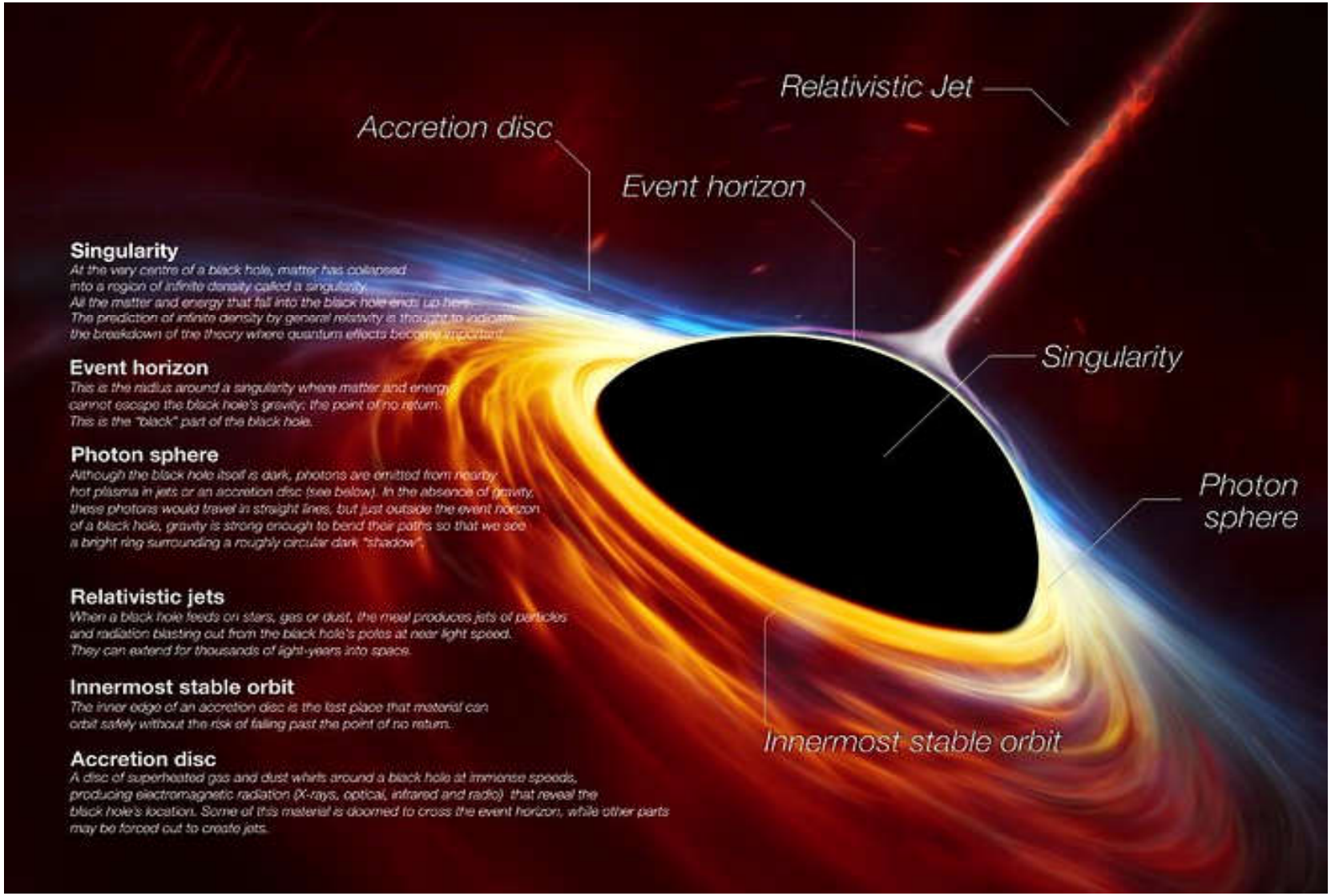

Conclusion

The shadow concept has been transformed from a purely theoretical category into an observable quantity which may be reconstructed from astronomical observations.

Therefore, VLBI observations and image reconstructions for M87* and Sgr A* are in a remarkable agreement with an existence of supermassive black holes in centers of these galaxies.

- Thanks for your kind attention!

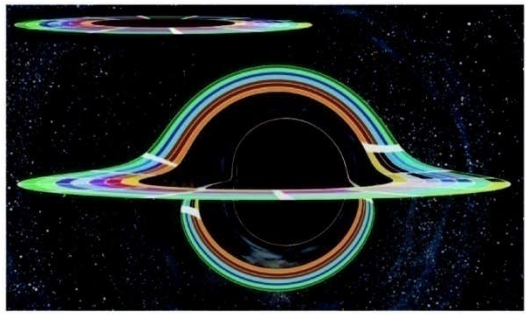

Figure 13. Inset: paint-swatch accretion disk with inner and outer radii $r = 9.26M$ and $r = 18.70M$ before being placed around a black hole. Body: this paint-swatch disk, now in the equatorial plane around a black hole with $a/M = 0.999$, as viewed by a camera at $r_c = 74.1M$ and $\theta_c = 1.511$ (86.56°), ignoring frequency shifts, associated colour and brightness changes, and lens flare. (Figure from *The Science of Interstellar* [40], used by permission of W. W. Norton & Company, Inc, and created by our Double Negative team, ™ & © Warner Bros. Entertainment Inc. (s15)).

itself. This entire image comes from light rays emitted by the disk's bottom face: the wide bottom portion of the image, from rays that originate behind the hole, and travel under the hole and back upward to the camera; the narrow top portion, from rays that originate on the disk's front underside and travel under the hole, upward on its back side, over its top, and down to the camera—making one full loop around the hole.

There is a third disk image whose bottom portion is barely visible near the shadow's edge. That third image consists of light emitted from the disk's top face, that travels around the hole once for the visible bottom part of the image, and one and a half times for the unresolved top part of the image.

In the remainder of this section 4 we deal with a moderately realistic accretion disk—but a disk created for *Interstellar* by Double Negative artists rather than created by solving astrophysical equations such as [32]. In appendix A.6 we give some details of how this and other Double Negative accretion disk images were created. This artists' *Interstellar* disk was chosen to be very anemic compared to the disks that astronomers see around black holes and that astrophysicists model—so the humans who travel near it will not get fried by x-rays and gamma-rays. It is physically thin and marginally optically thick and lies in the black hole's equatorial plane. It is not currently accreting onto the black hole, and it has cooled to a position-independent temperature $T = 4500$ K, at which it emits a black-body spectrum.

Figure 14 shows an image of this artists' disk, generated with a gravitational lensing geometry and computational procedure identical to those for our paint-swatch disk, figure 13

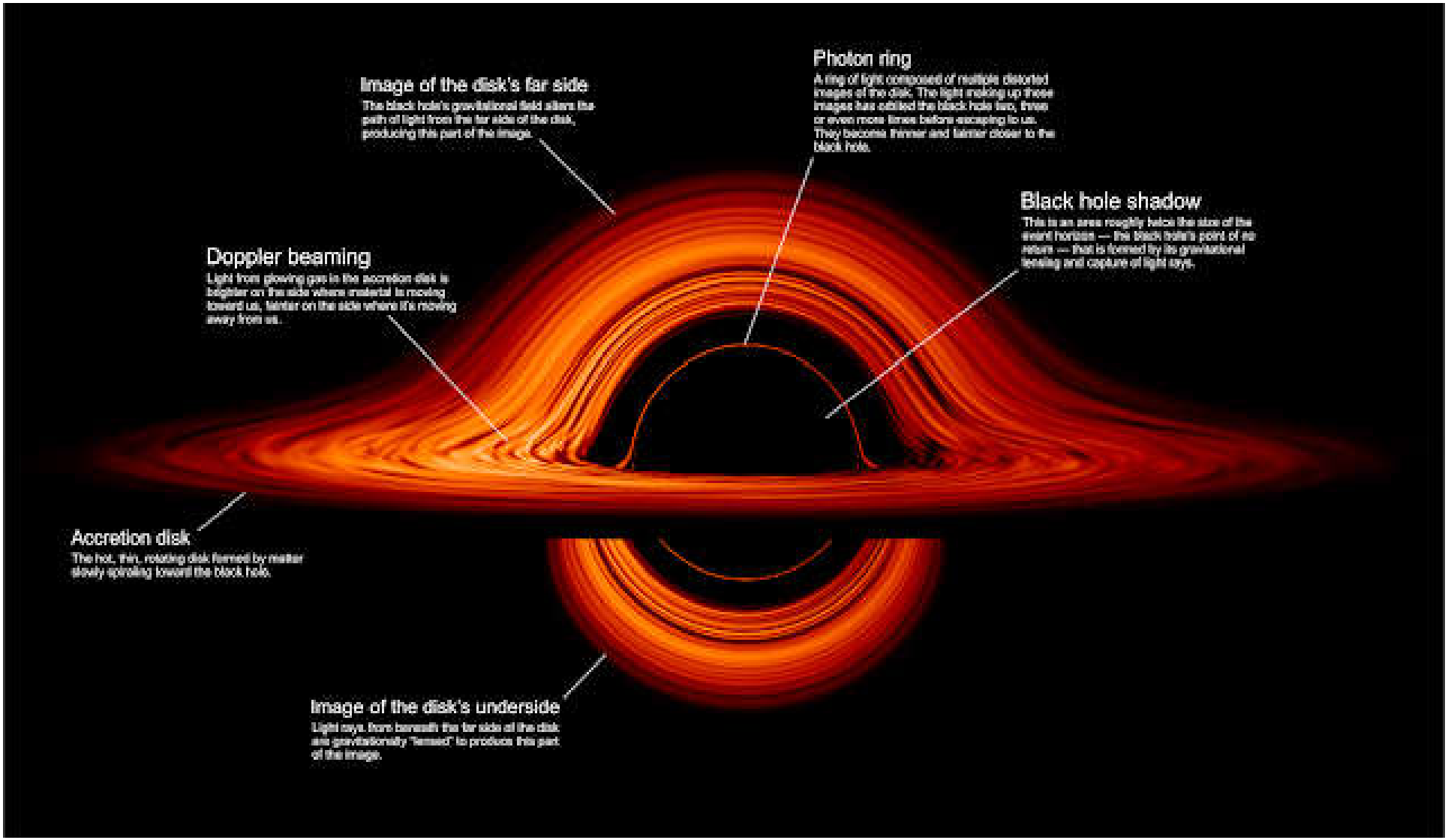
Image of the disk's far side
The black hole's gravitational field alters the path of light from the far side of the disk, producing this part of the image.
Photon ring
A ring of light composed of multiple distorted images of the disk. The light making up these images has orbited the black hole two, three or even more times before escaping to us. They become thinner and fainter closer to the black hole.
Black hole shadow
This is an area roughly twice the size of the event horizon — the black hole's point of no return — that is formed by its gravitational lensing and capture of light rays.
Doppler beaming
Light from glowing gas in the accretion disk is brighter on the side where material is moving toward us, fainter on the side where it's moving away from us.
Accretion disk
The hot, thin, rotating disk formed by matter slowly spiraling toward the black hole.
Image of the disk's underside
Light rays from beneath the far side of the disk are gravitationally "lensed" to produce this part of the image.

Fortschr. Phys. **56**, No. 4 – 5, 456 – 461 (2008) / **DOI** 10.1002/prop.200710519

Observational effects of strong gravity in vicinity of supermassive black holes

Predrag Jovanović[1,*] and **Luka Č. Popović**[1,2]

[1] Astronomical Observatory, Volgina 7, 11160 Belgrade, Serbia
[2] Alexander von Humboldt Fellow, presently at Max Planck Institute for Radioastronomy, Bonn, Germany

Received 27 November 2007, accepted 25 January 2008
Published online 8 April 2008

Key words Black holes, accretion and accretion disks, galactic nuclei, active and peculiar galaxies and related systems, quasars

PACS 97.60.Lf, 97.10.Gz, 98.62.Js, 98.54.Cm, 98.54.-h

Here we discuss the effects of strong gravity that can be observed in electromagnetic spectra of active galactic nuclei (AGN). According to the unification model of an AGN, there is a supermassive black hole ($10^7 - 10^9 M_\odot$) in its center, surrounded by an accretion disk that radiates in the X-ray band. Accretion disks could have different forms, dimensions, and emission, depending on the type of central black hole (BH), whether it is rotating (Kerr metric) or nonrotating (Schwarzschild metric). We modeled the emission of an accretion disk around supermassive BH using numerical simulations based on a ray-tracing method in the Kerr metric. A broad emission line Fe Kα at 6.4 keV with asymmetric profile (narrow bright blue peak and a wide faint red wing) has been observed in a number of type 1 AGN. The effects of strong gravitational field are investigated by comparison between the modeled and observed iron Kα line profiles. The results of our modeling show that the parameters of the Fe Kα line emitting region have significant influence on the line profile and thus, allow us to determine the space-time geometry (metric) in vicinity of the central BH of AGN, and also can give us information about the plasma conditions in these regions.

1 Introduction

It is now widely accepted that AGN derive their extraordinary luminosities (sometimes more than 10^4 times higher than luminosities of "ordinary" galaxies) from energy release by matter accreting towards, and falling into, a central supermassive BH. The accretion disks around the central BH represent an efficient mechanism for extracting gravitational potential energy and converting it into radiation, giving us the most probable explanation for the main characteristics of AGN (high luminosity, compactness, jet formation, rapid time variation in radiation and the profile of the Fe Kα spectral line). Thus, AGN are powerful sources of radiation in a wide spectral range: from γ rays to radio waves [1].

The most important feature of the X-ray radiation of AGN (which is generated in the innermost region around a central BH) is a broad emission line Fe Kα at 6.4 keV that may have an asymmetric profile (narrow bright blue peak and wide faint red peak). It was discovered in Seyfert 1 galaxy MCG-6-30-15 [2] and later on observed in a number of AGN. In some cases the line width corresponds to one third of speed of light, indicating that its emitters rotate with relativistic velocities. Therefore, the line is probably produced in a very compact region near the central BH of AGN and can provide us some essential information about the plasma conditions and the space-time geometry in vicinity of the BH [3].

* Corresponding author E-mail: pjovanovic@aob.bg.ac.yu, Phone: +381 11 3089 068, Fax: +381 11 2419 553

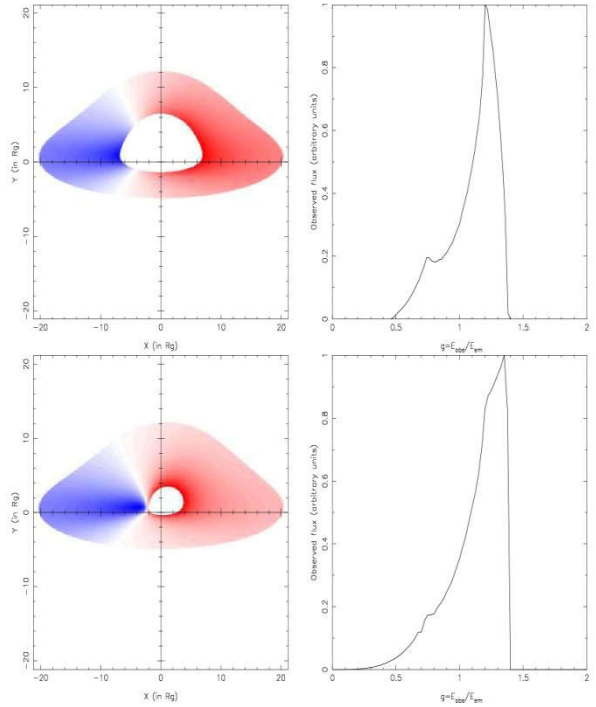

Fig. 2 (online colour at: www.fp-journal.org) The same as in Fig. 1 but for a highly inclined disk with $i = 75^{\circ}$.

asymmetric (see Fig. 3). If the line emission is originating at larger distances from the BH, the red peak of the line becomes brighter and line profile narrower and more symmetric. In majority of AGN, where the broad Fe Kα line is observed[1], its profile is more similar to the modeled profile as obtained under assumption that the line emitters are located close to the central BH. Therefore, comparisons between the observed and modeled Fe Kα line profiles can bring us some essential information about strong gravitational field in vicinity of central supermassive BH of AGN.

[1] Note here that in some AGN only the narrow Fe Kα line is observed, but it is supposed to be emitted in the disk corona that is located farther from the disk, and therefore, these relativistic effects cannot be detected in the line profile